SEISMIC RECORD OF WEST ANTARCTIC ICE SHEET DYNAMICS DURING THE LATE OLIGOCENE TO EARLY MIOCENE IN THE EASTERN BASIN, ROSS SEA

Seth Jennings Brazell

A dissertation submitted to the faculty of the University of North Carolina at Chapel Hill in partial fulfillment of the requirements for the degree of Doctor of Philosophy in the Department of Geological Sciences.

Chapel Hill
2017

Approved by:

Donna M. Surge

Larry K. Benninger

José A. Rial

Christopher C. Sorlien

Kevin G. Stewart

ABSTRACT

Seth Jennings Brazell: Seismic record of West Antarctic Ice Sheet dynamics during the late Oligocene to early Miocene in Eastern Basin, Ross Sea
(Under the direction of Donna M. Surge)

The Antarctic cryosphere is an important driver of global climate change and ocean circulation. The Antarctic Ice Sheet is comprised of the stable, terrestrially-based East Antarctic Ice Sheet (EAIS) and the marine-based West Antarctic Ice Sheet (WAIS) that may be prone to a collapse that would contribute over 3 m to global sea level rise. The Antarctic Ice Sheets have unique evolutionary histories and understanding how they have influenced and been influenced by global changes through the Cenozoic will yield a more robust understanding of their response to future climate change. 98% of Antarctica is currently covered in ice, posing challenges for investigators. Much of our understanding of the evolution of the Antarctic cryosphere has been developed from far field oxygen isotope records of global temperature and ice volume change; however, more direct records of Antarctic Ice Sheet dynamics from the continent and margin conflict with interpretations derived from these records. The Ross Sea embayment in Antarctic drains ~25% of the continent, receives input from both the EAIS and WAIS and contains a thick section of Cenozoic deposits, making it an important location to investigate the evolution of the Antarctic cryosphere. The Eastern Basin, Ross Sea contains a thick section of Cenozoic strata that records the evolution of the WAIS. This study reexamines legacy and recent seismic reflection data and uses spectral attribute analysis to enhance the resolution of the datasets. I document spectral decomposition techniques that enhance the temporal resolution of multi-

channel seismic profiles. Using the spectral decomposition technique, I develop a higher resolution, third-order sequence stratigraphic model of late Oligocene to early Miocene sequences within the Eastern Basin to test hypotheses about the evolution of the WAIS. I identify evidence of an expanding late Oligocene WAIS and waning ice volumes during the early Miocene. Using seismic-stratigraphic stacking patterns, I correlated relative sea level fluctuations recorded in the Eastern Basin to global eustatic and oxygen isotope events and refined chronostratigraphic correlations of regional horizons and unconformities. These findings have important implications for the initiation and evolution of the West Antarctic Ice Sheet during the late Paleogene and early Neogene.

ACKNOWLEDGEMENTS

I am grateful for the support and guidance of Donna Surge and Lou Bartek who were instrumental in this project. I offer a special thanks to Chris Sorlien who was generous with his time and resources and was a great mentor during my PhD. This work greatly benefited from our many conversations and your helpful insights and suggestions. This project was supported by the Department of Geological Sciences at the University of North Carolina – Chapel Hill and the Martin Fund, National Science Foundation grant PLR-1341585 to Christopher Sorlien and Bruce Luyendyk at the University of California – Santa Barbara, and dGB Earth Sciences. Technical support was provided by Nigel Wardell (OGS, Trieste, Italy), Suzanne Carbotte (LDEO, Columbia University) and the support team at OpendTect, dGB Earth Sciences. Seismic data was accessed via Marine Geoscience Data System: IEDA and Seismic Data Library System (OGS, Trieste, Italy) with the support of the ROSSMAP Project members. Gualtiero Bohm and Marvin Speece provided additional seismic data. I am thankful for my colleagues who made my time at Chapel Hill memorable. I am thankful to John Diemer for stoking my curiosity of geology and encouraging me to pursue a PhD. Finally, I would like to thank my family for their unwavering support in all my endeavors.

TABLE OF CONTENTS

LIST OF TABLES

Table

LIST OF FIGURES

LIST OF ABBREVIATIONS

ANTOSTRAT	The Antarctic Offshore Stratigraphy project
CIROS	Cenozoic Investigation in the Western Ross Sea
CRP	Cape Roberts Project
CWT	Continuous wavelet transform
DSDP	Deep Sea Drilling Project
EAIS	East Antarctic Ice Sheet
EB	Eastern Basin
GZW	Grounding zone wedge
HST	Highstand systems tract
IODP	Integrated Ocean Drilling Program
IRD	Ice rafted debris
LST	Lowstand systems tract
MCS	Multi-channel seismic
MFS	Maximum flooding surface
Mi	Miocene
MSSTS	McMurdo Sound Sediment and Tectonic Studies
Oi	Oligocene
Plio	Pliocene
RSL	Relative sea level
RSS	Ross Sea sequence
RSU	Ross Sea unconformity
SB	Sequence boundary

SCS	Single channel seismic
SMW	Shelf margin wedge
SWFFT	Short window fast Fourier transform
TST	Transgressive systems tract
TWTT	Two-way travel time
VE	Vertical exaggeration
WAIS	West Antarctic Ice Sheet

CHAPTER 1: SPECTRAL DECOMPOSITION AND SEISMIC ATTRIBUTE ANALYSIS AS A TOOL FOR 2D SEISMIC ENHANCEMENT: A CASE STUDY USING LEGACY SEISMIC DATA FROM THE ANTARCTIC MARGIN

1.1 Introduction

Seismic attribute analyses can enhance interpretation of 2D seismic data sets without the need for time-consuming reprocessing. The analysis of seismic attributes of 3D seismic datasets has been well documented (White 1991; Taner et al., 1994; Brown, 1996; Marfurt et al., 1998; Peyton et al., 1998; Barnes 2000, 2001; Chopra and Marfurt 2005). As the use and understanding of seismic attributes have improved over the last three decades, relatively little work has been recently conducted documenting the application of seismic attributes to legacy 2D seismic datasets. The work that follows is a case study discussing the application of short-window fast Fourier transform (SWFFT) and continuous wavelet transform (CWT) spectral decomposition as a tool to enhance the temporal resolution of seismic reflection profiles (Figure 1.1).

The Antarctic margin is a key area in which to investigate the application of post-stack seismic attributes on 2D seismic data. Legacy seismic data sets comprise a significant portion of seismic reflection data along the Antarctic margin and, in some places, seismic reflection data collected in the early 1990s and prior is the only available geophysical data. Reprocessing legacy data is a labor intensive and time-consuming method that often yields limited results. Additionally, poor data management practices may result in the corruption or loss of pre-stack seismic data making reprocessing impossible. Existing digital seismic data sets, however, can be re-examined with the use of post-stack seismic attributes, like spectral decomposition. Some post-stack techniques result in an enhancement of the legacy seismic data

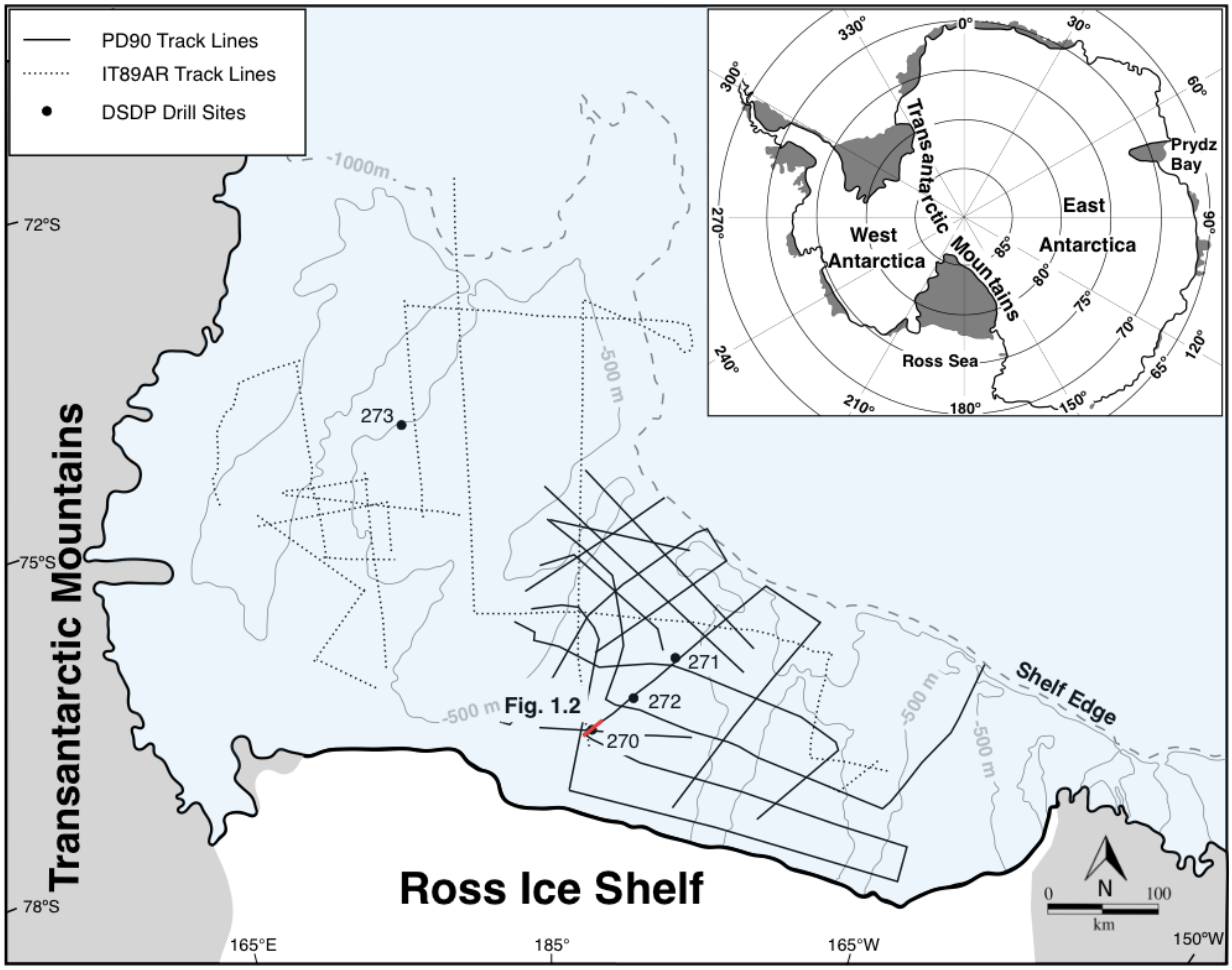

Figure 1.1 Location of study area: Ross Sea, Antarctica. Thin black and dashed lines are seismic track lines. Closed circles are DSDP Leg 28 drill sites along the Ross Sea margin.

that aids the interpreter by highlighting subtle features that are not obvious in standard amplitude section.

Extracting additional information from legacy seismic data may provide new direct records of glacial erosion surfaces and glacially associated seismic facies which are used to understand the evolution of the Antarctic Ice Sheet. Previous seismic stratigraphic studies, particularly in the Ross Sea, have used low-resolution multi-channel seismic (MCS) data to correlate regional unconformities (Houtz and Meijer, 1970; Houtz and Davey, 1973; Hinz and Block, 1984; Cooper et al., 1991; Busetti and Zayatz, 1994; and Brancolini et al., 1995). High- to

intermediate-resolution single channel seismic (SCS) surveys conducted by Anderson and Bartek (1992) and Bart (2004) showed that while SCS data do not clearly image below the sea floor multiple, their higher frequency sources are required to image detailed seismic facies that are not recognized in MCS data with lower source frequencies. MCS data from the Ross Sea can penetrate below the sea floor multiple and image older strata that may have been deposited or modified by mid-Cenozoic Antarctic glaciation. This study investigates the applicability of post-stack seismic attributes of 2D MCS data to enhance the resolution and extract additional information from the seismic data that may be useful for understanding seismic features and facies that are currently not imaged in traditional standard amplitude profiles.

1.2 Methods

The data sets used for this study include intermediate- and low-resolution seismic reflection data [BMR (Australia) 1982 multi-channel survey using a 460 cu. in air gun with a penetration depth of 6 seconds and vertical resolution of 30 meters; OGS Trieste (Italy) 1989 multi-channel survey using 2 arrays of air guns (45.16 liter volume) with a penetration depth of 6 seconds and a vertical resolution of 40 meters; Rice University (USA) 1990 single channel survey using a 150 cu. in air gun with a penetration depth of 1.5-2.0 seconds and a vertical resolution of 12 meters] and published lithologic descriptions from DSDP Leg 28, 119 and 188 drill sites (Hayes and Frakes, 1975; Stagg et al., 1983; Barron et al., 1991; De Santis et al., 1995; O'Brien et al., 2001).

Spectral decomposition was performed on MCS profiles using the OpendTect seismic attribute plugin. Two different discrete Fourier transforms were applied to MCS data in this study; 1) a short window, fast Fourier transform (SWFFT) with time gaps between +/- 8 to +/-14 milliseconds, and 2) a continuous wavelet transform (CWT) using the Morlet wavelet. Multiple

images of the frequency filtered seismic data were created at 1 Hz increments. Frequencies that displayed non-periodic absorption surfaces with the highest temporal resolution and within the data's bandwidth were used for subsequent interpretation.

Spectral decomposition images were then validated by comparison to overlapping, crossing or nearby higher resolution SCS profiles. Seismic reflection surfaces in SCS and MCS data and frequency absorption surfaces in spectrally decomposed MCS data were interpreted and averaged over a 1000 ms window to determine if spectrally decomposed MCS data resolution was improved compared to standard amplitude MCS data. Spectral absorption surfaces from spectrally decomposed MCS data were compared to SCS data reflection surfaces for validation.

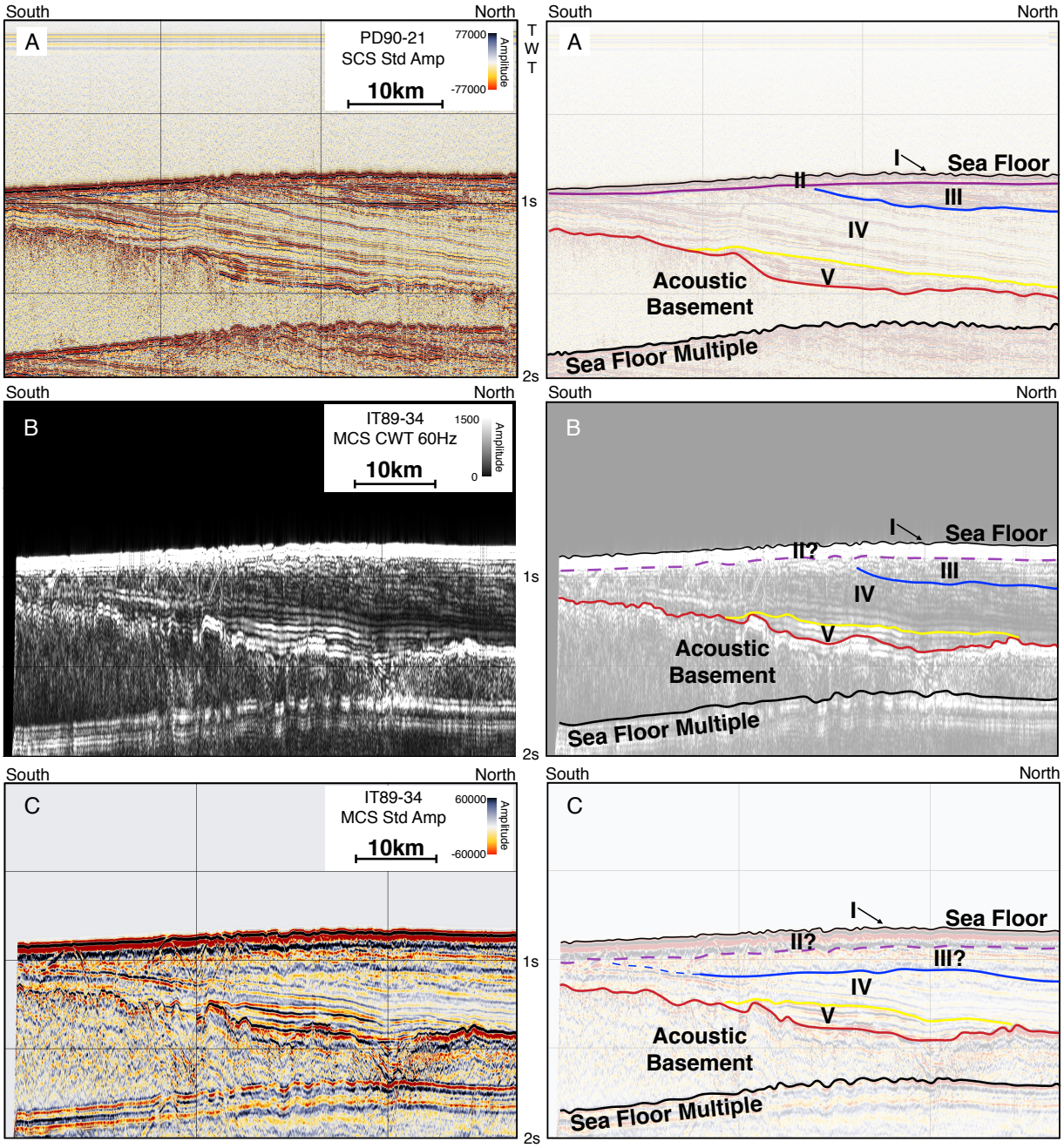

Figure 1.2. Comparison of moderate-resolution, low-resolution and spectral decomposition temporal enhancement images and their corresponding interpreted line drawings. **A)** Profile 1, PD90-21, moderate-resolution SCS profile showing scoured sea floor and seismic Units II-V separated by unconformities; **B)** Profile 2, IT89-AR34, CWT spectral decomposition image showing enhanced temporal resolution by resolving Units II-V with similar characteristics as identified in moderate-resolution seismic profile PD90-21; **C)** Profile 2, IT89-AR34, low-resolution MCS profile showing scoured sea floor and seismic Units II-V with different characteristics than PD90-21 or the spectral decomposition of IT89-AR3.

1.3 Results

Two obliquely overlapping seismic profiles, MCS IT89-AR34 and SCS PD90-21 (see Figure 1.1 for location), highlight differences in resolution between MCS and SCS profiles (Figure 1.2). Figure 1.2A shows PD90-21, an intermediate-resolution SCS profile with 5 distinct features and units. Sea floor morphology (Feature I) changes from smooth reflections to the south becoming wavy as the sea floor rises to the north. Diffraction hyperbolas are present at the sea floor and at the base of Unit I and extend below 1 second two-way travel time (twtt) and obscure portions of the profile. Beneath the sea floor Unit II is a thin package of discordant to sub-parallel reflections. Unit III is comprised of downlapping reflections dipping to the north and separated from Unit IV below by an unconformity that truncates closely spaced, sub-parallel, down dip converging reflections. Unit IV contains down-dip converging, acoustically laminated units. Reflections within Unit IV alternate between moderate to high-amplitude, laminated, continuous reflections and low-amplitude reflections that become discontinuous to acoustically transparent in the down-dip direction. Just above the base of Unit IV reflections become lower frequency and become discontinuous. The basal reflection of Unit IV truncates the top of Unit V and reflection character changes to high-amplitude and moderately continuous within a depression above acoustic basement.

Figure 1.2C shows IT89-34, a low-resolution MCS reflection profile with 3 distinct and 2 ambiguous features and units. Sea floor morphology (Feature I) changes from smooth reflections to the south, becoming wavy as the sea floor rises to the north and a return to smooth reflections at the northernmost section of the profile. Diffraction hyperbolas are present only at the sea floor of Unit II and extend below 1 second twtt and obscure portions of the profile. Unit II consists of a low-frequency, very high-amplitude, continuous and parallel reflectors. The sea floor reflection

has a thickness of approximately 100 milliseconds (ms) of travel time and the possible occurrence of a ghost multiple obscures any stratigraphic reflections close to it. Unit III contains sub-horizontal reflections that grade from discontinuous to the south and becoming more continuous, high-amplitude and high-frequency to the north. Unit III of IT89-34 contains reflections that dip slightly to the north but cannot be interpreted as foresets within a grounding zone wedge as interpreted in profile PD90-21. Unit IV is bounded on the top by truncation and at the base by onlap, downlap and a change in reflection character. Internal reflections gradually change from low-frequency, high-amplitude continuous and discontinuous to the south to higher-frequency, low-amplitude and continuous to the north. The alternating character of Unit IV in PD90-21 between high-frequency continuous to acoustically transparent is not present in Unit IV of IT89-34. Unit V in both MCS and SCS profiles is characterized by continuous, high-amplitude reflections occupying a depression above acoustic basement. Additionally, Unit V in IT89-34 contains low-frequency reflections, dissimilar to the high-frequency reflections contains in Unit V of PD90-21.

Figure 1.2B shows a spectral decomposition image of profile IT89-34 (Figure 1.2C) using a continuous Morlet wavelet transform at 60Hz. The spectral decomposition of profile IT89-34 reveals higher frequency information than can be resolved within the standard amplitude profile. Feature I and Unit II are similar to those identified in the standard amplitude profile of Figure 1.2C. However, directly below the high values of the sea floor the spectral decomposition image shows high-frequency, continuous to discontinuous reflections which are absent from the standard amplitude section. The base of Unit III can be identified as a high-frequency and continuous reflection dipping to the North in Figure 1.2B and not as a low-frequency, sub-horizontal reflection identified in Figure 1.2C. Unit IV is characterized by reflections that

converge down dip, to the north, with bed thicknesses decreasing with depth. The alternating patterns of high-frequency, continuous reflections and acoustically transparent facies is not apparent in Figure 1.2B, as it is in Figure 1.2A. Unit V is distinguished from Unit IV by its high amplitude values and continuous reflections that occupy a depression just above acoustic basement.

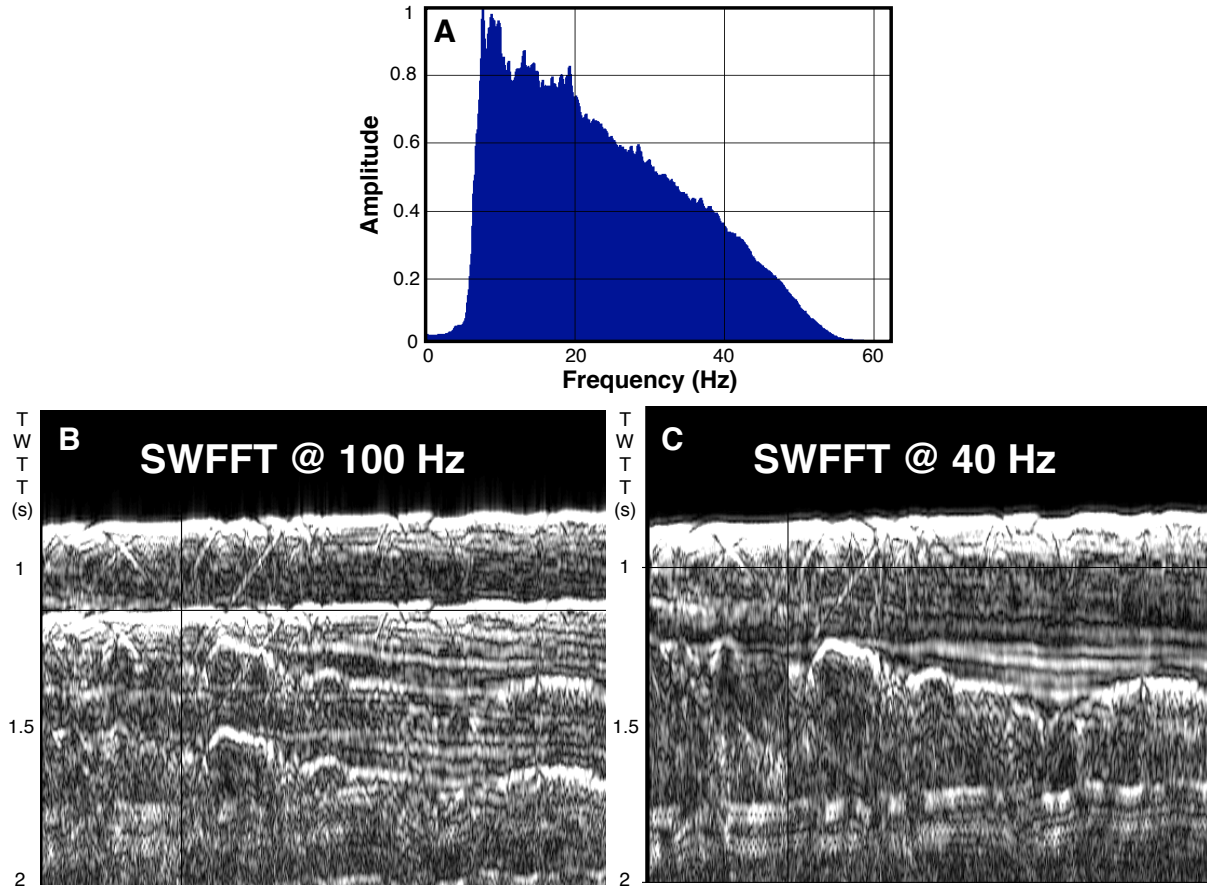

Figure 1.3. **A)** Frequency spectrum of profile IT89AR-34. **B)** Spectral decomposition at a frequency outside of the bandwidth of profile IT89AR-34 and **C)** spectral decomposition at a frequency within of the bandwidth of profile IT89AR-34. Spectral decomposition outside seismic bandwidth produces periodic, high frequency reflections that obscure the seismic image.

1.4. Discussion

SWFFT uses time gates to isolate temporal segments of the seismic trace upon which the fast Fourier transform is performed. The seismic trace frequency and resolution must be considered when selecting an appropriate time gate for a SWFFT operation. Selecting a time gate that is too small will result in a high temporal resolution, at the cost of frequency resolution. A large time gate will result in a high frequency resolution but with poor temporal resolution. Another spectral decomposition method that does not require the user to select a time gate is a continuous wavelet transform. A CWT function uses compressed and shifted variants of a mother wavelet, known as daughter wavelets, and the resulting spectral analysis contains higher frequency resolution for lower frequencies and higher temporal resolution for higher frequencies. Common mother wavelets include Gaussian, Morlet and Ricker wavelets. CWT analysis was the preferred method of spectral decomposition because it requires fewer input parameters and, unlike the SWFFT, it offers better time and frequency localization.

Multichannel seismic surveys have a vertical resolution between 40-100 m and are unable to resolve many important geologic features that exist on smaller scales but that are important to understand sedimentary processes and depositional environments. Spectral decomposition allows the interpreter to isolate higher portions of the frequency spectrum that are necessary to resolve features that may be tuned or aliased at the lower dominant frequency. However, high-frequency signals are rapidly attenuated by the Earth with depth and standard processing workflows filter out much of the high-frequency signal. Spectral decomposition at frequencies outside of the processed seismic data's bandwidth will produce unreliable results that should not be used for interpretation (Figure 1.3). Results from the analysis for spectral decomposition images show that temporal resolution is enhanced within 200 ms of the sea floor and that there is no temporal

resolution enhancement below 500 ms below the sea floor. As depth increases and high-frequency data is attenuated, spectral decomposition resolution will diminish and should not be used. Imaging a seismic profile at time depths below ~500 ms will require lower frequencies than were used to image reflections at shallower depths. It is recognized that increasing streamer tow depths (tow depth is typically increased in poor sea surface conditions) in addition to low pass filters applied to seismic data will reduce the ability of spectral decomposition to resolve higher frequency information, however, the effects of various pre- and post-stack processing should be investigated further to understand their impacts.

The wavy sea floor reflections to the north in Figure 1.2A are interpreted as ice scouring features that occurred during Last Glacial Maximum ice expansion when the West Antarctic Ice Sheet advanced across the Ross Sea towards the shelf edge (Anderson et al., 2013). Spectral decomposition did not appear to enhance the resolution of the sea floor. This result may be related to the large impedance contrast between ocean water and the sea floor and that no reflections occur above this interface, precluding seismic aliasing that may obscure additional detail. Unit II reflections are interpreted as a Plio-Pleistocene and younger deposits above an angular unconformity that separates it from Miocene and older seismic sequences Units III and IV (ANTOSTRAT, 1995). Unit II reflections are obscured in MCS profile IT89-AR34 standard amplitude section and the spectral decomposition image (Figures 1.2B and 1.2C). Unit III in profile PD90-21is interpreted as northward dipping forests within a prograding grounding zone wedge (GZW) of early to middle Miocene age (Anderson and Bartek, 1992; DeSantis et al., 1995). Standard amplitude profile IT89-AR34 (Figure 1.2C) displays Unit III as lower frequency, low-amplitude, sub-horizontal reflections extending nearly to the southern limit of the profile. The interpretation of Unit III from the MCS standard amplitude profile does not

correspond to the seismic characteristics imaged in nearby intermediate-resolution SCS profile PD90-21 (Figure 1.2A). Interpretation of profile IT89-AR34 standard amplitude image alone may lead to the incorrect interpretation that a thick package of sub-horizontal material exists below the sea floor and a failure to identify the seismic characteristics of Unit III properly. Spectral decomposition was helpful for enhancing shallow reflections (seismic units II & III) but shows little enhancement of deeper units IV and V. This may suggest that higher resolution imaging below the sea floor multiple may not be possible with this technique.

1.5. Conclusions

This work investigated the use of seismic attributes to enhance the resolution of legacy multi-channel seismic reflection data from the Antarctic margin and the implications of how these reinterpreted data sets may yield a more robust understanding of the evolution of the Antarctic Ice Sheets. Additionally, these techniques may be applied to a variety of modern or legacy 2D seismic data sets around the globe.

The results of this work show that spectral decomposition can increase the temporal resolution of MCS datasets and can resolve thin bedded stratigraphy and features that may be tuned when displayed as standard amplitude. Using a CWT spectral decomposition method, the highest temporal resolution enhancements occur in the upper 200-500 ms of the record, below which high-frequency signals are attenuated.

REFERENCES

Anderson, J.B., and Bartek, L.R., 1992. Cenozoic glacial history of the Ross Sea revealed by intermediate resolution seismic reflection data combined with drill site information, in The Antarctic Paleoenvironment: A perspective on global change. Antarctic Research Series, v. 56. edited by Kennett, J.P., and Warnke, D.A., AGU, Washington, D.C.

Anderson, J.B., Conway, H., Bart, P.J., Witus, A.E., Greenwood, S.L., McKay, R.M., Hall., B.L., Ackert, R.P., Licht, K., Jakobsson, M., and Stone, J.O., 2013. Ross Sea paleo-ice drainage and deglacial history during and since the LGM. Quaternary Science Review, v. 100, pp. 31-54.

ANTOSTRAT Project, 1995. Seismic Stratigraphic Atlas of the Ross Sea, Antarctica. *in*: Geology and Seismic Stratigraphy of the Antarctic Margin, v. 2. Editors, Cooper, A.K., Barker, P.F., and Brancolini, G., 1995. Antarctic Research Series. AGU, Washington D.C., v. 68. plates 1-22.

Barnes, A.E., 2000. Attributes for automated seismic facies analysis. 70th Annual International Meeting, SEG, Expanded Abstracts. pp. 553-556.

Barnes, A.E., 2001. Seismic attributes in your facies. Canadian Society of Exploration Geophysicists Recorder. v. 26. pp. 41-47.

Bart, P.J., 2004. West-directed flow of the West Antarctic Ice Sheet across Eastern Basin, Ross Sea during the Quaternary. Earth and Planetary Science Letters. v. 228, pp. 425-438.

Brancolini, et al., 1995. Descriptive text for the Seismic Stratigraphic Atlas of the Ross Sea. *in*: Geology and Seismic Stratigraphy of the Antarctic Margin, v. 2. Editors, Cooper, A.K., Barker, P.F., and Brancolini, G., 1995. Antarctic Research Series. AGU, Washington D.C., v. 68. p. 303.

Brown, A.R., 1996. Interpretation of three-dimensional seismic data, 4th ed. American Association of Petroleum Geologists Memoir 42.

Busetti, M., and Zayatz, I., and Ross Sea Regional Working Group, 1994. Distribution of seismic units in the Ross Sea. Terra Antarctica, v. 1, no. 2, pp. 345-348.

Chopra, S., and Marfurt, K.J., 2005. Seismic attributes – A historical perspective. Geophysics. v. 70, no. 5, pp. 3SO-28SO.

Cooper, A.K., Barrett, P.J., Hinz, K., Traube, V., Leitchenkov. G., and Stagg, H.M.J., 1991. Cenozoic prograding sequences of the Antarctic continental margin: a record of glacio-eustatic and tectonic events. Marine Geology, v. 102, pp. 175-213.

De Santis, L., Anderson, J.B., Brancolini, G., and Zayatz, I., 1995. Seismic record of Late Oligocene through Miocene glaciation on the central and eastern continental shelf of the Ross Sea. *in*: Geology and Seismic Stratigraphy of the Antarctic Margin, v. 2. Editors, Cooper, A.K., Barker, P.F., and Brancolini, G., 1995. Antarctic Research Series. AGU, Washington D.C., v. 68. pp. 235-260.

Hayes, D.E., and Frakes, L.A., 1975. Initial reports of the Deep Sea Drilling Project. v. 28, p. 1017. U.S. Government Printing Office, Washington D.C. pp. 211-278.

Hinz, K., and Block, M., 1984. Results of geophysical investigations in the Weddell Sea and in the Ross Sea, Antarctica. *in:* Proceedings of the 11th World Petroleum Congress, London. Wiley, New York. pp. 279-291

Houtz, R.E., and Meijer, R., 1970. Structure of the Ross Sea shelf from profiler data. Journal of Geophysical Research. v. 75, pp.6592-6597.

Houtz, R.E., and Davey, F.J., 1973. Seismic profiler and sonobouy measurements in the Ross Sea. Journal of Geophysical Research. v. 78, pp. 3448-3468.

Marfurt, K.J., Kirlin, R.L., and Farmer, S.L., Bahorich, M.S., 1998. 3-D seismic attributes using a semblance-based coherency algorithm. Geophysics. v. 63, no. 4, pp. 1150-1165.

Peyton, L., Bottjer, R., and Partyka, G., 1998. Interpretation of incised valleys using new 3-D seismic techniques: A case history using spectral decomposition and coherency. The Leading Edge. v. 17, pp. 1294-1298.

Taner, M.T., Schuelke, J.S., O'Doherty, R., an Baysal, E., 1994. Seismic attributes revisited. 64th Annual International Meeting, SEG, Expanded Abstracts, pp. 1104-1106.

White, R.E., 1991. Properties of instantaneous seismic attributes. The Leading Edge. v. 10, no. 7. p. 26-32. Discussion and reply in v.11, no. 8, p. 45-46. And v.11, no. 10, pp. 10-12.

CHAPTER 2: SEISMIC REFLECTION RECORD OF LATE OLIGOCENE TO EARLY MIOCENE THIRD-ORDER SEQUENCE STRATIGRAPHY IN EASTERN BASIN, ROSS SEA

2.1 Introduction

The late Oligocene to early Miocene glacial history of Antarctica, while poorly understood, is an important episode in the evolution of the West Antarctic Ice Sheet (WAIS). Far-field, stable isotope records (Abreu and Anderson, 1998; Lear et al., 2000; Zachos et al., 2001; Miller et al., 2005) indicate increased Antarctic ice volumes during the Oligocene; however, the contribution of the WAIS to the ice volume signal is poorly understood. More direct records from the margin and continent suggest variable timing of the presence of significant ice on West Antarctica from the Oligocene to Miocene (De Santis et al., 1999; Wilch and Mcintosh, 2000; Sorlien et al., 2007a; Gohl et al., 2013; Spiegel et al., 2016). More research is needed to resolve the conflicting interpretations of WAIS history. This study investigates the stratigraphic architecture and seismic reflection features and facies of late Oligocene to early Miocene strata in the Eastern Basin, Ross Sea that reveals information about multiple Oligocene glaciations along the margin of West Antarctica and the evolution of the WAIS.

The Ross Sea is a large embayment in Antarctica comprised of three primary basins separated by basement highs (Figure 2.1). The Eastern Basin, Ross Sea is bordered by basement highs, Central High to the west and Marie Byrd Land to the east. Within the eastern sector of the Eastern Basin, the Roosevelt Subbasin is bordered by the Roosevelt Ridge to the west and Marie Byrd Land to the east. The Eastern Basin and Roosevelt Subbasin contain thick sequences of Cenozoic strata that preserve a record of glacial erosion and deposition since at least the

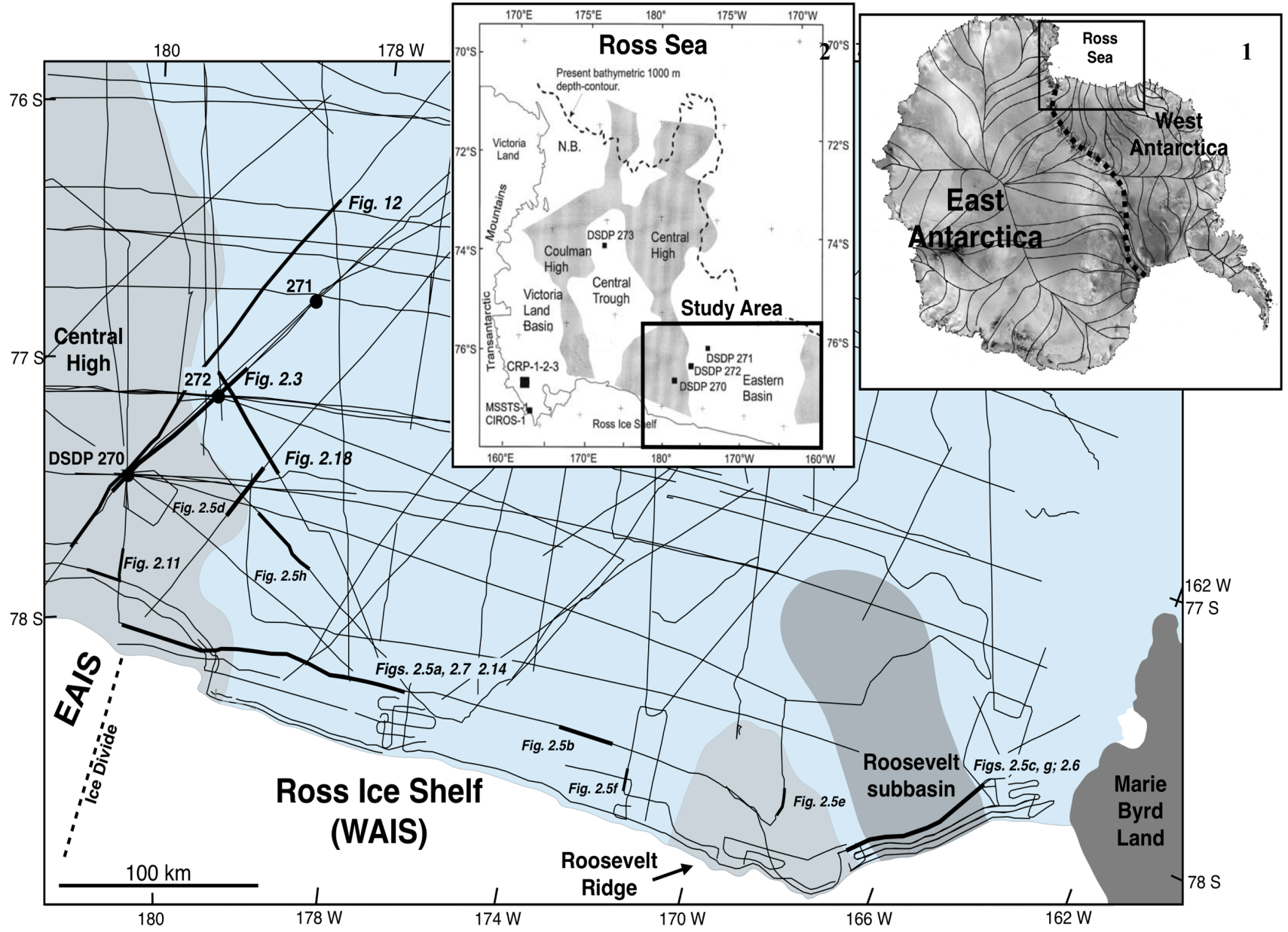
Ross Sea
2
Present bathymetric 1000 m depth-contour.
Victoria Land
N.B.
Mountains
Coulman High
DSDP 273
Central High
Central Trough
Victoria Land Basin
Transantarctic
Study Area
CRP-1-2-3
DSDP 271
DSDP 272
DSDP 270
Eastern Basin
MSSTS-1
CIROS-1
Ross Ice Shelf
Ross Sea
1
West Antarctica
East Antarctica
Fig. 12
271
Central High
272
Fig. 2.3
DSDP 270
Fig. 2.18
Fig. 2.5d
Fig. 2.11
Fig. 2.5h
Figs. 2.5a, 2.7 2.14
Fig. 2.5b
Fig. 2.5f
Fig. 2.5e
Roosevelt subbasin
Figs. 2.5c, g; 2.6
Marie Byrd Land
Roosevelt Ridge
EAIS
Ice Divide
Ross Ice Shelf (WAIS)
100 km
180
178 W
174 W
170 W
166 W
162 W
76 S
77 S
78 S

Figure 2.1. Location map of Eastern Basin, Ross Sea, Antarctica. showing ice divide (bold dashed back line) between East Antarctic Ice Sheet (EAIS) and West Antarctic Ice Sheet (WAIS), seismic tracks (thin black lines) and location of DSDP drilling sites marked with solid circles. Inset 1: boundary (bold dashed line) between East and West Antarctica and modern ice drainage of Antarctica (modified from Anderson et al., 2001). Inset 2: Ross Sea showing major basins, Deep Sea Drilling Project (DSDP), Cape Roberts Project (CRP), CIROS and MSSTS drill sites marked with solid squares (from Davey and DeSantis 2006).

Oligocene (Sorlien et al., 2007a). Over a third of the modern WAIS drains into the Ross Sea and likely has since the Neogene (Anderson and Shipp, 2001) which makes the Eastern Basin an important location to investigate the evolution of the WAIS.

Prior to recognition that the West Antarctic Rift system has been subsiding since 104 Ma (Luyendyk et al., 2001; Luyendyk et al., 2003), it was supposed that during the late Oligocene through early Miocene, ice in this region was comprised of several small ice caps atop islands of the West Antarctic archipelago (De Santis et al, 1995; Anderson and Shipp, 2001; DeConto and Pollard, 2003). However, recent modeling by Wilson and others (2012, 2013) suggest that the paleo-topography of West Antarctica was high enough to support a terrestrially based WAIS at the Eocene-Oligocene boundary that expanded in concert with the East Antarctic Ice Sheet. The timing of when the WAIS coalesced into an ice sheet large enough to impinge upon the continental shelf is uncertain. Controversial evidence from seismic reflection studies of Ross Sea suggest a grounded ice sheet in the western Ross Sea (Anderson and Bartek, 1992) and piedmont glaciers (De Santis, et al., 1995) were present on or near Central High as early as the late Oligocene and ice sheets advanced to the paleo-shelf edge by at least the middle Miocene (Barrett, 1996; Abreu and Anderson 1998; Bart 2004). The record of Oligocene ice advance and retreats in the Eastern Basin is poorly understood. The only direct sedimentological data from the Eastern Basin comes from DSDP Leg 28, drillcores from Sites 270, 271 and 272, which had poor recoveries (Hayes and Frakes, 1975). Due to limited sedimentologic data in the Eastern Basin, the seismic stratigraphic record may yield the most direct and complete records of late Oligocene through early Miocene glaciations.

Previous stratigraphic models of the Eastern basin have identified second-order sequences that were deposited over the course of 10 Myrs or more (Hinz and Block, 1984;

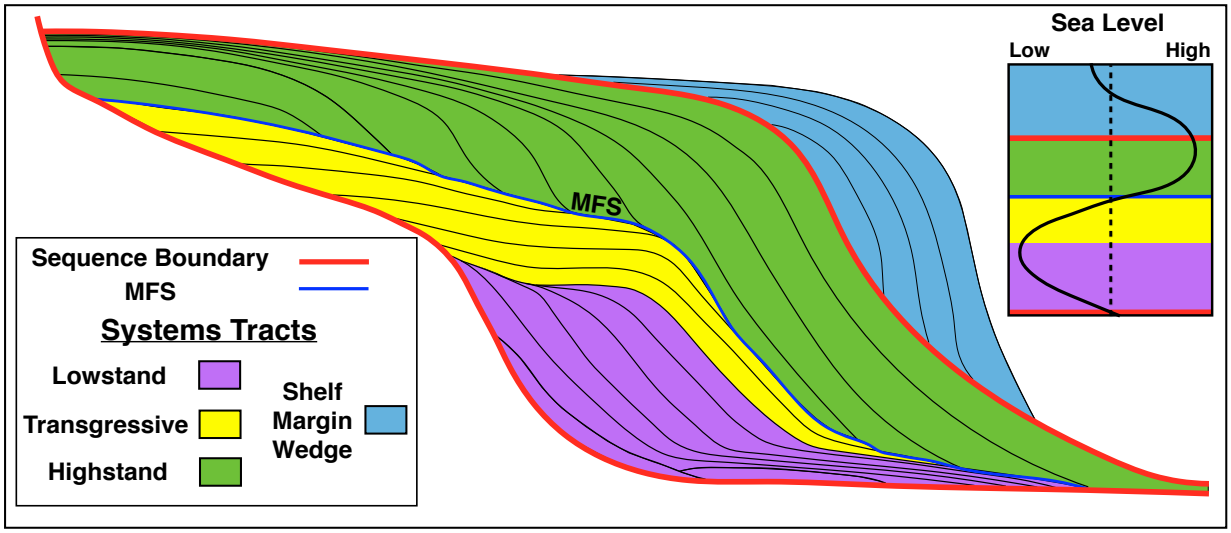

Figure 2.2. Sequence stratigraphic model adapted from Vail et al., (1977). Sequences are bounded by Sequence boundaries (bold red lines) that form during relative sea level falls. Within the lowstand systems tract (purple), strata onlaps the sequence boundary and thins basinward during relative sea level fall and just after the onset of relative sea level rise. Transgressive systems tract (yellow) is comprised of back-stepping strata that onlaps the sequence boundary with the rate of sea level rise exceeds the rate of sedimentation and is capped by a maximum flooding surface (**MFS** – blue line). The highstand systems tract (green) is comprised of prograding strata that is deposited as the rate of sea level rise falls below the rate of sedimentation. If sea level fall does not fall below the shelf break, a shelf margin wedge (light blue) is deposited.

ANTOSTRAT, 1995). To investigate higher frequency, third-order sequences (deposited over 0.5 Myrs to several Myrs) detailed correlation of higher resolution seismic data is required. Brazell (2017) describes a technique for enhancing low-resolution, multi-channel seismic data by spectral decomposition analysis. This technique, along with the recognition of seismic reflector staking patterns, was used to correlate sets of genetically related sequences that are arranged in distinctive patterns, or “composite sequences”.

Composite sequences stack into systems tracts, (lowstand, transgressive and highstand) that reflect changes in basin accommodation and relative sea level (Kerans and Kempter, 2002). A complete stratigraphic sequence contains a basal lowstand and transgressive systems tract,

TABLE 2.1: Seismic data

Seismic source (L)	Vertical resolution (m)	Penetration depth (s)	Cruise abbreviation
Air Gun 2.46	12	2.0	PD90[1]
Air Gun 23.45	30	6.0	BGR[2]
Air Gun 22.5	20-30	3.0-4.0	IT88[3], IT89[3], IT94[3]
Air Gun 10	60-70	6.0	SEV87[4], SEV89[4]
Air Gun 35.54	30	6.0	IFP[5]
Air Gun 9.2	30	6.0	TH82[6], TH92[6]
Air Gun 3.44	30	6.0	NBP9601[7]
Air Guns: 1.72; 6.88; 10.3; & 49.2	10-60	2.0-6.0	NBP0301[8], NBP0306[9]
Air Gun 0.8	10	2.0	NBP0802[10]

Table 2.1. Seismic data used for this study. [1] Rice University (USA) 1990; [2] Bundesanstalt für Geowissenchaften und Rohstoffe (Germany) 1980; [3] Osservatorio Geofisico Sperimentale di Trieste (Italy) 1988, 1989, 1994; [4] Joint Stock Company Marine Arctic Geological Expedition (Russia) 1987, 1989; [5] Institute Fançaise du Pétrole (France) 1982; [6] Japanese National Oil Company 1982, 1992; [7] University of Alabama (USA) 1990; [8] University of North Carolina at Chapel Hill (USA) 1996; [9] University of California at Santa Barbara (USA) 2003; [10] University of Southern California (USA) 2008.

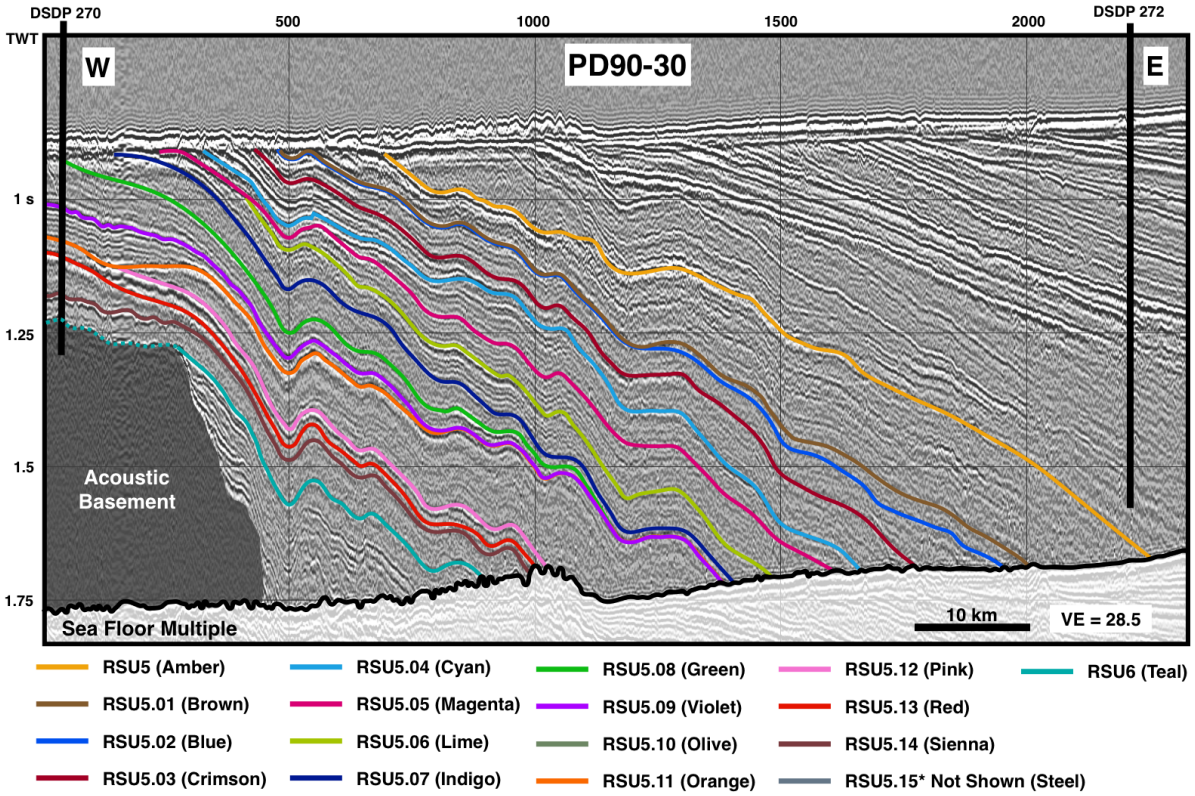

Figure 2.3. Dip-oriented, single channel seismic profile PD90-30 , RSS-2-EB horizons and locations of DSDP drillcore, Sites 270 and 272 (see Figure 2.1 for locations). Horizon colors are consistent across figures.

capped by a highstand systems tract and enveloped by sequence boundaries (Figure 2.2). The lowstand systems tract is deposited during a relative sea level fall and directly after the onset of relative sea level rise. The transgressive systems tract is deposited during the onset of coastal transgression and is capped by a maximum flooding surface that marks the most landward position of marine sediments and is associated with a period of reduced sedimentation. The highstand systems tract is deposited when the rate of sediment accumulation exceeds the rate of accommodation increase, resulting in a transition from back-stepping to aggradational and progradational stacking patterns.

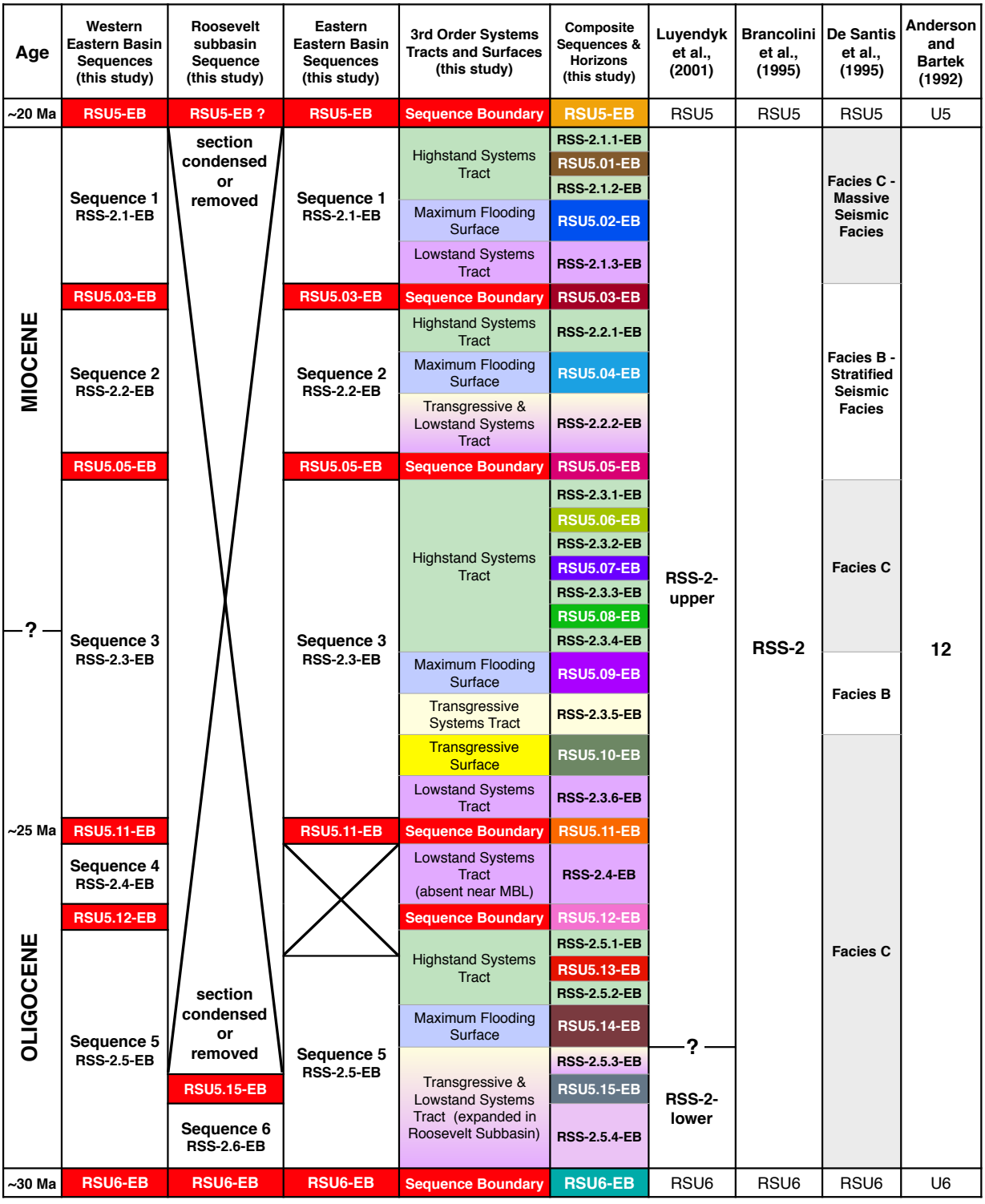
Age
Western Eastern Basin Sequences (this study)
Roosevelt subbasin Sequence (this study)
Eastern Eastern Basin Sequences (this study)
3rd Order Systems Tracts and Surfaces (this study)
Composite Sequences & Horizons (this study)
Luyendyk et al., (2001)
Brancolini et al., (1995)
De Santis et al., (1995)
Anderson and Bartek (1992)
~20 Ma
RSU5-EB
RSU5-EB ?
RSU5-EB
Sequence Boundary
RSU5-EB
RSU5
RSU5
RSU5
U5
MIOCENE
Sequence 1
RSS-2.1-EB
section condensed or removed
Sequence 1
RSS-2.1-EB
Highstand Systems Tract
RSS-2.1.1-EB
RSU5.01-EB
RSS-2.1.2-EB
Maximum Flooding Surface
RSU5.02-EB
Lowstand Systems Tract
RSS-2.1.3-EB
Facies C - Massive Seismic Facies
RSU5.03-EB
RSU5.03-EB
Sequence Boundary
RSU5.03-EB
Sequence 2
RSS-2.2-EB
Sequence 2
RSS-2.2-EB
Highstand Systems Tract
RSS-2.2.1-EB
Maximum Flooding Surface
RSU5.04-EB
Transgressive & Lowstand Systems Tract
RSS-2.2.2-EB
Facies B - Stratified Seismic Facies
RSU5.05-EB
RSU5.05-EB
Sequence Boundary
RSU5.05-EB
?
Sequence 3
RSS-2.3-EB
Sequence 3
RSS-2.3-EB
Highstand Systems Tract
RSS-2.3.1-EB
RSU5.06-EB
RSS-2.3.2-EB
RSU5.07-EB
RSS-2.3.3-EB
RSU5.08-EB
RSS-2.3.4-EB
RSS-2-upper
RSS-2
Facies C
12
Maximum Flooding Surface
RSU5.09-EB
Facies B
Transgressive Systems Tract
RSS-2.3.5-EB
Transgressive Surface
RSU5.10-EB
Lowstand Systems Tract
RSS-2.3.6-EB
~25 Ma
RSU5.11-EB
RSU5.11-EB
Sequence Boundary
RSU5.11-EB
Sequence 4
RSS-2.4-EB
Lowstand Systems Tract (absent near MBL)
RSS-2.4-EB
Facies C
RSU5.12-EB
Sequence Boundary
RSU5.12-EB
OLIGOCENE
Highstand Systems Tract
RSS-2.5.1-EB
RSU5.13-EB
RSS-2.5.2-EB
Sequence 5
RSS-2.5-EB
section condensed or removed
Sequence 5
RSS-2.5-EB
Maximum Flooding Surface
RSU5.14-EB
?
RSU5.15-EB
Transgressive & Lowstand Systems Tract (expanded in Roosevelt Subbasin)
RSS-2.5.3-EB
RSU5.15-EB
RSS-2-lower
Sequence 6
RSS-2.6-EB
RSS-2.5.4-EB
~30 Ma
RSU6-EB
RSU6-EB
RSU6-EB
Sequence Boundary
RSU6-EB
RSU6
RSU6
RSU6
U6

Figure 2.4. Summary of third-order sequence stratigraphic units in the Eastern Basin, Ross Sea (including the western sector [column 2], Roosevelt Subbasin [column 3] and eastern sector [column 4]) and interpretations of correlations from published units. Column 1, chronostratigraphic correlations from DSDP Site 270 (Leckie and Webb, 1983). Column 2, Third-order sequences and boundaries from this study. Column 5, systems tracts and major surfaces. Column 6, composite sequences and surface from this study. Horizon colors are used to identify horizons on seismic lines. Column 7, late Oligocene to early Miocene units interpreted from Luyendyk et al., 2001. Column 8, interpretation of late Oligocene to early Miocene sequence from Brancolini et al., 1995. Column 9, seismic facies interpreted within RSS-2 from De Santis et al., 1995. Column 10, late Oligocene to early Miocene sequences interpreted by Bartek et al., 1992.

2.2. Methods

The data sets used for this study consist of intermediate- and low-resolution multichannel seismic reflection data (MCS), and higher resolution single channel seismic reflection data (SCS) from Eastern Basin, Ross Sea, Antarctica (Table 2.1) and facies, lithologic and biostratigraphic descriptions and synthetic seismograms from DSDP Leg 28 drill Site 270 (Hayes and Frakes, 1975; Balshaw-Biddle, 1981; and Leckie and Webb, 1986; ANTOSTRAT, 1995).

This study focuses on late Oligocene through early Miocene strata, Ross Sea Sequence – 2 (RSS-2), as defined by ANTOSTRAT (1995), (referred to here as RSS-2-EB) based on correlation to DSDP Leg 28, Site 270 (Figure 2.3). I compare multi-resolution seismic reflection data sets collected in Eastern Basin over nearly four decades and use spectral analysis techniques to enhance the resolution of portions of the seismic data. This study builds upon previous seismic stratigraphic interpretations (Hinz and Block, 1984; Cooper et al., 1991; Anderson and Bartek, 1992; Busetti and Zayatz, 1994; Brancolini et al., 1995; De Santis et al., 1995; Luyendyk et al., 2001; Sorlien et al., 2007b). I develop a detailed stratigraphic model for RSS-2-EB by interpreting higher frequency horizons and correlating them to Site 270, which penetrates the lower section of RSS-2-EB (Figures 2.3, 2.4). I identified and mapped various seismic facies and

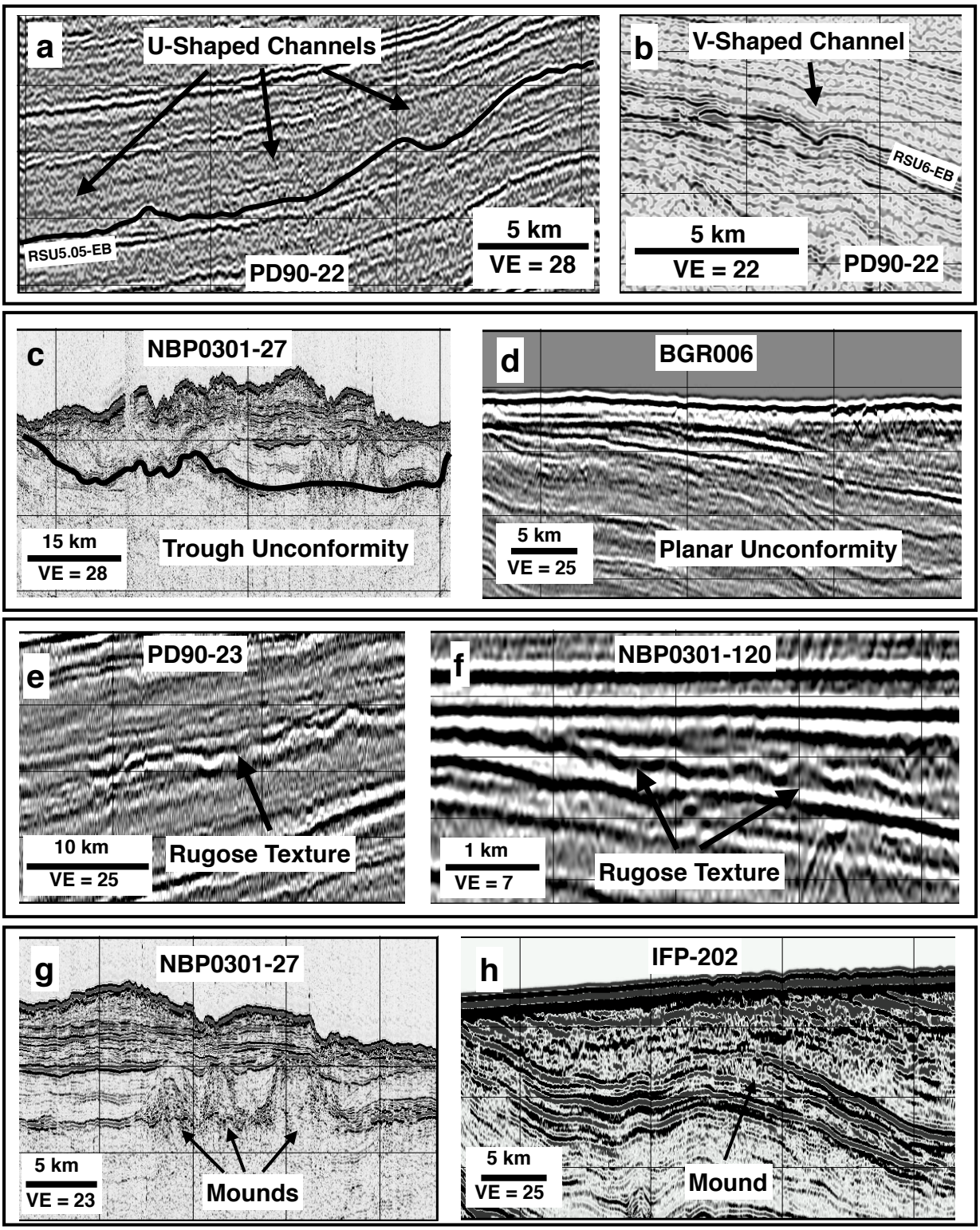

Figure 2.5. Examples of seismic features identified within RSS-2-EB (see Figure 2.1 for locations). **a**) U-shaped channel, **b**) V-shaped channels, **c**) trough shaped unconformities, **d**) planar unconformities, **e**) long wavelength rugose texture, **f**) short wavelength rugose texture, **g**) tall, narrow mounds, **h**) broad mounds.

features within RSS-2 which I interpret as glaciogenic features associated with each horizon including: glacial erosion surfaces, glacial mounds (e.g. moraines and grounding zone wedges) and channels and placed them within a context of subglacial, ice-proximal or ice-distal paleoenvironments.

I interpret stratal stacking patterns from seismic profiles using the Posamentier and Allen (1999) nomenclature and identified multiple third-order sequences separated by time-transgressive sequence boundaries created during the fall of relative sea level. Facies models developed from drill cores from the Ross Sea were used to calibrate the interpreted systems tracts to allow predictions regarding lateral and vertical succession of facies within Eastern Basin where direct sedimentological evidence is absent.

Seismic velocities of 2100 m/s at the sea floor was used for RSS-2-EB strata (Davey et al., 1982) and a 1D linear velocity gradient:

$$Z = (e^{0.4t} - 1) \times \frac{2100}{0.8}$$

2.3. Description of Seismic Features

2.3.1 Erosional Features

Erosional features are identified as seismic surfaces that truncate reflectors below them. U- and V-shaped channels are present throughout the basin, generally along the flanks of basement highs and near the modern ice shelf edge. Widths of channels range from 1 – 6 km with depths ranging from 10 – 50 m (Figure 2.5a, 2.5b). Three types of unconformities are recognized: broad trough, planar angular and rugose textured unconformities (Figure 2.5c, 2.5d, 2.5e, 2.5f). The dimensions of broad trough and planar unconformities range from several kilometers to 10s of km wide and 10s of m deep (Figure 2.c; 2.5d; Sorlien et al, 2007a). Large

distances (up to 50 km) between in seismic reflection profiles limited our ability to quantify these feature's 3D morphologies precisely.

2.3.2 Depositional Features

Mound-shaped depositional features on 2D seismic profiles (possible ridges in 3D) were recognized by their positive relief and internal seismic character (Figure 2.5g, 2.5h). Dimensions of identified mounds range from 3 to several 10s of km in width and 30 to 250 m in height. The internal seismic character of the mounds ranges from internally stratified to chaotic/transparent.

2.3.3 Rugose Textured Features

Rugose textures appear as corrugated seismic reflectors that do not clearly truncate reflectors below and do not have a distinct internal seismic character. Rugose textured horizons have wavelengths between 0.25 – 2 km and amplitudes of 10 – 50 m (Figure 2.5e, 2.5f). Rugose reflectors often appear on multiple closely-spaced seismic profiles, downdip of broad trough and updip of U- and V-shaped erosional features and mounded depositional features. Rugose textured unconformities are shallow and extend for 100s of meters laterally (Figure 2.5e, 2.5f). Rugose reflectors of similar dimensions identified along the modern sea floor of the Ross Sea are interpreted as ice-contact and/or ice-proximal features (Spagnolo et al., 2014).

2.4. Description of Seismic Sequences and Horizons

This study details the seismic sequence stratigraphy of RSS-2 (after ANTOSTRAT, 1995) in the Eastern Basin (referred to here as RSS-2-EB, Figure 2.4). RSS-2-EB is enveloped by regional unconformities, RSU6-EB, (~30 Ma) at its base and RSU5-EB (ca. ~20 Ma) above. Sixteen composite sequences and a minimum of six third-order sequences (Figure 2.4) have been

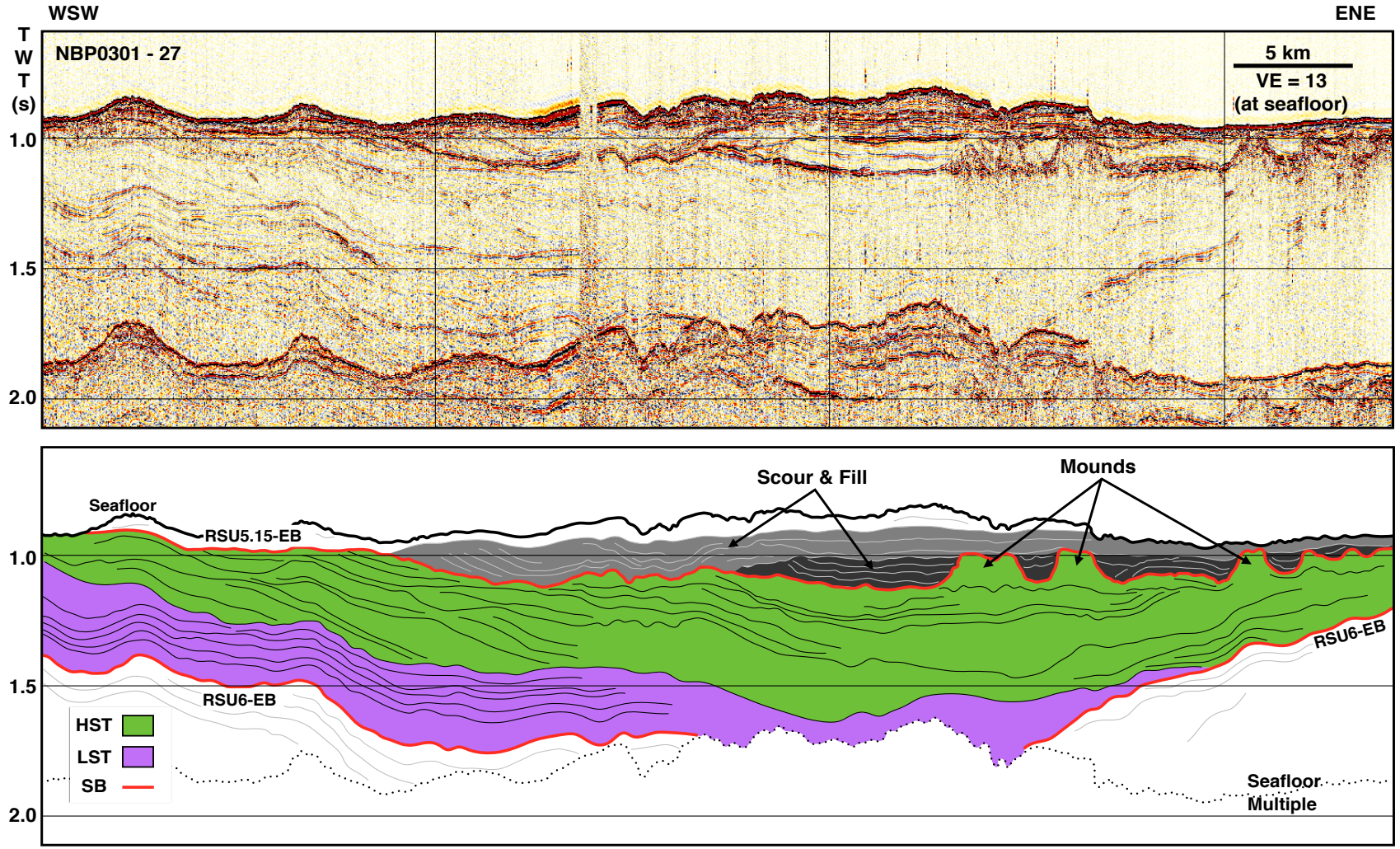

Figure 2.6. Strike-oriented single channel seismic profile NBP0301-27A (see Figure 2.1 for location). Standard amplitude above and interpreted profile below. Sequence 6, bounded by horizons RSU6-EB and RSU5.15-EB, is show with interpreted systems tracts: lowstand systems tract (**LST**) in purple, overlain by green highstand systems tract (**HST**) that shows basinward progradation Flat topped mounds within erosional troughs on RSU5.15-EB are interpreted as moraines (Sorlien et al., 2007. Scour and fill sections are highlighted in grey.

identified within RSS-2-EB that record fluctuations of RSL within Eastern Basin during the late Oligocene through early Miocene.

2.4.1 Sequence 6 (RSS-2.6-EB): Roosevelt subbasin

Sequence 6 (RSS-2.6-EB) exists as a local, expanded sequence within the Roosevelt subbasin and is enveloped by a regionally extensive lower horizon correlated to RSU6-EB, and an upper horizon correlated to RSU5.15-EB (Figure 2.4). Previous work by Sorlien and others (2007b) also correlates the section identified in Roosevelt subbasin to lower RSS-2-EB. RSU6-EB is a regionally extensive, high amplitude, continuous reflector that onlaps basement highs, is a downlap surface for overlying reflectors and occurs above syn-rift reflectors that fill extensional basins within Ross Sea. Age constraints for RSU6-EB are poor because it is uncertain whether it was sampled at DSDP Site 270 (Figure 2.3). RSU6-EB has a putative age of ~30 Ma (ANTOSTRAT, 1995; Levy et al., 2012) based on correlations to a large eustatic sea level fall at 30 Ma formerly proposed by Haq and others (1987). Upper horizon, RSU5.15-EB, cannot be definitively correlated to the base of Site 270, therefore, no age for the horizon has been interpreted. RSU5.15-EB, is an erosional unconformity at the top of sequence 6 onto which flat-topped mounds (possible ridges in 3D) that have a stratified to chaotic internal seismic character are deposited (Figure 2.6). Outside of the Roosevelt subbasin, on the flanks of Central High and the Marie Byrd Land margin, RSU5.15-EB appears as a conformable horizon and above a thin (< 100 m), seismically transparent section above RSU6-EB.

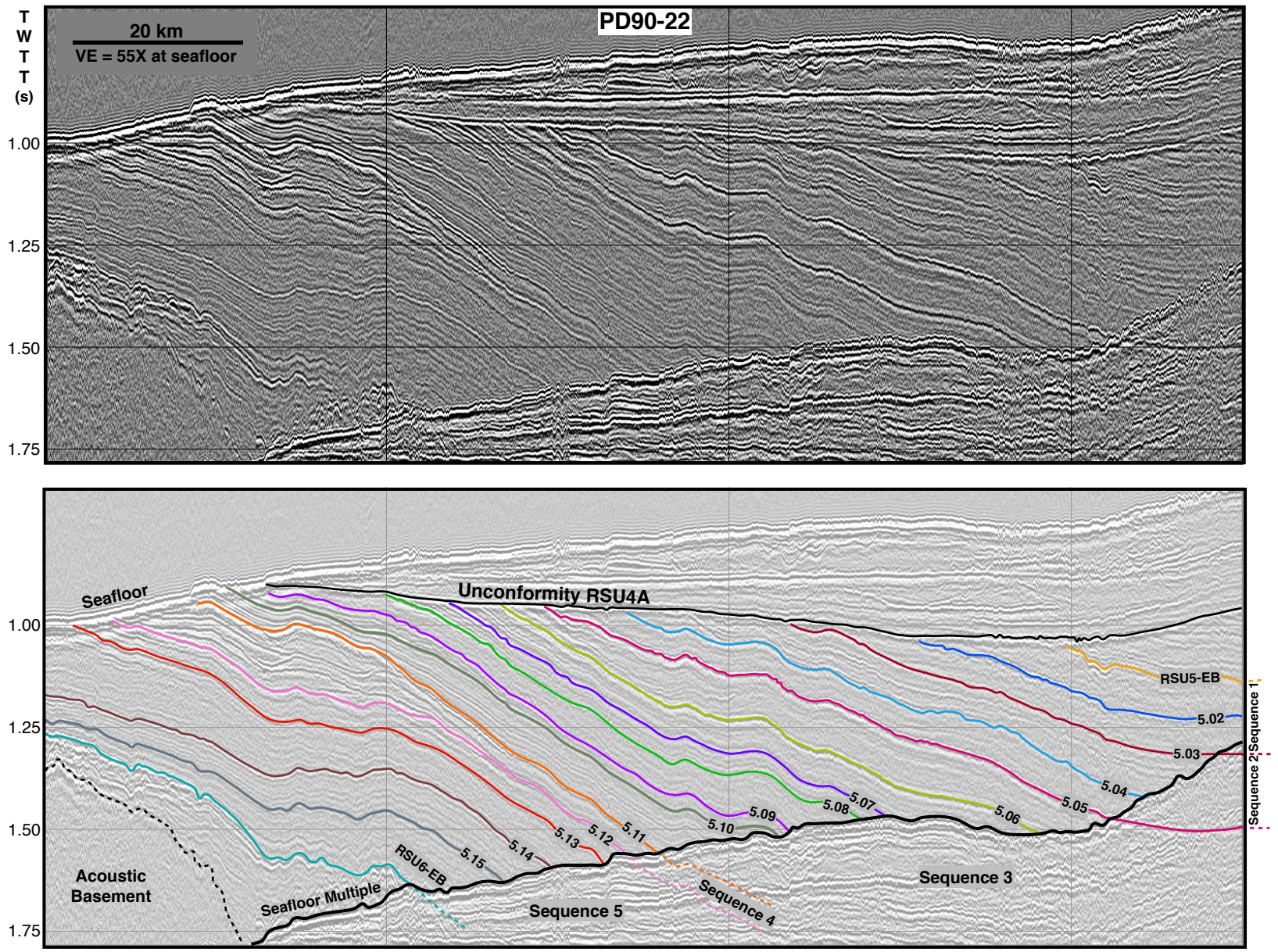
PD90-22
20 km
VE = 55X at seafloor
TWTT (s)
1.00
1.25
1.50
1.75
Seafloor
Unconformity RSU4A
RSU5-EB
5.02
5.03
5.04
5.05
5.06
5.07
5.08
5.09
5.10
5.11
5.12
5.13
5.14
5.15
RSU6-EB
Seafloor Multiple
Acoustic Basement
Sequence 5
Sequence 4
Sequence 3
Sequence 2
Sequence 1

Figure 2.7. Seismic reflection profile of SCS PD90-22 and line drawing of regional horizons and sequences within RSS-2-EB (see Figure 2.1 for location). Middle Miocene unconformity, RSU4A, truncates horizons RSU5.08-EB and younger. Horizons RSU5.09-EB and older outcrop at the modern sea floor. Horizon RSU5.01-EB is not present in this section.

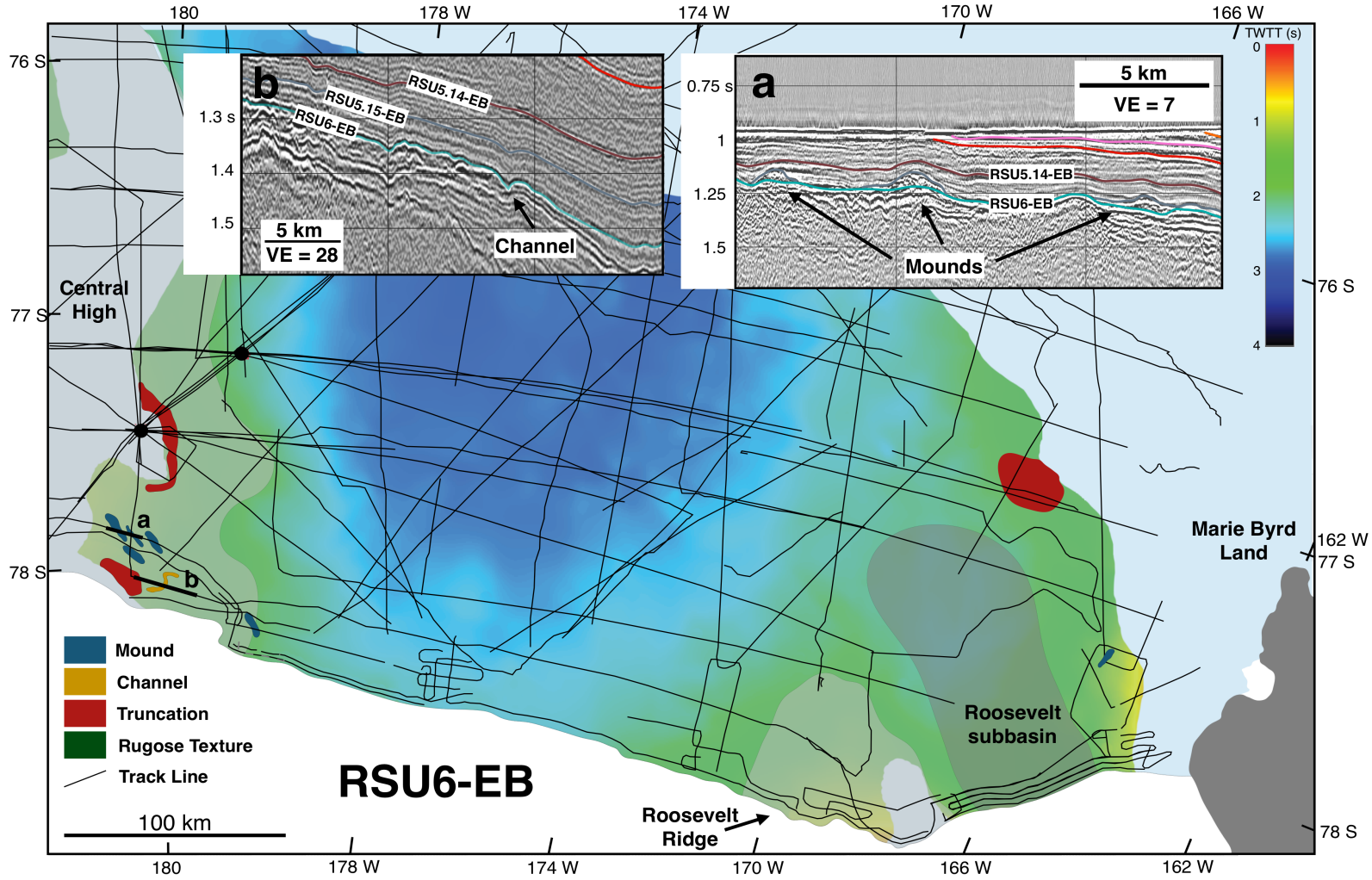

Figure 2.8. Time-depth structure map of horizon RSU6-EB with mounds, channels and erosional truncation interpreted from seismic date. Inset **a**) seismic profile NBP0301-13A showing horizons, RSU6-EB (teal), RSU5.15-EB (steel), RSU5.14 (sienna), RSU5.13 (red), RSU5.12 (pink) and RSU5.11 (orange) and mounds above RSU6-EB and below RSU5.15-EB. Inset **b**) seismic profile PD90-22 showing horizons RSU6-EB (teal), RSU5.15-EB (steel), RSU5.14 (sienna) and RSU5.13 (red), and V-shaped channel along RSU6-EB.

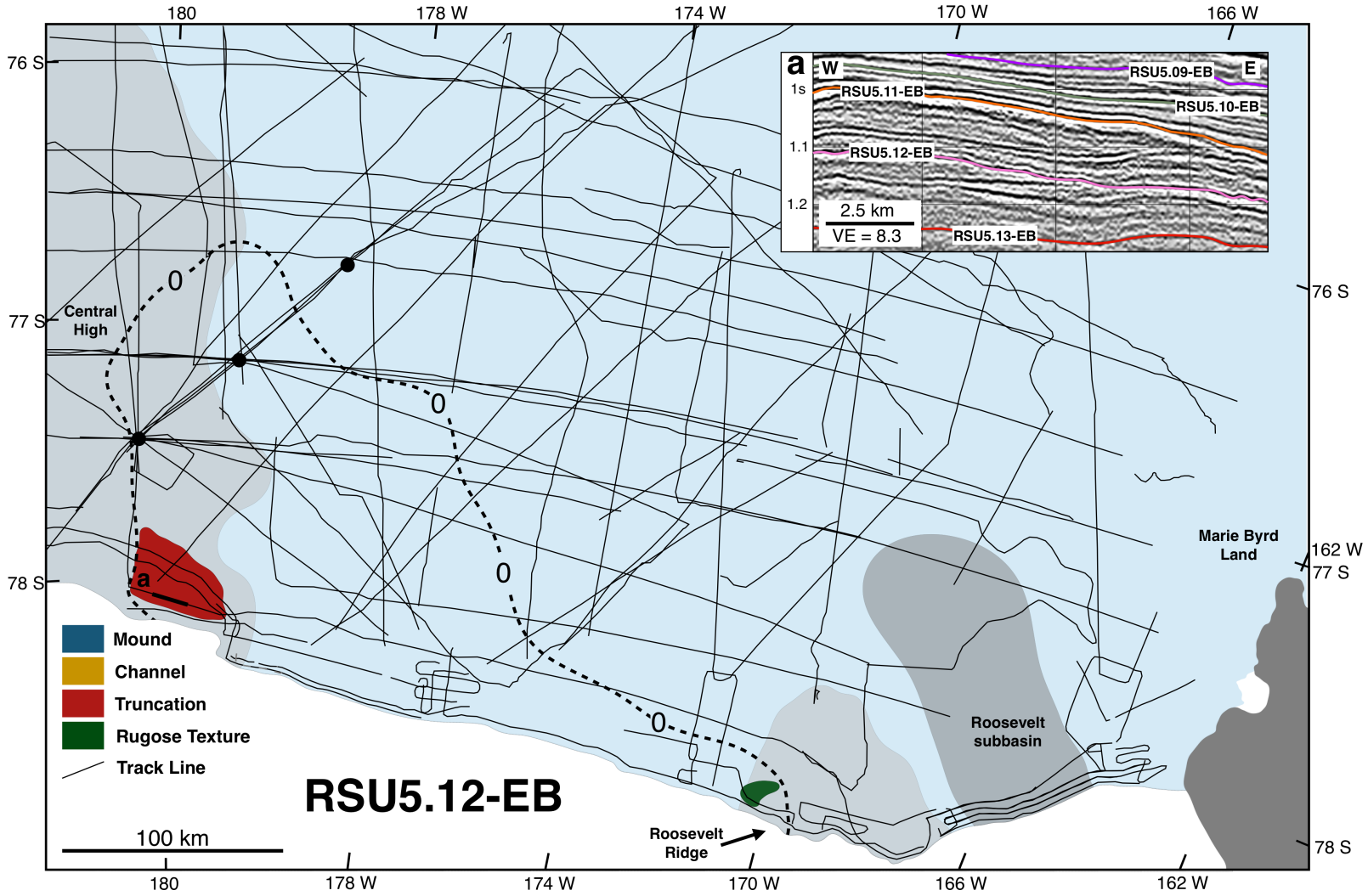

Figure 2.9. Feature map of horizon RSU5.12-EB showing location of erosional truncation, rugose texture and RSS-2.4.1-EB 0-thickness line (bold dashed line) interpreted from seismic date. Inset **a**) seismic profile PD90-22 showing horizons RSU5.13 (red), RSU5.12 (pink) and RSU5.11 (orange) RSU5.10 (olive) and RSU5.09 (violet). Stacked and cross cutting unconformities occur between horizons RSU5.12-EB and RSU5.11-EB.

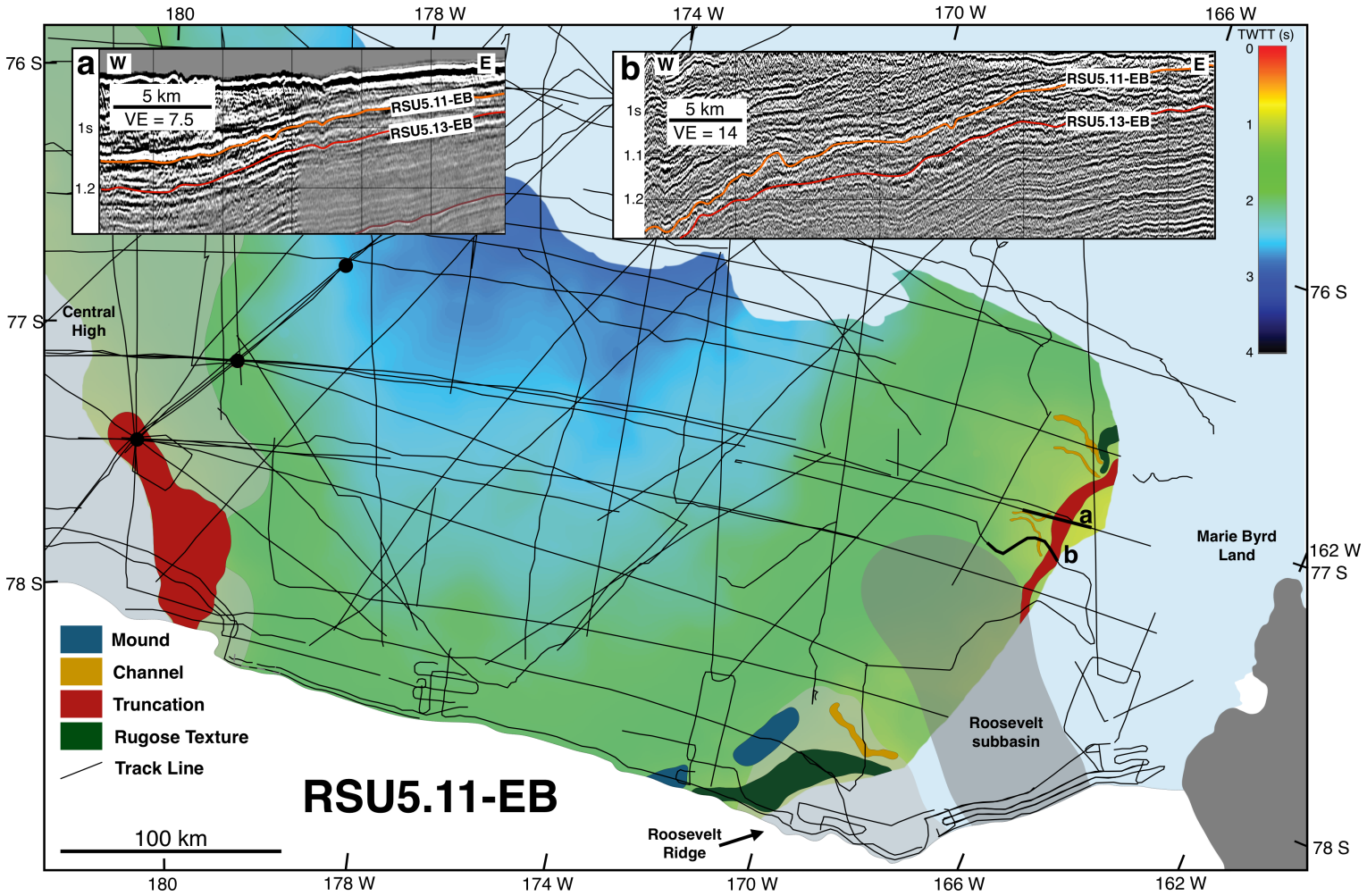

Figure 2.10. Time-depth structure map of horizon RSU5.11-EB, a regional unconformity and sequence boundary. Mounds, channels, rugose textures and erosional truncation interpreted from seismic date. Inset **a**) single channel seismic profile NBP9601L082A showing horizons, RSU5.14-EB (sienna), RSU5.13-EB (red) and RSU5.11-EB (orange). RSU5.11 (orange) has truncated RSS-2.4.1. A small channel can been see on horizon RSU5.11 and is interpreted as a pro-glacial meltwater channel. Inset **b**) single channel seismic profile NBP0802-4B showing horizons RSU5.13-EB (red) and RSU5.11-EB (orange). Erosional truncation, U-shaped channel, and a mound can be seen on this seismic profile.

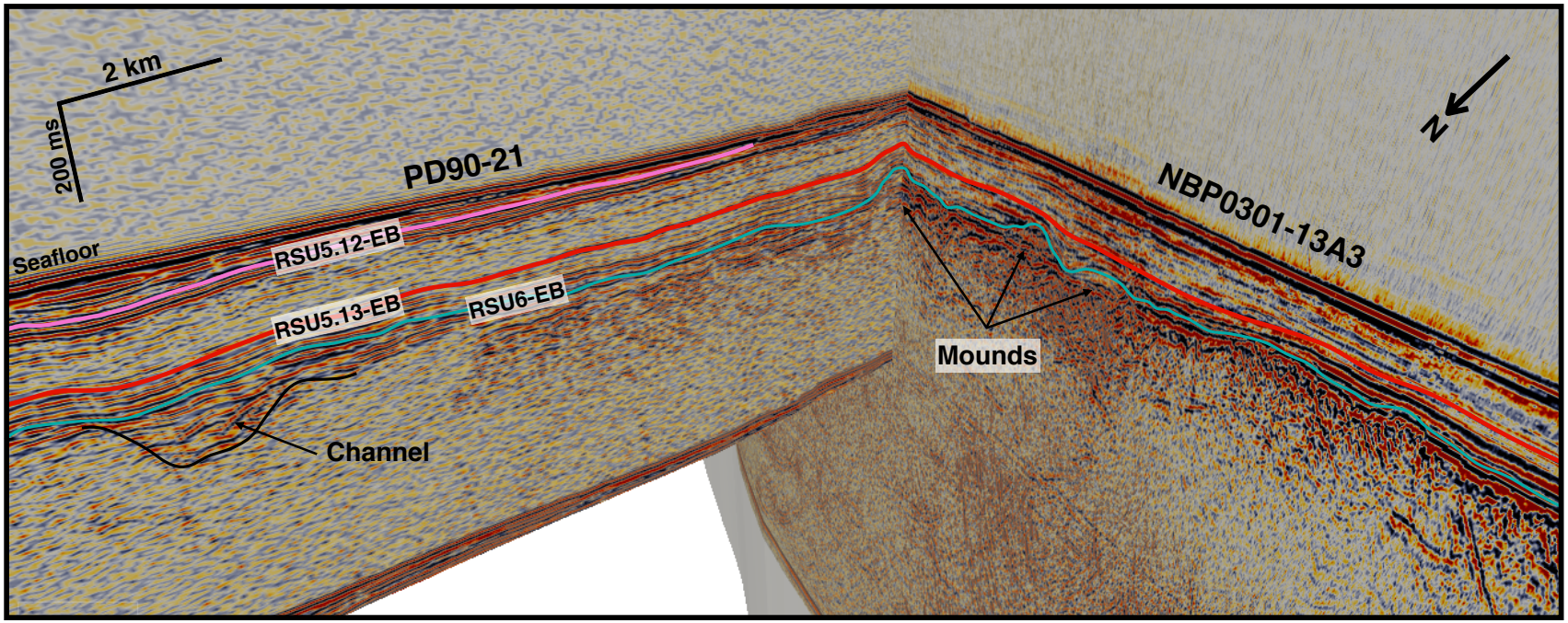

Figure 2.11. Fence diagram of seismic profiles PD90-21 and NBP0301-13A3 on the eastern flank of Central High (see Figure 2.1 for location) looking to the southeast. U-shaped channel carved into acoustic basement, below RSU6-EB is highlighted on seismic profile PD90-21. RSS-2-EB horizons RSU6-EB (teal), RSU5.13-EB (red) and RSU5.12-EB (pink) are highlighted with much up upper RSS-2-EB section removed by erosion. Internally stratified, asymmetric mounds are located on horizon RSU6-EB. The intersection of profiles PD90-21 and NBP0301-13A3 reveal that these mounds are not elongated in 3D. These mound features exceed 100 in height and are interpreted as drumlins deposited by piedmont glaciers flowing from a subaerial Central High.

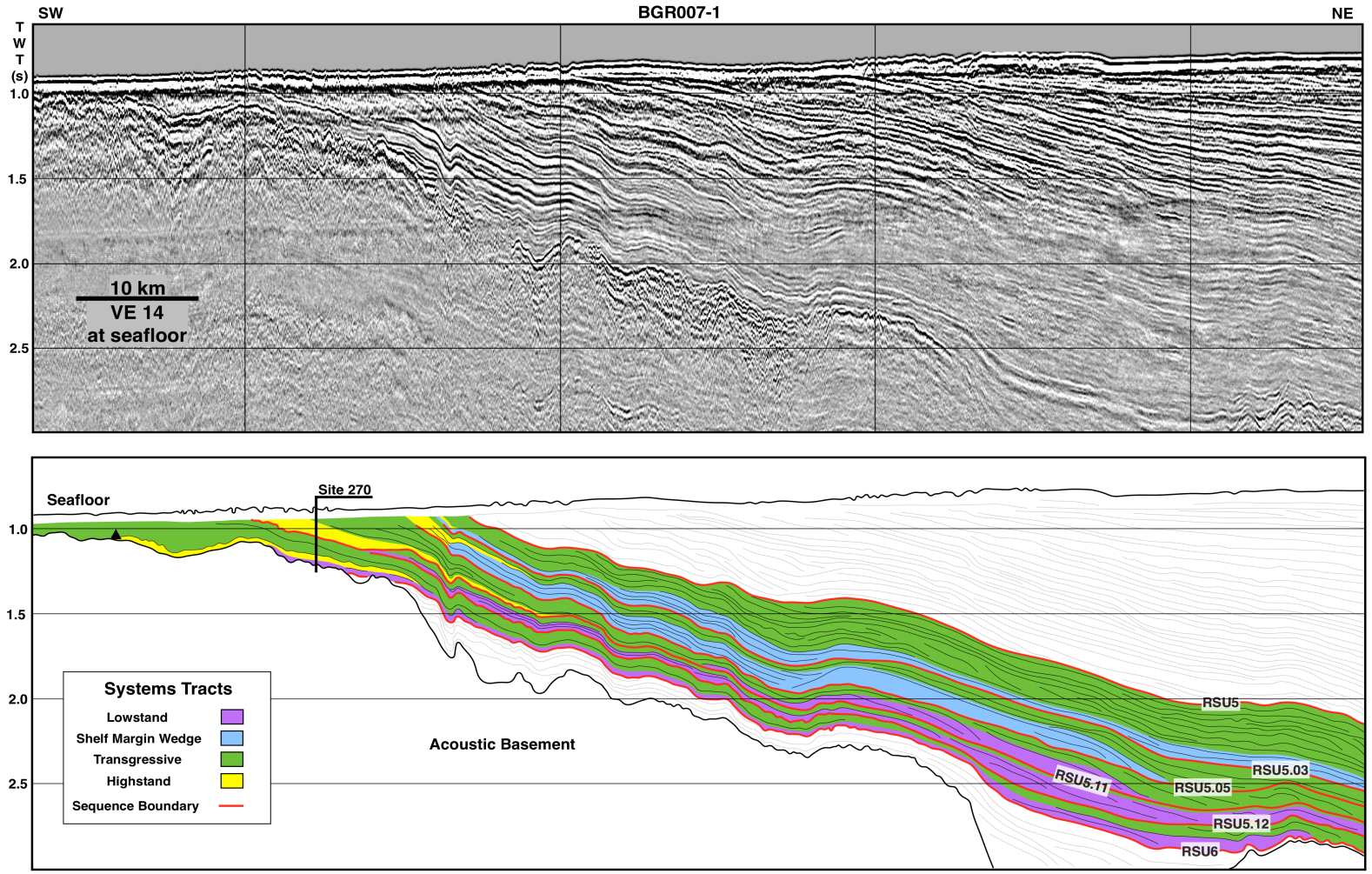

Figure 2.12. Seismic profile BGR007-1 in the western sector of Eastern Basin (see Figure 2.1 for location), interpreted above and line drawing interpretation below. Sequence boundaries (red lines) are labeled (refer to Figure 2.4). Up-dip portions of RSS-2-EB have been removed by erosion. There is a change in stacking pattern character from lowstand systems tracts (purple) being deposited above sequence boundaries to shelf margin wedges (light blue). This suggests that relative sea level falls during lower RSS-2-EB deposition were falling below the shelf break and after RSU5.05-EB time, relative sea level falls were lower magnitude and did not fall below the shelf break.

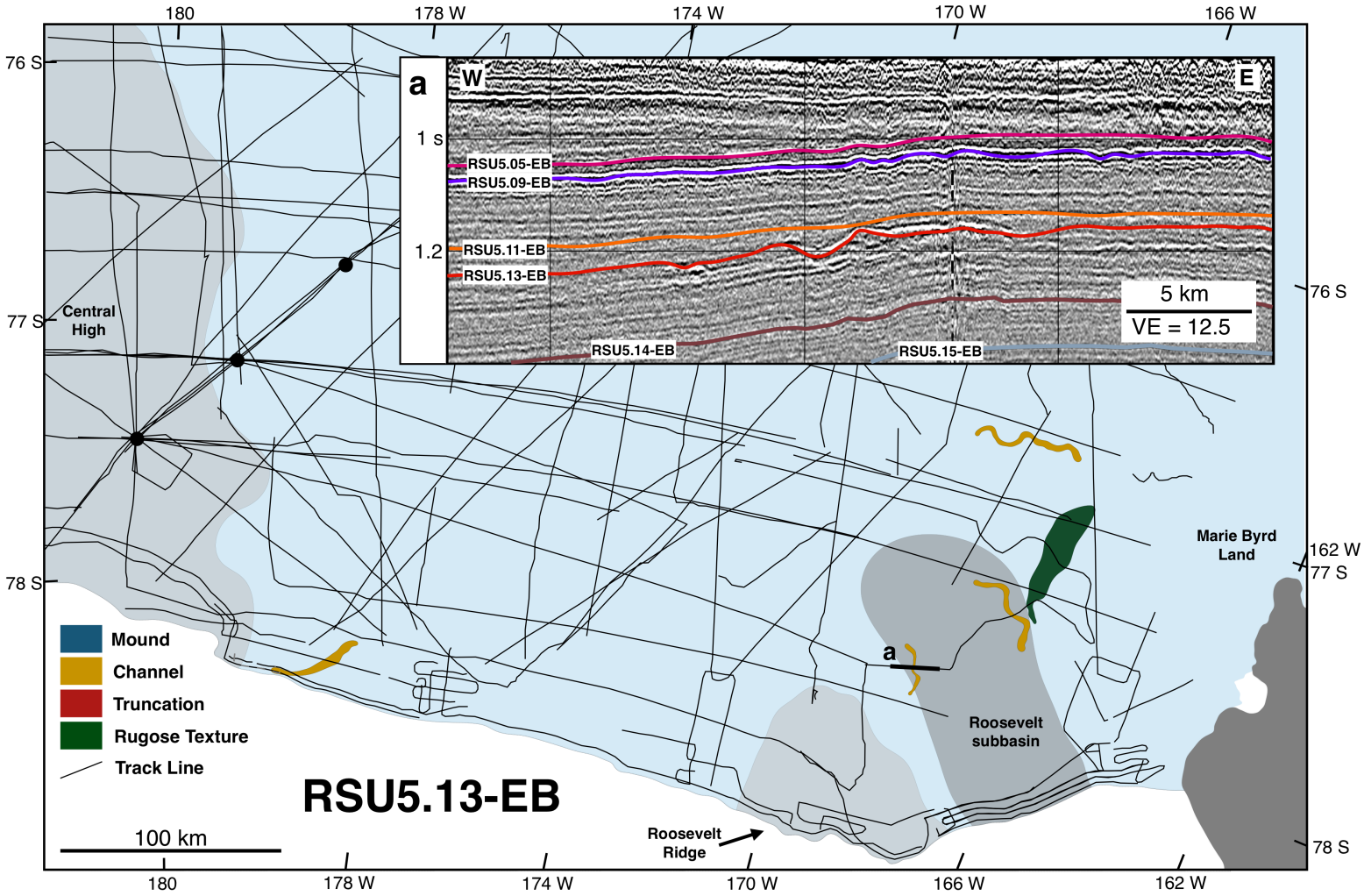

Figure 2.13. Feature map of horizon RSU5.13-EB showing location of channels and rugose texture interpreted from seismic date. **a**) seismic profile NBP0802-5A showing horizons RSU5.15-EB (steel), RSU5.14-EB (sienna), RSU5.13-EB (red), RSU5.11-EB (orange), RSU5.09-EB (violet) and RSU5.05-EB (magenta). Channels are interpreted in RSU5.13-EB (red) as sediment bypass channels.

2.4.2 Sequence 5 (RSS-2.5-EB)

Sequence 5 is enveloped by lower horizon RSU6-EB and upper horizon RSU5.12-EB (Figures 2.4, 2.7). RSU6-EB is a regionally extensive, high-amplitude, continuous reflector that onlaps basement highs and is a downlap surface for overlying reflectors. RSU6-EB is a planar unconformity that truncates older strata along the eastern flank of Central High (Figures 2.7, 2.8). RSU5.12-EB is a broad, sub-planar erosional unconformity where it is present in the southwestern sector of Eastern Basin (Figure 2.9). Horizon RSU5.12-EB displays rugose textured seismic characteristics along the western flank of Roosevelt Ridge and is truncated by horizon RSU5.11-EB in the eastern sector of Eastern Basin (Figure 2.10). Along RSU6-EB, near the eastern flank of Central High, internally stratified mounds in 3D, 100 – 130 m high are identified (Figure 2.11). Whether RSU6-EB drapes preexisting mounds or they are coeval is uncertain.

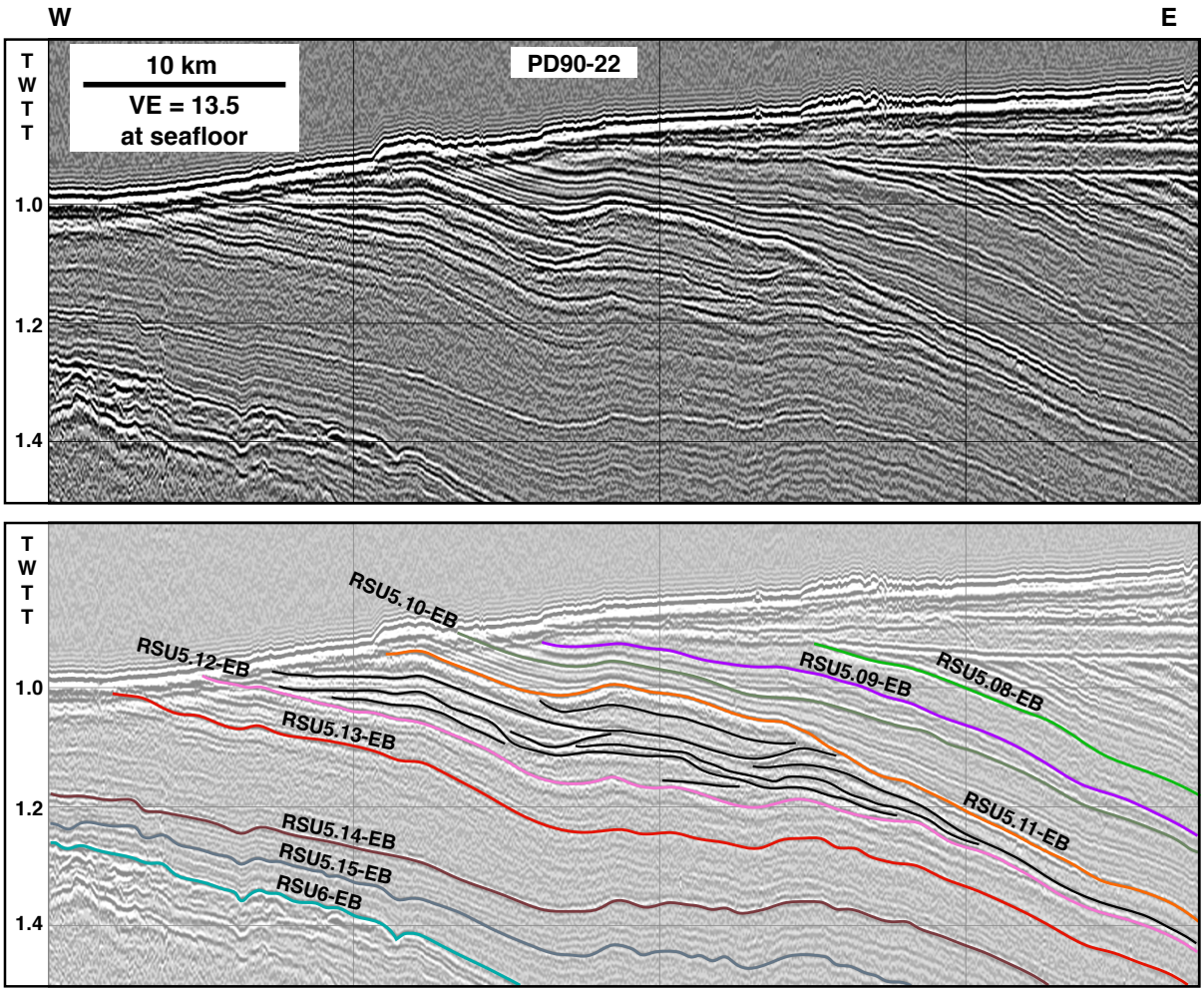

Figure 2.14. Seismic profile PD90-22 (see Figure 2.1 for location) showing multiple stacked unconformities (black lines) of Sequence 4 (refer to Figure 2.4). The section of stacked unconformities is interpreted to represent a series of high-frequency ice advances and retreats into the Eastern Basin correlated to ~25 Ma and associated with stacked unconformities from the western Ross Sea at drill core CRP (Figure 2.1, inset 2).

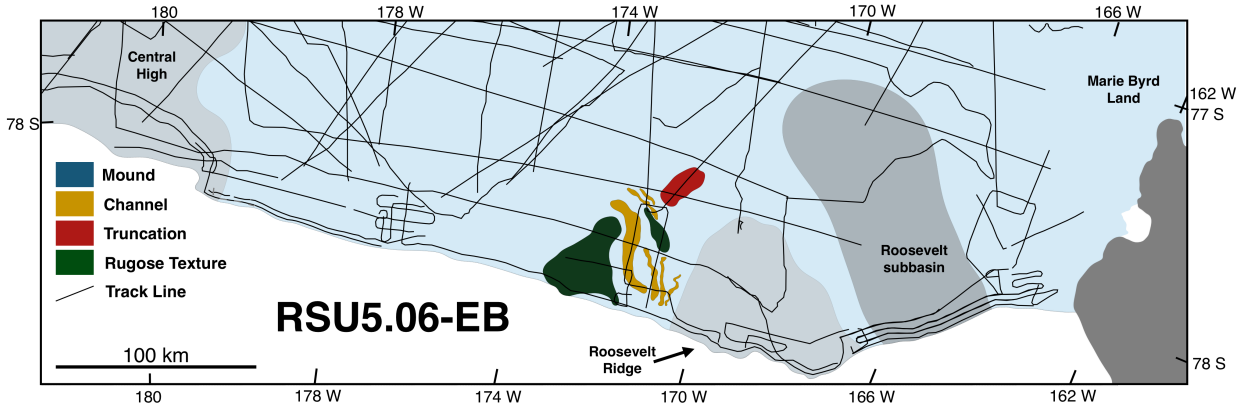

Figure 2.15. Feature map of horizon RSU5.06-EB showing the location of Rugose reflectors, channels and truncation. Horizon RSU5.06-EB is a horizon within Sequence 3 highstand systems tract. The features identified along RSU5.06-EB corresponds to interglacial conditions and therefore are not interpreted as glaciogenic in origin.

2.4.3 Sequence 4 (RSS-2.4-EB)

Sequence 4 is bounded by horizons RSU5.12-EB below and RSU5.11-EB above (Figure 2.4). Sequence 4 has limited preservation in the southwestern sector of Eastern Basin, near Central High with a maximum thickness of <150 m (Figure 2.14). Sequence 4 is comprised of multiple, stacked high-amplitude cross-cutting and truncating reflectors. These unconformities are broad, trough shaped and occur along approximately 100km section of southwestern Eastern Basin, on the flanks of Central High (2.14). General seismic reflection character between stacked unconformities is low- to moderate-amplitude weakly stratified and reflectors downlap onto horizon RSU5.12-EB or are truncated by horizon RSU5.11-EB (Figure 2.14). Horizon RSU5.11-EB is a regionally extensive, high-amplitude horizon that is correlated to DSDP Site 270 and has a preliminary age of ~25 Ma (Levy et al., 2012).

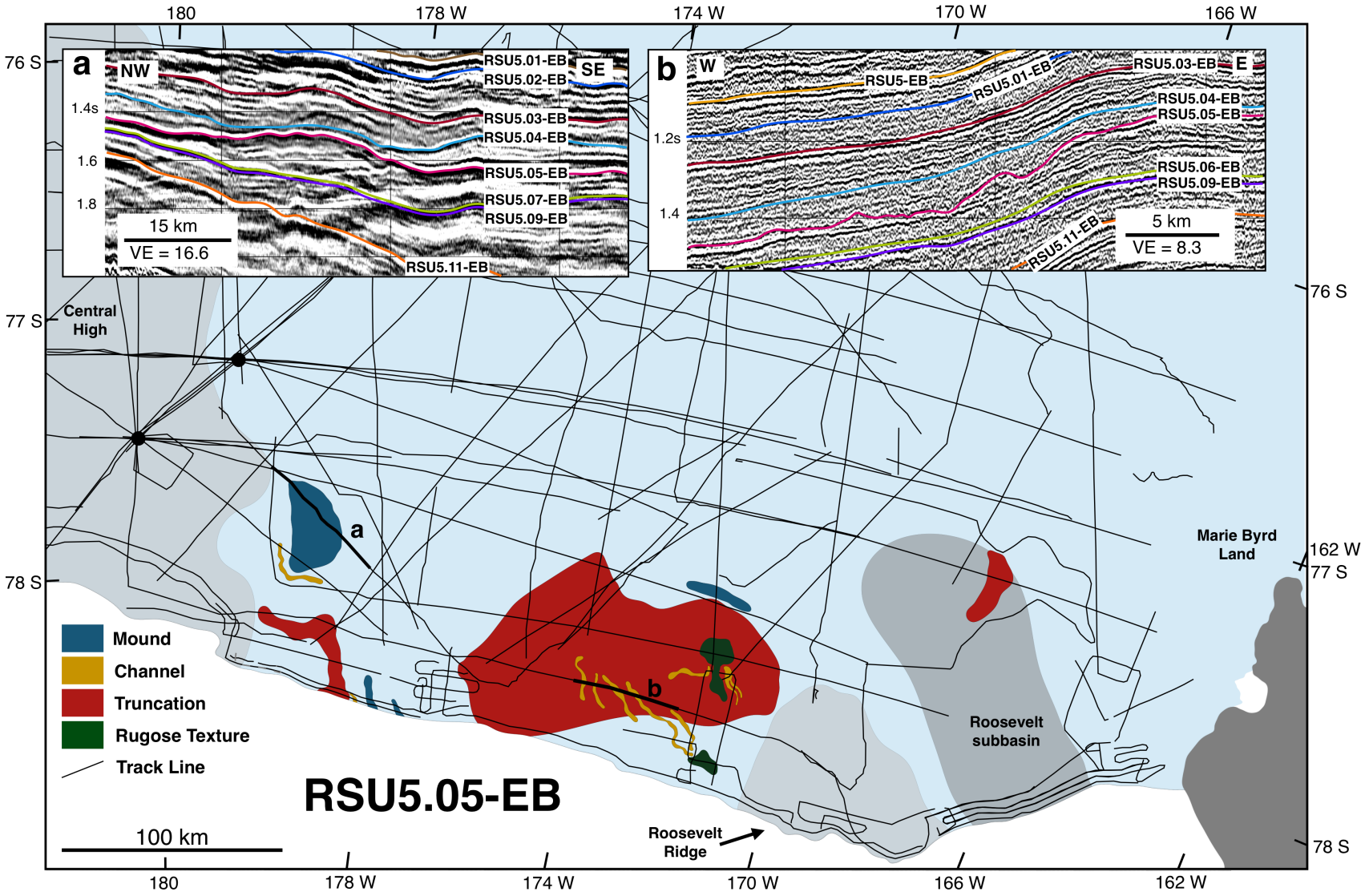
180
178 W
174 W
170 W
166 W
162 W
76 S
77 S
78 S
a
NW
SE
1.4s
1.6
1.8
15 km
VE = 16.6
RSU5.01-EB
RSU5.02-EB
RSU5.03-EB
RSU5.04-EB
RSU5.05-EB
RSU5.07-EB
RSU5.09-EB
RSU5.11-EB
b
W
E
1.2s
1.4
5 km
VE = 8.3
RSU5-EB
RSU5.01-EB
RSU5.03-EB
RSU5.04-EB
RSU5.05-EB
RSU5.06-EB
RSU5.09-EB
RSU5.11-EB
Central High
Marie Byrd Land
Roosevelt subbasin
Roosevelt Ridge
Mound
Channel
Truncation
Rugose Texture
Track Line
RSU5.05-EB
100 km

Figure 2.16. Feature map of RSU5.05-EB, a regional unconformity and sequence boundary. Mounds, channels, erosional truncation and rugose textures are interpreted from seismic data. **a)** Multi-channel seismic profile, IFP202, showing horizons RSU5.11-EB (orange), RSU5.09-EB (violet), RSU5.06-EB (olive), RSU5.05-EB (magenta), RSU5.04-EB (cyan), RSU5.03-EB (crimson), RSU5.02-EB (blue) and RSU5.01-EB (brown). A large mound, interpreted as a grounding zone wedge, is present beneath RSU5.05-EB (magenta). **b)** Single channel seismic line PD90-22 showing horizons, RSU5.08-EB (green), RSU5.07-EB (indigo), RSU5.06-EB (lime), RSU5.05-EB (magenta), RSU5.04-EB (cyan), RSU5.03-EB (crimson), RSU5.02-EB (blue), and RSU5-EB (amber). Numerous channels are present along RSU5.05-EB (magenta) and interpreted as subglacial meltwater channels or grounded ice streams.

2.4.4 Sequence 3 (RSS-2.3-EB)

Sequence 3 contains a thick section of parasequences enveloped by horizon RSU5.11-EB at its base and horizon RSU5.05-EB above (Figure 2.4). Horizon RSU5.11-EB truncates reflectors and displays rugose textures, channels and mounds along the Roosevelt Ridge basement high and the Marie Byrd Land margin (Figure 2.10). Back-stepping clinoforms above RSU5.10-EB are capped by a regionally extensive, high-amplitude horizon RSU5.09-EB (Figure 2.3). Above horizon RSU5.09-EB clinoforms prograde basinward (Figure 2.3). A large asymmetric mound capped by RSU5.05-EB that thickens down-dip is present along the eastern flank of Central High (Figure 2.16, inset a).

2.4.5 Sequence 2 (RSS-2.2-EB)

Sequence 2 is enveloped by horizons RSU5.05-EB and RSU5.03-EB (Figure 2.4). Numerous channels are observed on RSU5.05-EB within an area of erosional truncation near the modern ice shelf edge (Figure 2.16).

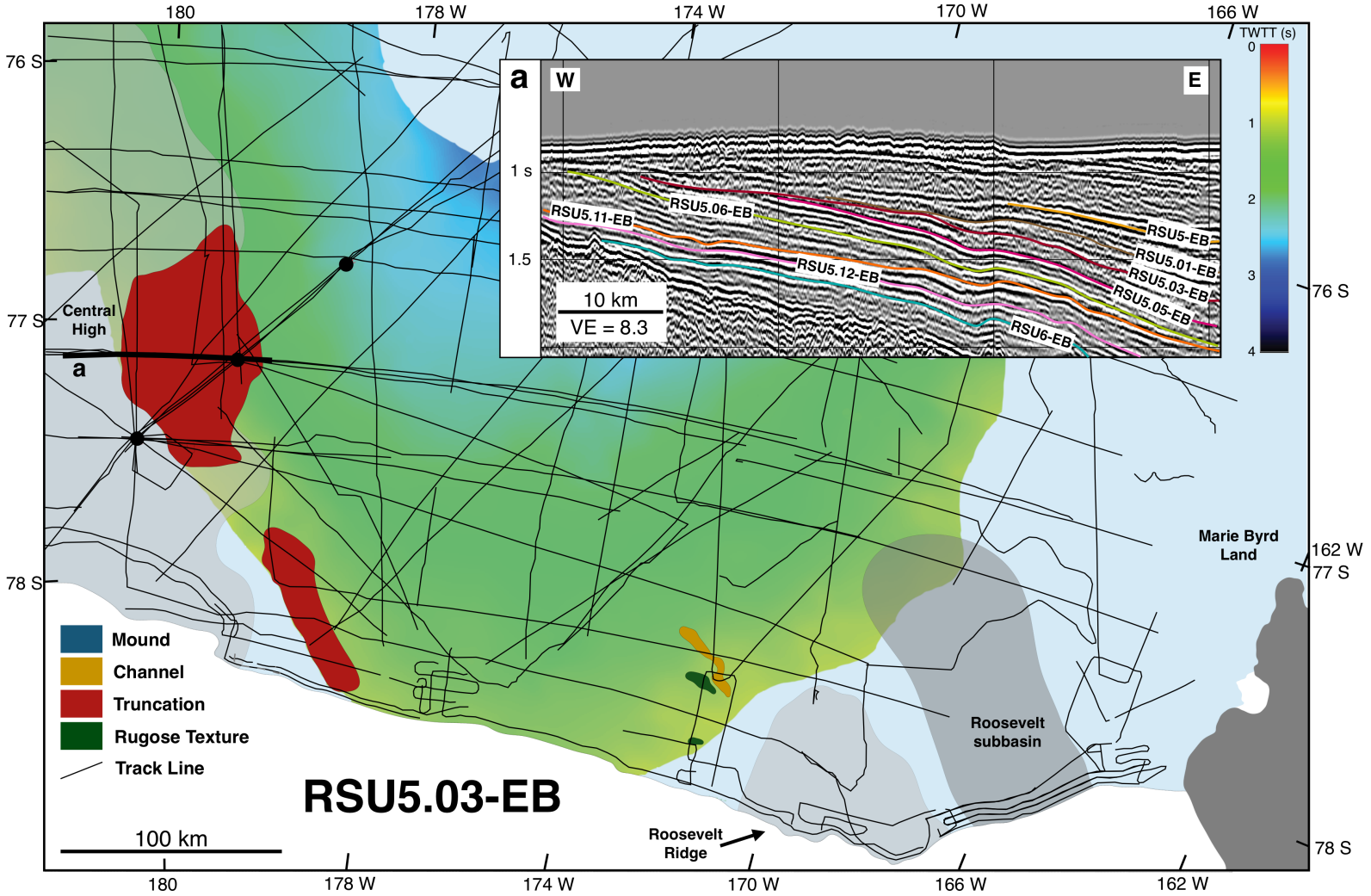

Figure 2.17. Structure map of RSU5.03-EB a regional unconformity and sequence boundary. Channel, rugose textures and erosional truncation interpreted from seismic date. **a)** Multi-channel seismic profile BGR-002-1 showing horizons: RSU6-EB (teal), RSU5.12-EB (pink), RSU5.11-EB (orange), RSU5.06-EB (lime), RSU5.05-EB (magenta), RSU5.03-EB (crimson), RSU5.01-EB (brown) and RSU5-EB (amber). Horizon RSU5.03-EB (crimson) truncates horizon RSU5.05-EB (pink) and RSS-2.2-EB along Central High.

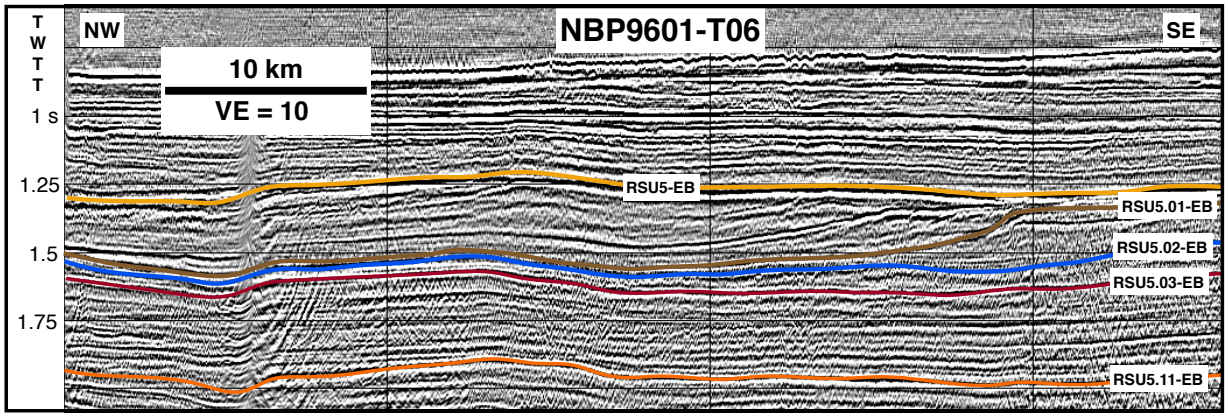

Figure 2.18. Strike-oriented Multi-channel seismic profile NBP9601-T06 (see Figure 2.1 for location) showing prograding clinoforms within Sequence 1 highstand systems tract (refer to Figure 2.4). RSU5-EB (amber), RSU5.01-EB (brown), RSU 5.02-EB (blue), RSU, 5.03-EB (crimson), and RSU5.11-EB (orange).

2.4.6 Sequence 1 (RSS-2.1-EB)

Sequence 1 is bounded at its base by horizon RSU5.03-EB and above by RSU5-EB (Figure 2.4). Sequence 1 thins to the east where reflectors amalgamate and the sequence subcrops near the margin of Marie Byrd Land. RSU5-EB was recognized as a regionally extensive reflector by Hinz and Block (1984). Horizon RSU5-EB truncates reflectors along the western sector of Eastern Basin where it is truncated by an overlying unconformity (Figure 2.18, inset a). A thick section of northeastward prograding clinoforms is present east of DSDP Site 272 and is capped by RSU5-EB. A younger, planar unconformity, RSU4A, truncates a significant portion of sequence 1 throughout the Eastern Basin (Figure 2.7).

2.5. Interpretation of Seismic Features and Sequences

2.5.1 Erosional and Depositional Seismic Features

2.5.1.1 Channels

Shallow, U- and V-shaped erosional features with dimensions of 100s of meters wide and 10s of meters deep are recognized as channels. Facies and features associations are used to

interpret whether channels are the product of glaciogenic, fluvial, or deep water transport processes. Glaciogenic channels, channels carved directly by ice or ice-proximal processes (e.g. sub-ice meltwater erosion), are identified as U-shaped channels (Figure 2.5a) that are associated with terrestrial or near-shore deposits coeval with glacial maxima, relative sea level falls, sequence boundaries, laterally extensive up-dip truncation and down-dip terminal moraines. Meltwater channels have similar morphologies and internal facies as fluvial channels but are associated with submarine rugose textured reflectors. Worldwide, fluvial channels typically display V-shaped (e.g. Figure 2.5b), leveed and avulsing channel morphologies and are associated with terrestrial deposits, up-dip tributary networks and down-dip deltaic deposits that display broad, lobate morphologies. Deep-water erosional channels associated with turbidites are U-or V-shaped, typically leveed and avulsing channels that occur on shelf slopes. Turbidites are often associated with down-dip distributary networks and submarine fan complexes.

2.5.1.2 Troughs

Large, broad erosional troughs (Figure 2.5c), with dimensions from several kilometers to 10s of km wide are interpreted as glaciogenic features that are carved by grounded ice streams or sheets (Sorlien et al., 2007a). The axes of large troughs observed in sequence RSS-2-EB are perpendicular to paleo-depositional strike (Figure 2.6). The troughs interpreted within RSS-2-EB strata have similar dimensions to ice stream troughs have been recognized along the modern sea floor (Anderson et al., 2014), from Plio-Pleistocene age strata (Bart, 2004), and from Miocene age strata (Anderson and Bartek, 1992). Wider troughs that extend further north are interpreted as the product of erosion from thicker ice sheets that could remain grounded well below sea level. A stack of trough shaped unconformities along the eastern flank of Central High (Figures 2.7, 2.14) may represent a series of ice advances and retreats.

2.5.1.3 Mounds

Several mounds, in 2D are identified within RSS-2-EB strata. Mounds have dimension of 1-5 km wide and heights exceeding 100 m (Figures 2.5g, 2.5h, 2.10, 2.15). Several mounds in 2D are likely ridges in 3D, and are interpreted as moraines produced by piedmont glaciers or streaming ice. Several mounds were only imaged on a single seismic profile so their 3D shapes and dimensions are unknown. Mounds that were imaged on two or more closely spaced profiles suggest ridges that are consistent with moraines.

The largest mound identified within RSS-2-EB strata occurs along the eastern flank of Central High, with a maximum width of ~15 km (Figure 2.5g, 2.5h, 2.15). This mound has a distinct internal seismic character of stratified internal reflectors that are truncated updip and downlap downdip. This feature is interpreted as a grounding zone wedge and the product of a significant ice sheet that was grounded below sea level. This feature has dimensions similar to modern and ancient grounding zone wedges documented from the Antarctic shelf and the Arctic (Bart and DeSantis, 2012; Dowdeswell and Fugelli, 2012; Batchelor and Dowdeswell, 2015).

2.5.1.4 Rugose Reflectors

Rugose reflectors (Figure 2.5e, 2.5f) are distinct corrugated reflector that are recognized throughout RSS-2-EB strata. Rugose reflectors are present at the modern seafloor and are associated with mega-scale lineations, ice-berg furrows and ice-proximal processes (Loth et al. 2007). Rugose reflectors resemble modern, deep-water sediment waves imaged on single channel seismic profiles on the slope offshore Amundsen Sea (Nitsche et al., 2000); however, rugose reflectors identified within the Eastern Basin are associated with horizons correlated to paleo water-depths of 500 m or less (Leckie and Webb, 1985; De Santis et al., 1999). Another possible interpretation that cannot be ruled out is that the rugose textured reflectors are the

product of fluvial small tributary or deep water distributary channels; however, lack of association of rugose reflectors with large updip channels or downdip fans does not support this interpretation.

2.5.2 Seismic Sequences and Stratigraphy

RSS-2, as defined by Brancolini and others (1995) (Figure 2.4), has been examined in detail using all publically available multichannel seismic reflection data and additional single channel data. I interpreted the seismic datasets using a sequence stratigraphic approach (Vail et al., 1977) to understand changes of accommodation. Detailed seismic stratigraphic analysis allowed me to interpret and correlate regional composite sequences which were then grouped into systems tracts defined by their stacking patterns. A minimum of 6 relative sea level cycles are recorded in the strata of the Eastern Basin, Ross Sea. A discussion of the newly defined third-order sequence stratigraphy follows.

2.5.2.1 Sequence 6 – Roosevelt Subbasin

Sequence 6 is locally identified within the Roosevelt subbasin and contains some of the earliest evidence of Oligocene glaciation along the West Antarctica margin. Along the upper sequence boundary, RSS5.15-EB, several 2D mound deposits are imaged to the east and are interpreted as lateral moraines (Figure 2.6). The moraines correspond to a period of decreasing accommodation that is likely associated with a relative sea level fall and glacial maximum.

Above sequence 6 is a series of cross-cutting broad troughs up to 20 km wide (Figure 2.6) that suggests multiple scour-and-fill cycles and are interpreted as multiple ice advance and retreats into the Roosevelt subbasin during the late Oligocene to early Miocene (Sorlien et al., 2007a) and younger.

Outside of Roosevelt subbasin, RSU6-EB to RSU5.15-EB exist as a thin (<150 m thick, Figure 2.7) sequence and is interpreted as the lowstand systems tract of sequence 5 that does not display evidence of glaciogenic processes. The anomalous expanded section of lower RSS-2-EB strata within the Roosevelt subbasin has been documented by previous investigators (Luyendyk et al., 2001; Decesari et al., 2007a; Sorlien et al., 2007a). This anomalously thick section of lower RSS-2-EB strata may be explained by: 1) the early development of a more gently sloping shelf within the Roosevelt subbasin while shelf morphology beyond the subbasin was more steeply dipping, 2) sedimentation rates that kept pace with subsidence within the Roosevelt subbasin while sedimentation rates were outpaced by subsidence beyond the Roosevelt subbasin, or 3) a combination of the two.

The morphology of the shelf is an important factor when considering differences in stratal stacking patterns (O'Grady et al., 2000). When a shelf has a steep slope, sediments are preferentially transported downslope by sediment gravity flow processes. These deeper deposits are less well imaged on seismic reflection profiles and interpretations of stratal architecture are limited. Deep currents impinging upon the margin may redistribute sediments deposited at depth, thus destroying primary stacking patterns. A subsiding, gently sloping shelf is more likely to develop and preserve stacking patterns at a sufficiently shallow depth that they may be well imaged on a seismic reflection profile. Decesari and others (2007b) model a late phase subsidence history for the Ross Sea at RUS6-EB time that depicts greater subsidence rates in the western Eastern Basin, near Central High, than in the east. This model suggests that areas around Marie Byrd Land would have developed a more gently sloping shelf and were more likely to preserve stacking patterns that can be better resolved on seismic. Both shelf morphology and

sedimentation rates may have resulted in thicker accumulations of RSS-2.4-EB along Marie Byrd Land and Roosevelt subbasin than adjacent to Central High and the modern ice shelf edge.

The shelf morphology of the Roosevelt subbasin during the late Oligocene is poorly understood. Limited seismic data from the Roosevelt subbasin and no seismic profiles oriented along dip prevents investigators from identifying the position of the shelf break during sequence 6 time. The processes responsible for a thick lower RSS-2 sequence within the Roosevelt remains equivocal and these hypotheses require additional data to be properly tested.

2.5.2.2 Sequence 5

Sequence 5 (Figure 2.4) is the first regionally extensive sequence deposited above horizon RSU6-EB. The lower sequence boundary, RSU6-EB is interpreted to have formed during a relative sea level fall and is generally conformable throughout the Eastern Basin. Small portions of Central High, near Site 270, may have been subaerialy exposed or shallow submarine during RSU6-EB time (Decesari et al., 2007a; Wilson and Luyendyk, 2009; Wilson et al., 2012). It is unclear if Site 270 sampled RSU6-EB, however 23 m of sedimentary breccia and a 3.5 m layer of well-developed regolith above metamorphic basement was recovered that suggest the area was subaerial before marine sedimentation commenced (Hayes and Frakes, 1975).

U-shaped channels are cut into acoustic basement (Figure 2.11) are interpreted as glaciogenic in origin (De Santis et al., 1995, Brazell 2017). A series of mounds, in 3D, occur along RSU6-EB on the southeastern flank of Central High (Figures 2.8, 2.11) and are interpreted as glaciogenic, though they have similar morphologies to volcanic vent complexes or bioherms. The mounds display weak internal stratification, have slightly asymmetric morphologies similar to drumlins and multiple mounds are clustered (Figure 2.8). Erosional truncation occurs along RSU6-EB along Central High (Figure 2.8) with a lateral extent up to 50 km and downdip

moraine-like features suggest an ice sheet, rather than small piedmont glaciers that would likely have carved U-shaped channels during RSU6-EB time. De Santis and others (1995) proposed small ice caps along subaerialy exposed portions of Central High during Oligocene time; however, this study supports the interpretations made by Anderson and Bartek (1992) that suggests a thin ice sheet and localized areas of streaming ice.

Several lines of evidence suggests a glaciated Eastern Basin margin during the Oligocene. Below horizon RSU-6-EB, U-shaped troughs have been recognized and interpreted as glacial features (De Santis et al., 1995). The presence of glacial features prior to RSU6-EB time suggests that ice was present along the margin of Eastern Basin and likely persisted after RSU6-EB. Geomorphic characteristics of piedmont glaciers that may be imaged on seismic include: U-shaped troughs ≤5 km, well-formed lateral moraines, end moraine with associated stratified lacustrine deposits and lobed outwash terraces (Benn et al., 2003). These features are not imaged on horizon RSU6-EB, instead the association of broad updip truncation and downdip mounds and channels supports a glaciated environment with a thin ice sheet and narrow regions of streaming ice, rather than localized piedmont glaciers.

U-shaped leveed channels are recognized within sequence 5 highstand systems tract (Figure 2.13) and are interpreted to be related to sediment bypass along the shelf during decreasing accommodation. Rugose reflectors along the margin of Marie Byrd Land are not associated with up-dip truncation or down-dip mounds and are, therefore, not interpreted to be the product of ice-proximal processes. Sequence 5 highstand systems tract reflectors are truncated by horizon RSU5.12-EB (Figures 2.3; 2.7).

2.5.2.3 Sequence 4

Sequence 4 is poorly preserved and is removed in the eastern sector of Eastern Basin. Internally, sequence 4 is comprised of a series of stacked, broad trough unconformities that cross-cut one another (Figure 2.14). The broad, trough unconformities within sequence 4 are interpreted as the product of ice advances and scouring, ice retreat and backfilling following by re-advancing ice that cannibalized previously deposited strata. Multiple cross-cutting unconformities are identified within sequence 4 (Figure 2.14). This suggests that multiple ice expansion and contractions, with possible frequencies of 100 kyr or more were occurring during this time. Levy and others (2012) estimate the age of horizon RSU5.11-EB to be ca. 25 Ma. Drill core from CRP2/2A in the Victoria Land Basin, western Ross Sea, contain late Oligocene deposits that record high frequency unconformities correlated to ~25 Ma and associated with an expanded East Antarctic Ice Sheet (Naish et al., 2001). Additionally, oxygen isotope data and eustacy calculations display high frequency variability during this time (Kominz and Pekar, 2001; Pekar et al., 2002; Miller et al., 2005) This correlation suggests a major expansion of both the East and West Antarctic Ice Sheets during the late Oligocene.

2.5.2.4 Sequence 3

Sequence 3's basal sequence boundary, RSU5.11-EB, is an extensive erosional surface along the eastern flank of Central High and the margin of Marie Byrd Land (Figure 2.10). Rugose reflectors and channels are present up-dip of mounds or ridges along Roosevelt Ridge and the Marie Byrd Land margin. These features and facies associations suggest a glaciogenic origin and that the WAIS advanced onto the margin.

Above sequence 3 lowstand, reflectors of the transgressive systems tract are correlated with deposits at Site 270 that contain a fining up sequence and evidence that water depths

increase from <50 m to possibly 500 m (Leckie and Webb, 1986) suggesting a high magnitude relative sea level rise with most of this related to subsidence. Highstand systems tract reflectors have an aggradational to sigmoid-oblique stacking pattern. Upper sequence boundary, RSU5.05-EB, truncates sequence 3 highstand systems tract reflectors along the modern ice shelf edge where it is recognized as a laterally extensive unconformity (Figures 2.3, 2.16).

2.5.2.5 Sequence 2

Sequence 2's lower sequence boundary is a regionally significant unconformity (Figure 2.16 that truncates upper sequence 3 and contains numerous channels near the modern ice shelf edge (Figure 2.16). Truncation, rugose reflectors are recognized along Roosevelt Ridge with mounded (moraine?) features located down-dip (Figure 2.16) are interpreted as glaciogenic or ice-proximal features and facies.

The unique spatial positions of features and facies on horizon RSU5.05-EB are interpreted as the product of a a greatly expanded WAIS. Paleo-water depth indicators at DSDP Site 270 for the strata below sequence 2 suggest depths greater than 300 m. A large mound is present on the southeastern flank of Central High (Figure 2.16) that has a similar morphology and internal seismic character as grounding zone wedges identified in the Ross Sea and high-latitude glaciated margins (Bart and DeSantis et al., 2012; Batchelor and Dowdeswell, 2015). This mound further supports the interpretation that the Eastern Basin margin may have been impinged upon by a well-developed WAIS.

The presence of shelf margin wedge suggests a relative sea level lowstand that did not fall below the shelf break. Above sequence 3 lowstand systems tract, a thin transgressive systems

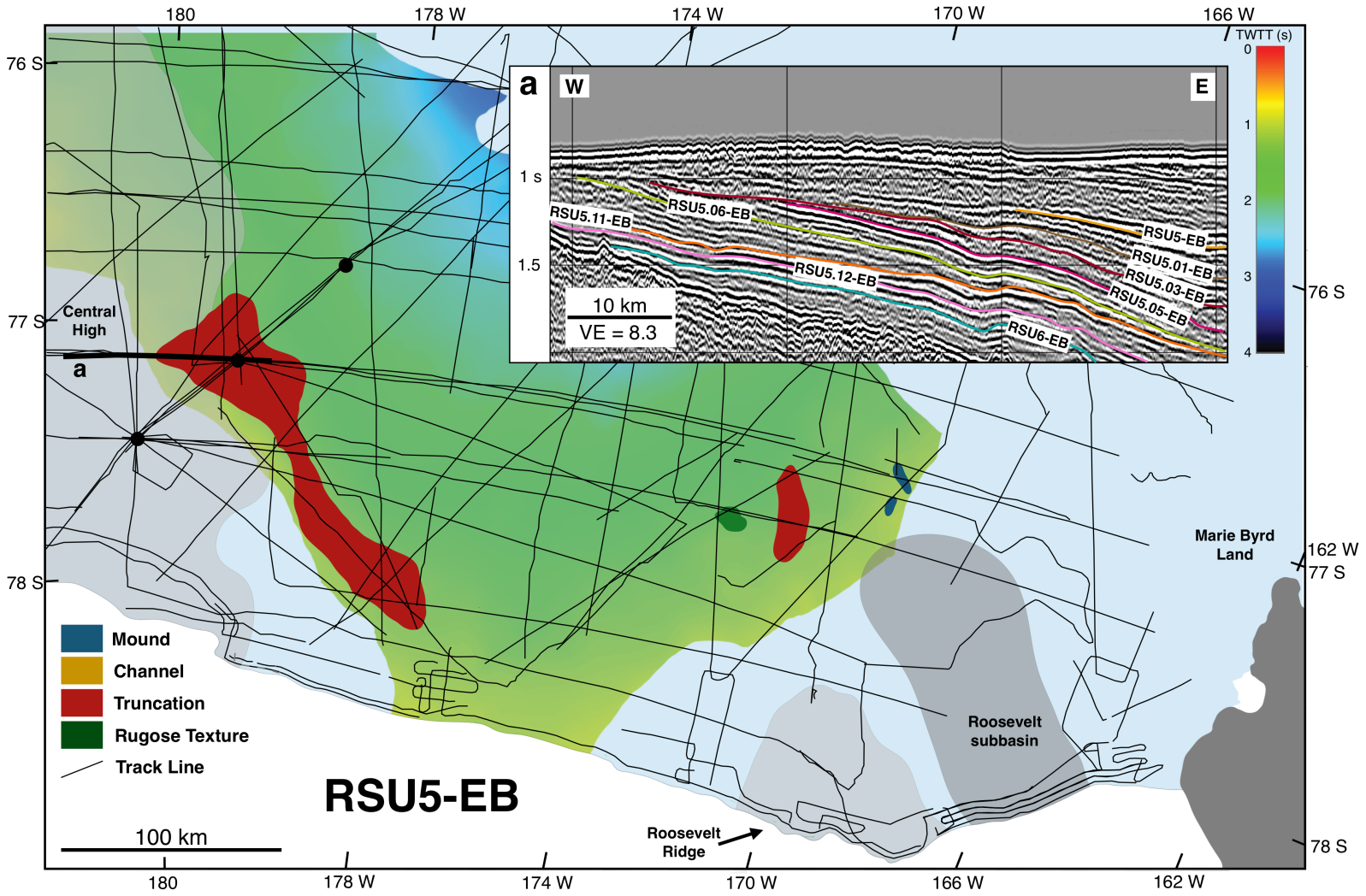

Figure 2.19. Structure map of RSU5-EB a regional unconformity and sequence boundary. Channel, rugose textures and erosional truncation interpreted from seismic date. **a)** Multi-channel seismic profile BGR-002-1 showing horizons: RSU6-EB (teal), RSU5.12-EB (pink), RSU5.11-EB (orange), RSU5.06-EB (lime), RSU5.05-EB (magenta), RSU5.03-EB (crimson), RSU5.01-EB (brown) and RSU5-EB (amber). Horizon RSU5-EB (amber) is truncated by an overlying reflector along Central High.

tract exists below a largely prograding highstand systems tract. Few seismic features are recognized within sequence 2 and the reflectors appear conformable. Upper sequence 2 is truncated by sequence boundary RSU5.03-EB, a regionally extensive unconformity (Figure 2.17).

2.5.2.6 Sequence 1

Unlike previous sequence boundaries, no evidence of rugose reflectors, channels or mounds are identified along RSU5.03-EB (Figure 2.17). A lack of glaciogenic features and facies associates suggests the Eastern Basin was an open marine environment during sequence 1 deposition and may be associated with early Miocene warming and glacial minimum.

2.5.3 Late Oligocene to early Miocene Glacial History of Eastern Basin

The glacial history of Eastern Basin in the Ross Sea during the late Oligocene to early Miocene has been developed from the stratal stacking patterns identified in the seismic record and from associated features, facies, and direct sedimentologic evidence, where available. Stratal stacking patterns are controlled by the morphology of the shelf, fluctuations in relative sea level, tectonic subsidence and sedimentation rates.

RSU6-EB is an unconformity created during a relative sea level fall correlated to a eustatic sea level fall ~30 Ma (Levy et al., 2012). Sediments from the bottom of Site 270 contain regolith and paleosols (Hayes and Frakes, 1975) suggesting subaerial exposure. Additionally, erosional truncation is noted along Central High downdip of Site 270 and off the modern coast of Marie Byrd Land. Mound-like features along RSU6-EB in the southwest sector of Eastern Basin (Figures 2.8, 2.11) are interpreted as moraines over 100m high at the base of outlet glaciers flowing from southern Central High.

During sequence 6, a thick section of strata was deposited and preserved within Roosevelt subbasin than along the modern ice shelf edge or Central High (Figure 2.6). The anomalously thick section within sequence 6 may be a function of slope morphology. Scour and fill features and moraines preserved in Roosevelt subbasin (Sorlien et al., 2007a) suggest that ice existed near Marie Byrd Land during the late Oligocene and may represent some of the earliest evidence of WAIS glaciation along the margin of West Antarctica.

Sequence 5 displays glaciogenic features including U-shaped channels that are associated with down-dip mounds interpreted as drumlins (Figure 2.8). The results of this study may suggest that subaerialy exposed portions of Central High may have been covered by a thin ice sheet and piedmont glaciers during RSU6-EB time.

Sequence 4 is interpreted to record multiple, high-frequency glaciations in West Antarctica that are correlated to high-frequency fluctuations of East Antarctica ice volume recorded in the western Ross Sea (Naish et al., 2001). Stacked and cross-cutting unconformities are interpreted as glacial surfaces of erosion and may records a period, ~25 Ma, when the WAIS was advancing and retreating from the Eastern Basin margin over time periods of 100 kyrs or more.

Sequence 3 is bounded, at its base, by a laterally extensive unconformity that truncates most of sequence 4 and contains glaciogenic features associates along the Marie Byrd Land Margin (Figure 2.10). Sequence 3 contains evidence of an expanded WAIS and a large amplitude sea level fall during the latest Oligocene.

Sequence 2 displays a unique stratal stacking pattern and contains a shelf margin wedge (Figures 2.3, 2.12) that suggests sequence 2 sea level lowstand did not fall below the position of the shelf break. Evidence of laterally extensive truncation along the modern ice shelf edge

highlights the northernmost extent of erosion, and a potentially glaciated margin, during RSS2-EB time.

Sequence 1 does not contain glaciogenic features or facies associations (Figure 2.17) and is interpreted as a period of ice-distal or ice-free deposition. This sequence may be correlated to early Miocene warming, recorded in the oxygen isotope record (Miller et al., 2005). This suggests that early Miocene ice volume fluctuations derived from stable isotope proxies may be a function of East Antarctic Ice Sheet dynamics alone during the early Miocene.

The record of WAIS dynamics contained within the Ross Sea appears to be unique along the West Antarctic margin. Records from the Amundsen Sea do not show significant glacial events until the mid-Miocene (Gohl et al., 2013). This study suggests that there was a significant volume of ice within West Antarctica along the Ross Sea margin. The volume of ice along other portions of West Antarctica, beyond the Ross Sea, during the late Oligocene to early Miocene is still poorly understood.

2.6. Conclusions

Detailed seismic correlation of RSS-2-EB (Figure 2.4) has identified seventeen regional seismic horizons and sixteen composite sequences in Eastern Basin, Ross Sea, Antarctica. Lower RSS-2-EB composite sequences were correlated to age and lithologic control at DSDP Site 270. Multiple features were identified from seismic profiles including: U- and V-shaped channels, mounds, broad trough and planar truncation and rugose reflectors. The occurrence of these features and their spatial associations were used to interpret depositional environment. This study uses stratal stacking patterns to place glaciogenic features associations into a context of accommodation and relative sea level. From these relationships, I interpret the glacial history of

WAIS during the late Oligocene to early Miocene. The history of glaciation in the Eastern Basin consists of:

1) Piedmont glaciation, ice caps or thin ice sheets existed along subaerialy exposed portions of Central High and early Oligocene glaciers advanced into Roosevelt subbasin during RSU6-EB time (ca. 30 Ma?).

2) Multiple, high frequency glacial advances occurred in both East and West Antarctica ca. 25 Ma and suggests Antarctic Ice Sheet instability during this time.

3) Ice persisted and impinged upon the margin of Eastern Basin and perhaps reached its maximum extent along the shelf during the latest Oligocene.

4) Ice volume decreased during the early Miocene and the Eastern Basin, Ross Sea was dominated by open marine deposition.

The results from the sequence stratigraphic model, developed from multi-resolutional seismic reflection data in Eastern Basin, document some of the earliest evidence that ice existed in West Antarctica. This study identifies that strata of Roosevelt subbasin as potentially containing a direct record of incipient WAIS formation and should be the target of future drilling efforts. The lack of glaciogenic features and facies associations after RSU5.05-EB time suggests that WAIS ice volume decreased during the early Miocene and that ice volume fluctuations during this time may be related to East Antarctic Ice Sheet dynamics.

A forthcoming revised age model for DSDP Site 270 (Levy and Kulhanek, electronic communication, January 2017) will be helpful by providing age control for the stratigraphic model of RSS-2-EB, and may allow for comparison to eustatic sea level models. Additional drill cores in Eastern Basin, along the modern ice shelf edge, within Roosevelt subbasin and on the

shelf of western Marie Byrd Land is needed to test hypotheses developed from our sequence stratigraphic model.

REFERENCES

Abreu, V. S., and Anderson, J. B., 1998. Glacial eustasy during the Cenozoic: Sequence stratigraphic implications. American Association of Petroleum Geologists Bulletin, v. 82, pp. 1385–1400.

Anderson, J. B., and Bartek, L. R., 1992. Cenozoic Glacial History of the Ross Sea Revealed by Intermediate Resolution Seismic Reflection Data Combined with Drill Site Information. Antarctic Research Series. American Geophysical Union, Washington, DC, v. 56, pp. 231–263.

Anderson, J.B., Conway, H., Bart, P.J., Witus, A.E., Greenwood, S.L., McKay, R.M., Hall, B.L., Ackert, R.P., Licht, K., Jakobsson, M., and Stone, J.O., 2014. Ross Sea paleo-ice sheet drainage and deglacial history during and since the LGM. Quaternary Science Reviews, v. 100, pp. 31-54.

Anderson, J.B., and Shipp, S.S., 2001. Evolution of the West Antarctic Ice Sheet, In: Alley, R.B., and Bindschadle, R.A., (Eds). The West Antarctic Ice Sheet: behavior and environment. Antarctic Research Series, v. 77, pp. 45-57.

ANTOSTRAT Project, 1995. Seismic Stratigraphic Atlas of the Ross Sea, Antarctica. In: Geology and Seismic Stratigraphy of the Antarctic Margin, v. 2. Editors, Cooper, A.K., Barker, P.F., and Brancolini, G., 1995. Antarctic Research Series. AGU, Washington D.C., v. 68, plates 1-22.

Balshaw-Biddle, K. M., 1981. Antarctic glacial chronology reflected in the Oligocene through Pliocene sedimentary section in the Ross Sea. M.A. Thesis, Rice University, Houston, TX, 140 pp.

Barrett, P. J., 1996. Antarctic paleoenvironment through Cenozoic times: A review. Terra Antartica, v. 3, pp. 103–119.

Bart, P.J., 2004. West-directed flow of the West Antarctic Ice Sheet across Eastern Basin, Ross Sea during the Quaternary. Earth and Planetary Science Letters, v. 228, pp. 425-438.

Bart, P.J., and DeSantis, L., 2012. Glacial intensification during the Neogene: A review of seismic stratigraphic evidence from the Ross Sea, Antarctica, continental shelf. Oceanography v. 25, no. 3, pp. 166-183.

Batchelor, C.L., and Dowdeswell, J.A., 2015. Ice-sheet grounding-zone wedges (GZWs) on high-latitude continental margins. Marine Geology, v. 363, pp. 65-92.

Benn, D.I., Kirkbride, M.P., Owen, L.A., and Brazier, V., 2003. Glaciated valley landsystems. *in* Evans, D.J.A., (Ed.) Glacial Landsystems, Hodder Arnold. London. 2003. pp. 372-404.

Brancolini, G., Cooper, A. K., and Coren, F., 1995. Seismic Facies and Glacial History in the Western Ross Sea (Antarctica), Antarctic Research Series. American Geophysical Union, Washington, DC, v. 68, pp. 209–234.

Brazell, 2017. Seismic record of West Antarctic Ice Sheet dynamics during the late Oligocene to early Miocene in the Eastern Basin, Ross Sea. PhD Dissertation. University of North Carolina at Chapel Hill, Chapel Hill, NC, USA.

Busetti, M. and I. Zayatz and Ross Sea Regional Working group 1994. Distribution of seismic units in the Ross Sea, Terra Antarctica, v. 1, pp. 345-348.

Cooper, A. K., Barrett, P. J., Hinz, K., Traube, V., Leitchenkov, G., and Stagg, H. M. J., 1991. Cenozoic prograding sequences of the Antarctic continental margin: A record of glacio-eustatic and tectonic events. Marine Geology, v. 102, pp.175–213.

Davey, F.J., Bennett, D.J., and Houtz, R.E., 1982. Sedimentary basins of the Ross Sea, Antarctica. New Zealand Journal of Geology and Geophysics. v. 25, i. 2, pp. 245-255.

Decesari, R.C., Wilson, D. S., Luyendyk, B. P., and Faulkner, M., 2007a. Cretaceous and Tertiary extension throughout the Ross Sea, Antarctica. *in* Cooper, A.K., and Raymond, C.R., (Eds.) Antarctica: A Keystone in a Changing World – Online Proceedings of the 10th ISAES, USGS Open File Report 2007-1047, Short Research Paper 052, p. 6.

Decesari, R.C., Sorlien, C.C., Luyendyk, B.P., Wilson, D.S., Bartek, L.R., Diebold, J., and Hopkins, S.E., 2007b. Regional seismic stratigraphic correlations of the Ross Sea: Implications for the tectonic history of the West Antarctic Rift System, *in* Cooper, A.K., and Raymond, C.R., (Eds.) Antarctica: A Keystone in a Changing World – Online Proceedings of the 10th ISAES, USGS Open File Report 2007-1047, Short Research Paper 052, p. 4.

DeConto, R.M., and Pollard, D., 2003. Rapid Cenozoic glaciation of Antarctica induced by declining atmospheric CO2. Nature. v. 421, pp. 245-249.

De Santis, L., Anderson, J. B., Brancolini, G., and Zayatz, I., 1995. Seismic Record of Late Oligocene Through Miocene Glaciation on the Central and Eastern Continental Shelf of the Ross Sea. Antarctic Research Series. American Geophysical Union, Washington, DC, v. 68, pp. 253–260.

De Santis, L., Prato, S., Brancolini, G., Lovo, M., and Torelli, L. 1999. The eastern Ross Sea continental shelf during the Cenozoic: Implications for the West Antarctic Ice Sheet development. *in*: F. M. Van der Wateren, and S. A. P. L. Cloetingh (Eds). Lithosphere dynamics and environmental change of the Cenozoic West Antarctic Rift System. Global Planetary Change, v. 23 (Special Issue), pp. 173–196.

Dowdeswell, J.A., and Fugelli, E.M.G., 2012. The seismic architecture and geometry of grounding-zone wedges formed at the marine margins of past ice sheets. GSA Bulletin, v. 124, no. 11/12, pp. 1750-1761.

Gohl, K., Uenzelmann-Neben, G., Larter, R.D., Hillenbrand, C.D., Hochmuth, K., Kalberg, T., Weigelt, E., Davy B., Kuhn, G., and Nitsche, F.O., 2013. Seismic stratigraphic record of the Amundsen Sea Embayment shelf from pre-glacial to recent times: Evidence for a dynamic West Antarctic ice sheet. Marine Geology, v. 344, pp. 115-131.

Haq, B. U., Harnderbol, J., and Vail, P. R., 1987. Chronology of fluctuating sea level since Triassic. Science, v. 235, pp. 156–1167.

Hayes, D. E., and Frakes, L. A. (Eds)., 1975. Initial Reports of the Deep-Sea Drilling Project Leg 28. US Government Printing Office, Washington, DC, 28, 1017.

Hinz, K., and Block, M., 1984. Results of geophysical investigations in the Weddell Sea and in the Ross Sea, Antarctica. In: Proceedings of the 11th World Petroleum Congress, London 1983. Wiley, New York, v. 2, pp. 79–91.

Kerans, C., and Kempter, K., 2002. Hierarchical stratigraphic analysis of a carbonate platform, Permian of the Guadalupe Mountains. The University of Texas at Austin, Bureau of Economic Geology. American Association of Petroleum Geologists. Datapages Discover Series No. 5. CD-ROM.

Kominz, M.A., and Pekar, S.F., 2001. Oligocene eustasy from two-dimensional sequence stratigraphic backstripping. Geological Society of America Bulletin, v. 113, pp. 291-304.

Lear C.H., Elderfield, H., and Wilson, P.A., 2000. Cenozoic deep-sea temperatures and global ice volumes from Mg/Ca in benthic foraminiferal calcite. Science, v. 287, pp. 269-272.

Lear, C.H., Rosenthal, Y., Coxall, H.K., and Wilson, P.A., 2004. Late Eocene to early Miocene ice-sheet dynamics and the global carbon cycle: Paleoceanography, v. 19, PA4915.

Leckie, R. M., and Webb, P. N., 1986. Late Paleogene and early Neogene foraminifers of deep sea drilling project site 270, Ross Sea, Antarctica. In: J. P. Kennett, C. C. von der Borch, et al. (Eds). Initial Reports of the Deep-Sea Drilling Project. Leg 90. US Government Printing Office, Washington, DC, pp. 1093–1118.

Levy, R. H., Harwood, D. M., Sorlien, C. C., Wilson, D. S., Luyendyk, B. P., Decesari, R. C., and Tuzzi, E., 2012. A Revised Chronostratigraphy for Ross Sea Sediments and Predicted Age of the ANDRILL Coulman High Sequences, Abstract PP23C-2070 presented at 2012 Fall Meeting, AGU: San Francisco, Calif., 3-7 Dec.

Levy, R.H., and Kulhanek, D.K., (electronic communication, January 3, 2017).

Loth, A.S., Bartek, L.R., Luyendyk, B.P., Wilson, D.S., and Sorlien, C.C., 2007. Scale of subglacial to sub-ice shelf facies variability, Eastern Basin, Ross Sea. Related Publications from ANDRILL Affiliates, Paper 13.

Luyendyk, B.P., Sorlien, C.C., Wilson, D.S., Bartek. L.R., and Siddoway, C.H., 2001 Structural and tectonic evolution of the Ross Sea rift in the Cape Colbeck region, Eastern Ross Sea, Antarctica. Tectonics, v. 20, pp. 933-958.

Luyendyk, B.P., Wilson, D.S., and Siddoway, C.S., 2003. Eastern margin of the Ross Sea Rift in western Marie Byrd Land, Antarctica: Crustal structure and tectonic development. Geochemistry Geophysics Geosystems. v. 4, no. 10, pp. 1-25.

Miller, K. G., Kominz, M. A., Browning, J. V., Wright, J. D., Mountain, G. S., Katz, M. E., Sugarman, P. J., Cramer, B. S., Christie-Blick, N., and Pekar, S. F., 2005. The Phanerozoic record of sea-level change. Science, v. 310, pp. 1293–1298.

Naish, T.R., Barrett, P.J., Dunbar, G.B., Woolfe, K.J., Dunn, A.G., Henrys, S.A., Claps, M., Powell, R.D., and Fielding C.R., 2001. Sedimentary cyclicity in CRP drillcore, Victoria Land Basin, Antarctica. Terra Antartica. v. 8, i. 3, pp. 225-244.

Nitsche, F. O., Cunningham, A. P., Larter, R. D., and Gohl, K., 2000. Geometry and development of glacial continental margin depositional systems in the Bellingshausen Sea. Marine Geology, v. 162, pp. 277–302.

O'Grady, D.B., Syvitski, J.P.M., Pratson, L.P., and Sarg, J.F., 2000. Categorizing the morphologic variability of siliciclastic passive continental margins. Geology. v. 28, i. 3, p. 313-332.

Pekar, S.F., Christie-Blick, N., Kominz, M.A., and Miller, K.G., 2002. Calibration between eustatic estimates from backstripping and oxygen isotopic records for the Oligocene. Geology, v. 30, pp. 903-906.

Posamentier, H. W., and Allen, G. P., 1999. Siliciclastic sequence stratigraphy: concepts and applications. SEPM Concepts in Sedimentology and Paleontology no. 7, 210 pp.

Sorlien, C. C., B. P. Luyendyk, D. S. Wilson, R. C. Decesari, L. R. Bartek, and J. B. Diebold, 2007a. Oligocene development of the West Antarctic Ice Sheet recorded in eastern Ross Sea strata, Geology, v. 35, pp. 467-470.

Sorlien C.C., Wilson, D.S., Luyendyk, D.S., Bartek, L.R., Decesari, R.C., and Diebold, J.B., 2007b. Buried Oligocene glacial topography beneath a smooth middle Miocene unconformity in the southeast Ross Sea: Evolution of West Antarctic glaciation. U.S. Geological Survey and The National Academies, USGS OF-2007-1047. Extended Abstract 099. p. 4.

Spagnolo, M., Clark, C.D., Ely, J.C., Stokes, C.R., Anderson, J.B., Andreassen, K., Graham, A.G.C., and King E.C., 2014. Size, shape and spatial arrangement of mega-scale glacial lineations from a large and diverse dataset. Earth Surface Processes and Landforms. DOI: 10.1002/esp.3532

Spiegel, C., Lindow, J, Kamp, P.J.J., Meisel, O., Mukasa, S., Lisker, F., Kuhn, G., and Gohl, K., 2016. Tectonomorphic evolution of Marie Byrd Land – Implications for Cenozoic rifting activity and onset of West Antarctic glaciation. Global and Planetary Change. v., 145, pp. 98-115.

Vail, P.R., Mitchum, R.M., Jr., and Thompson, S., III, 1977. Seismic stratigraphy and global changes of sea level, part 3: relative changes of sea level from coastal onlap; in C.E. Payton (ed.) Seismic Stratigraphy - Applications to Hydrocarbon Exploration: American Association of Petroleum Geologists Memoir 26, p. 63-81.

Wilch, T.I., and McIntosh, W.C., 2000. Eocene and Oligocene volcanism at Mount Petras, Marie Byrd Land: implications for middle Cenozoic ice sheet reconstructions in West Antarctica. Antarctic Science. v. 12, i. 4, pp. 477-491.

Wilson D.S., and Luyendyk, B.P., 2009. West Antarctic paleotopography estimated at the Eocene-Oligocene climate transition. Geophysical Research letters. v., 36, L16302.

Wilson D.S., Jamieson S.S.R., Barrett, P.J., Leitchenkov, G., Gohl, K., and Later, R.D., 2012. Antarctic topography at the Eocene-Oligocene boundary. Palaeogeography, Palaeoclimatology, Palaeoecology. v. 335-336, pp. 24-34.

Wilson, D.S., Pollard, D., DeConto, R.M., Jamieson, S.S.R., and Luyendyk, B.P., 2013. Initiation of the West Antarctic Ice Sheet and estimates of total Antarctic ice volume in the earliest Oligocene. Geophysical Research Letters, v. 40, pp. 4305-4309.

Zachos, J. C., Pagani, M., Sloan, L., Thomas, E., and Billups, K., 2001. Trends, rhythms, and aberrations in global climate 65 Ma to present. Science, v. 292, pp. 686–693.

CHAPTER 3: ANTARCTIC CRYOSPHERE EVOLUTION DURING THE LATE OLIGOCENE TO EARLY MIOCENE FROM THE EASTERN BASIN, ROSS SEA

3.1. Introduction

The history of Antarctic glaciation has been interpreted from a combination of indirect deep sea and low-latitude proxy records and incomplete direct records from the margin and continent. These records offer an inconsistent account of initial Antarctic cryosphere development and conflicting evidence about the magnitudes of ice growth and decay during the

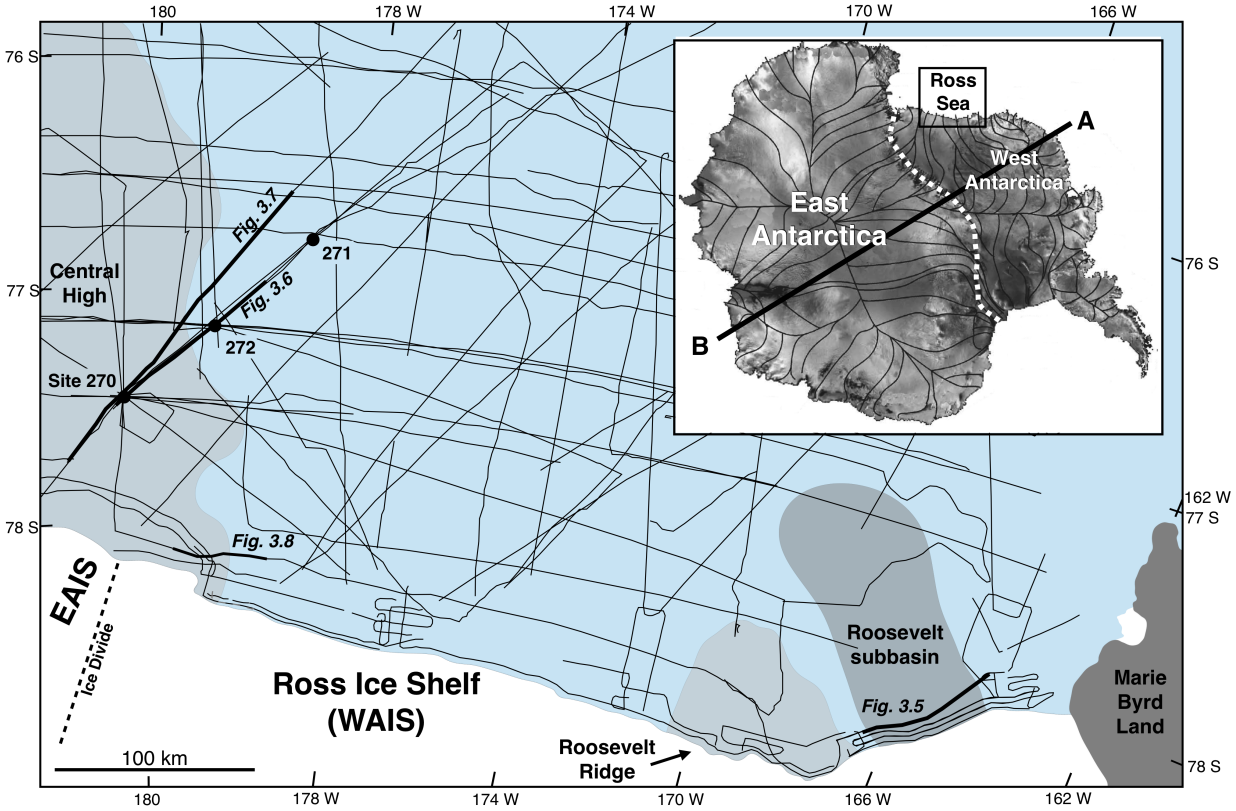

Figure 3.1. Location map of Eastern Basin, Ross Sea. Inset map: boundary of East and West Antarctica (bold white dashed line), ice drainage pathways (black solid lines). Primary map: modern Ross Ice Shelf (blue), modern EAIS and WAIS ice divide (dashed black line), basement highs: Central High, Roosevelt Ridge, Marie Byrd Land (light and dark grey), Roosevelt subbasin (medium grey), seismic tracks (thin black lines) and DSDP drill sites (black circles).

Cenozoic. The Eastern Basin, Ross Sea (Figure 3.1) contains a thick record of margin sedimentation during the Cenozoic (ANTOSTRAT, 1995). A third-order sequence stratigraphic model for late Oligocene to early Miocene strata in the Eastern Basin, Ross Sea (Brazell, 2017) is used to develop a relative sea level curve that can be compared to continuous deep-sea proxy records.

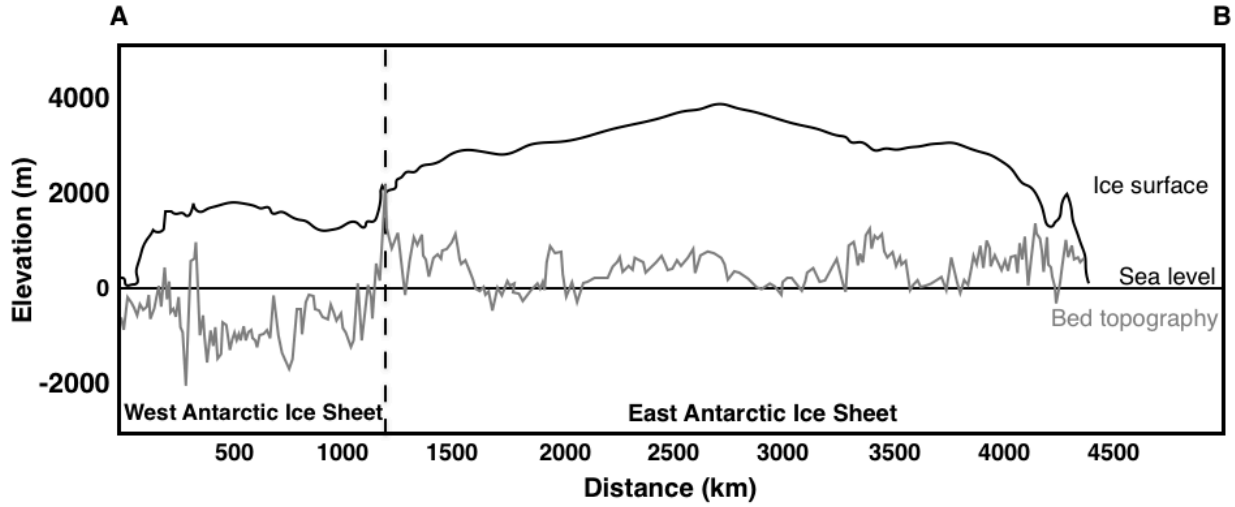

Figure 3.2. Cross section of Antarctica showing ice surface and BEDMAP bed elevations along transect A-B (Figure 3.1 inset). Much of the West Antarctic Ice Sheet is grounded below sea level (modified from Fretwell et al., 2013).

The Antarctic Ice Sheet is comprised of two fundamentally different ice sheets, the East Antarctic Ice Sheet (EAIS) and the West Antarctic Ice Sheet (WAIS) (Figure 3.2). The EAIS is a terrestrially-based and relatively stable ice sheet (Sugden et al., 1993). The WAIS, currently grounded below sea level, is believed to be more sensitive to fluctuations in global climate and ocean temperature (Joughin and Alley, 2011). This part of the Antarctic Ice Sheet is of scientific and public concern because a total collapse of the WAIS could result in a global sea level rise of

3.2 m (Bamber et al., 2009). The timing of EAIS and WAIS initiation likely occurred asynchronously but is poorly constrained (Miller et al., 1998; Anderson and Shipp, 2001; O'Brien et al., 2001; Zachos et al., 2001; DeConto and Pollard, 2003; Naish et al., 2008; Wilson et al., 2013). Developing a more robust understanding of how the EAIS and WAIS have responded and contributed to global climate change throughout the Cenozoic will result in a better understanding of the interactions between the Antarctic cryosphere and future global climate change.

Distal oxygen isotope records suggest incipient Antarctic glaciation as early as the late Eocene (Zachos et al., 2001) and as recently as the late Oligocene (Miller et al., 1991; Lear et al., 2000). Rapid and large amplitude $\delta^{18}O$ variations define global isotopic events and presumably indicate global cooling and Antarctic ice volume growth through the Pliocene, after which northern hemisphere ice volume contributes to the signal; however, estimates of ice volume and temperature dynamics from the oxygen isotope record alone are difficult to deconvolve. Mg/Ca ratios can provide an independent measurement of seawater temperatures and when combined with $\delta^{18}O$ records, may constrain estimates of ice volume. Continuous $\delta^{18}O$ records from deep sea sediment cores depict a dynamic Antarctic Ice Sheet throughout the late Paleogene and Neogene; however, Mg/Ca ratios do not record bottom water cooling prior to marine oxygen isotope event Mi1 (Lear et al., 2000; 2004) suggesting an unrealistic Oligocene Antarctic Ice Sheet more than twice as large as the modern (Coxall et al., 2005). Ice volume modeling by Wilson and others (2013) suggests the Eocene development of the EAIS with WAIS development in the earliest Oligocene and that there may have been significant ice volume on the Antarctic continent during the Oligocene.

Proximal records of Antarctic glaciations are interpreted from seismic reflection data, ice-rafted debris (IRD), sediment cores, paleontological remains, and sparse outcrop data. The

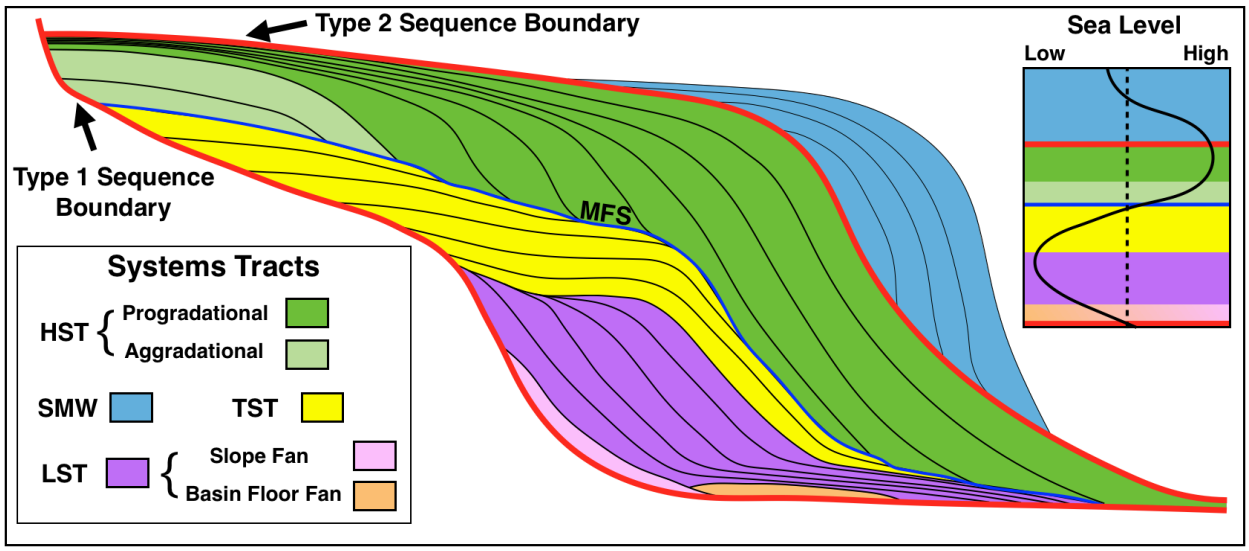

Figure 3.3. Sequence stratigraphic model adapted from Vail et al., 1977. **Type 1 sequence boundary** consists of an up-dip erosional unconformity and its down-dip correlative conformity created when sea level falls below the shelf break. Within the **LST** (lowstand systems tract) slope and basin floor fan are deposited below a prograding wedge of strata. As sea level begins to rise the **TST** (transgressive systems tract) is deposited and consists of landward thickening parasequences with landward onlap and downlap trajectories. A **MFS** (maximum flooding surface) marks the end of the TST when the shoreline is at its maximum landward position. During the early **HST** (highstand systems tract) parasequences are aggradational and become progradational as the rate of sea level rise decreases. A **Type 2 sequence boundary** consists of an up-dip erosional unconformity and its down-dip correlative conformity created when sea level does not fall below the position of the shelf break and is followed by the deposition of a **SMW** (shelf margin wedge).

earliest direct records of Antarctic glaciations are from sediment cores collected during Deep Sea Drilling Project (DSDP) Leg 119 in Prydz Bay and suggest glaciers existed on East Antarctica as early as the late middle Eocene, and an ice sheet existed by the late Oligocene (Barron et al., 1991; Hambrey et al., 1991). Seismic reflection data from the Amundsen Sea does not show evidence of significant West Antarctica glaciation until the middle Miocene (Gohl et al., 2013),

while seismic reflection data from the Ross Sea suggests possible West Antarctic glaciation prior to the late Oligocene (Sorlien et al., 2007a).

Distal proxy records provide the most continuous records of Antarctic glaciation; however, proxy records are unable to deconvolve the individual contributions of EAIS and WAIS ice volumes. Since approximately 98% of the modern Antarctic continent is obscured by ice, evidence from the margin may provide the most direct and complete records of the timing and evolution of the AIS.

The principles of sequence stratigraphy relate stratal stacking patterns to changes in basin accommodation (Figure 3.3), which is a product of changes in sedimentation, tectonic subsidence, and eustasy (Vail et al., 1977; Posamentier and Allen, 1999; Catuneanu et al., 2011). Sequences are enveloped by sequence boundaries that are products of falling relative sea-level (RSL) and are identified as up-dip erosional unconformities and their correlative down-dip conformities. Genetically related strata stack into predictable patterns based on the amount and rate of change of accommodation within a basin. These stacking patterns are referred to as "systems tracts". The lowstand systems tract is deposited during a RSL fall and is characterized by reflectors that onlap the sequence boundary and prograding clinoforms with reflectors that downlap onto the sequence boundary in the deep basin. During the ensuing RSL rise, as the rate of accommodation is increasing, a transgressive systems tract is deposited. The transgressive systems tract contains back-stepping parasequences that onlap the sequence boundary in a landward trajectory. The transgressive systems tract is capped by a maximum flooding surface that represents the surface of deposition at the time the shoreline is at its maximum landward position. As the rate of accommodation and rising RSL decreases below the rate of sediment accumulation, the highstand systems tract is deposited and parasequences downlap onto the

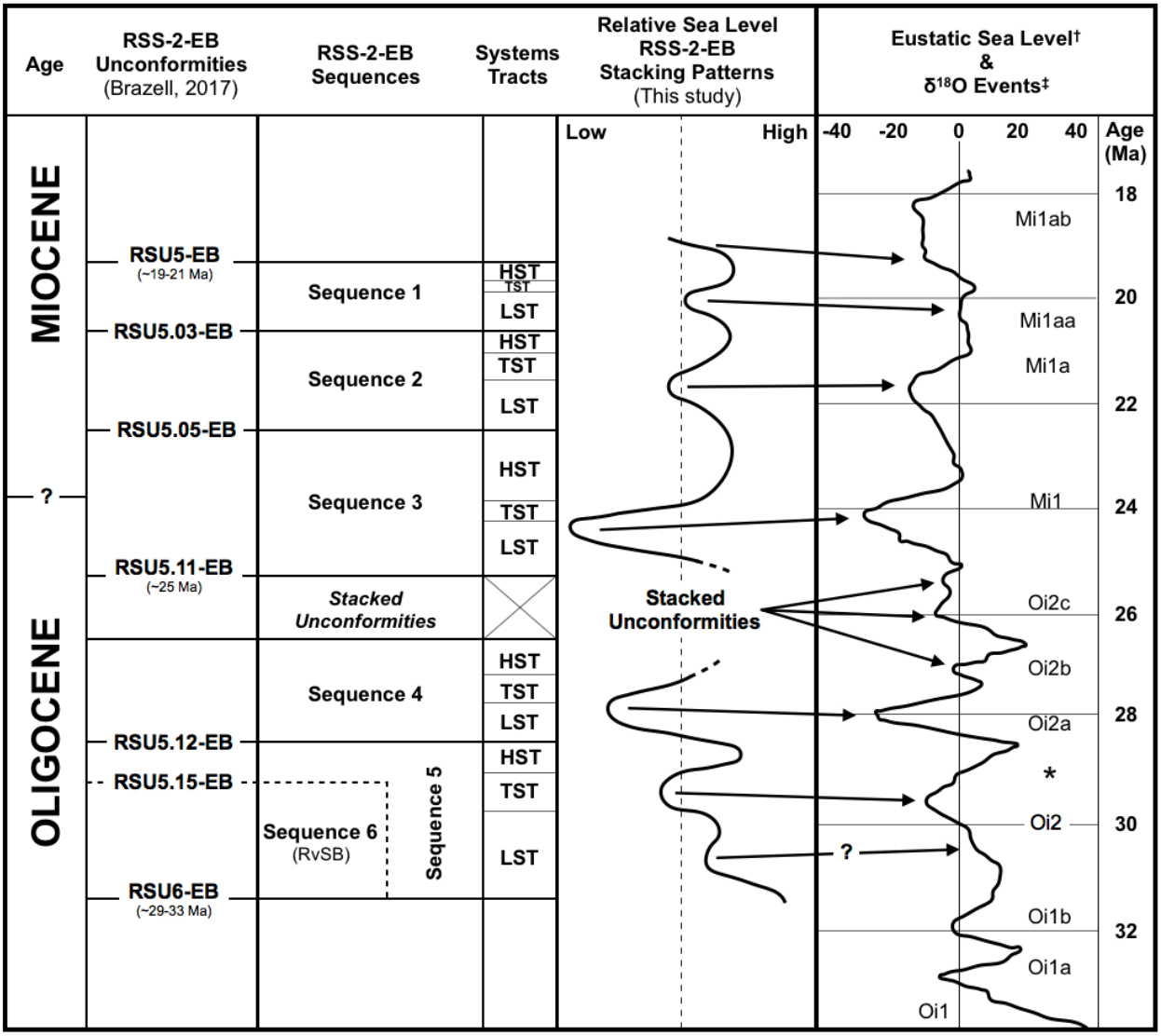

Figure 3.4. Correlation chart of Eastern Basin, Ross Sea sequence stratigraphy and relative sea level curve to eustatic sea level curve and oxygen isotope events. RSS-2-EB (Ross Sea Sequence 2 – Eastern Basin) unconformities, sequences and systems tracks (Brazell, 2017) were used to interpret the seismo-stratigraphic stacking patterns and develop a relative sea level curve that is not representative of absolute magnitude or duration. RSS-2-EB relative sea level curve was correlated to the eustatic sea level curve †(Miller et al., 2005) and oxygen isotope events ‡(Pekar et al., 2002; Pekar and DeConto, 2006). Based on the correlation between eustatic sea level fluctuations, RSS-2-EB sequences are interpreted to reflect glacio-eustatic fluctuations in sea level with further constrains in the chronology of RSS-2-EB sequences

maximum flooding surface and clinoforms prograde basinward. A subsequent RSL fall will produce another sequence boundary that constrains the top of the sequence.

Sea level curves are constructed from a combination of: 1) biostratigraphic records of sediment age and water depth; 2) seismic data that records the position of coastal onlap; 3) sediment compaction models; and 4) tectonic subsidence models (Greenlee et al., 1988). Stratigraphic sequences are fractal on all geologically relevant time-scales. First-order sequences are deposited over 100s of millions of years and may correspond with Wilson-cycle scale events. First-order sequences are comprised of multiple second-order sequences which are deposited over 10 – 100 Myrs, and are themselves comprised of higher order sequences deposited over shorter durations. Third-order sea level fluctuations occur on time scales of 0.5 to 10 Myrs and are below the resolution required to capture discrete glacial/interglacial cycles which occur on time-scales of 40 – 100 kyrs; however, third-order cycles may represent significant changes in the composition of the Antarctic cryosphere (e.g., significant changes in ice-volume and thermal regime).

Limited chronostratigraphic control for late Oligocene to early Miocene Ross Sea Sequence 2 in the Eastern Basin (RSS-2-EB) (Figure 3.4) from DSDP Sites 270 and 272 reduces certainty in the timing and duration of third-order glacio-eustatic sea level changes. Examining the stratal architecture and stacking patterns of the sequences within RSS-2-EB will allow for comparison to continuous, deep-sea records of eustatic change during the Cenozoic. RSS-2-EB is enveloped by regional sequence boundaries Ross Sea Unconformities 6 and 5 in the Eastern Basin (RSU6-EB and RSU5-EB, respectively) (Figure 3.4) with assumed ages of ca. 33 - 29 Ma and ca. 21 -19 Ma, respectively (Leckie and Webb, 1983; Levy et al., 2012). Additional chronostratigraphic constraints include a regional sequence boundary, RSU5.11-EB (a.k.a. Mid-

270 horizon) that is correlated to Site 270 with an assumed age of ca. 25 Ma (Sorlien et al., 2007b; Levy et al., 2012). Paleo-water depths are poorly constrained from foraminiferal data; however, data show a general trend of increasing water depth from 10-50 m post RSU6-EB time to 300 m and possibly as deep as 500 m by 25 Ma, suggesting an average subsidence rate of 68-95 m/Myr (Leckie and Webb, 1983). Interpretation of seismic profiles in Eastern Basin indicate that post RSU6-EB erosion has removed large sections of up-dip strata including paralic deposits that would provide information about the position and depth of coastal onlap.

Despite limited data needed to constrain the absolute timing and magnitude of RSL fluctuations, stratal stacking patterns are used to test hypotheses about the relative magnitudes and rates of RSL fluctuations during the late Oligocene to early Miocene in the Eastern Basin. Data from continuous, deep-sea cores and passive margins show that fluctuations in eustatic sea level during the early Cenozoic were quasi-periodic and unequal in magnitude. This study tests the hypotheses that the seismic-stratigraphic architecture of the Eastern Basin is the product of: 1) periodic changes in accommodation that were of equal magnitude and duration; 2) periodic changes in accommodation that were of unequal magnitude and duration; 3) aperiodic changes in accommodation that were of equal magnitude and duration; or 4) aperiodic changes in accommodation that were of unequal magnitude and duration. If the seismic architecture of the Eastern Basin can be correlated to the deep-sea proxy record of eustatic fluctuation, it can be used to further constrain the timing and influence of WAIS evolution. Additionally , a better understanding of intervals that are preserved within the Eastern Basin will permit comparison to previous interpretations of Antarctic cryosphere history derived from distal proxy records (Zachos et al., 2001; Miller et al., 2005; Pekar and Lear, 2007; Naish et al., 2008) and more proximal geophysical and sedimentological records from the margin and continent (Bartek et al.,

1996; De Santis et al., 1999; Wilch and McIntosh, 2000; Naish et al., 2001; Sorlien et al., 2007a; Gohl et al., 2013; Spiegel et al., 2016).

TABLE 3.1: Seismic data

Seismic source (L)	Vertical resolution (m)	Penetration depth (s)	Cruise abbreviation
Air Gun 2.46	12	2.0	PD90[1]
Air Gun 23.45	30	6.0	BGR[2]
Air Gun 22.5	20-30	3.0-4.0	IT88[3], IT89[3], IT94[3]
Air Gun 10	60-70	6.0	SEV87[4], SEV89[4]
Air Gun 35.54	30	6.0	IFP[5]
Air Gun 9.2	30	6.0	TH82[6], TH92[6]
Air Gun 3.44	30	6.0	NBP9601[7]
Air Guns: 1.72; 6.88; 10.3; & 49.2	10-60	2.0-6.0	NBP0301[8], NBP0306[9]
Air Gun 0.8	10	2.0	NBP0802[10]

Table 3.1. Seismic data used for this study. [1] Rice University (USA) 1990; [2] Bundesanstalt für Geowissenchaften und Rohstoffe (Germany) 1980; [3] Osservatorio Geofisico Sperimentale di Trieste (Italy) 1988, 1989, 1994; [4] Joint Stock Company Marine Arctic Geological Expedition (Russia) 1987, 1989; [5] Institute Fançaise du Pétrole (France) 1982; [6] Japanese National Oil Company 1982, 1992; [7] University of Alabama (USA) 1990; [8] University of North Carolina at Chapel Hill (USA) 1996; [9] University of California at Santa Barbara (USA) 2003; [10] University of Southern California (USA) 2008.

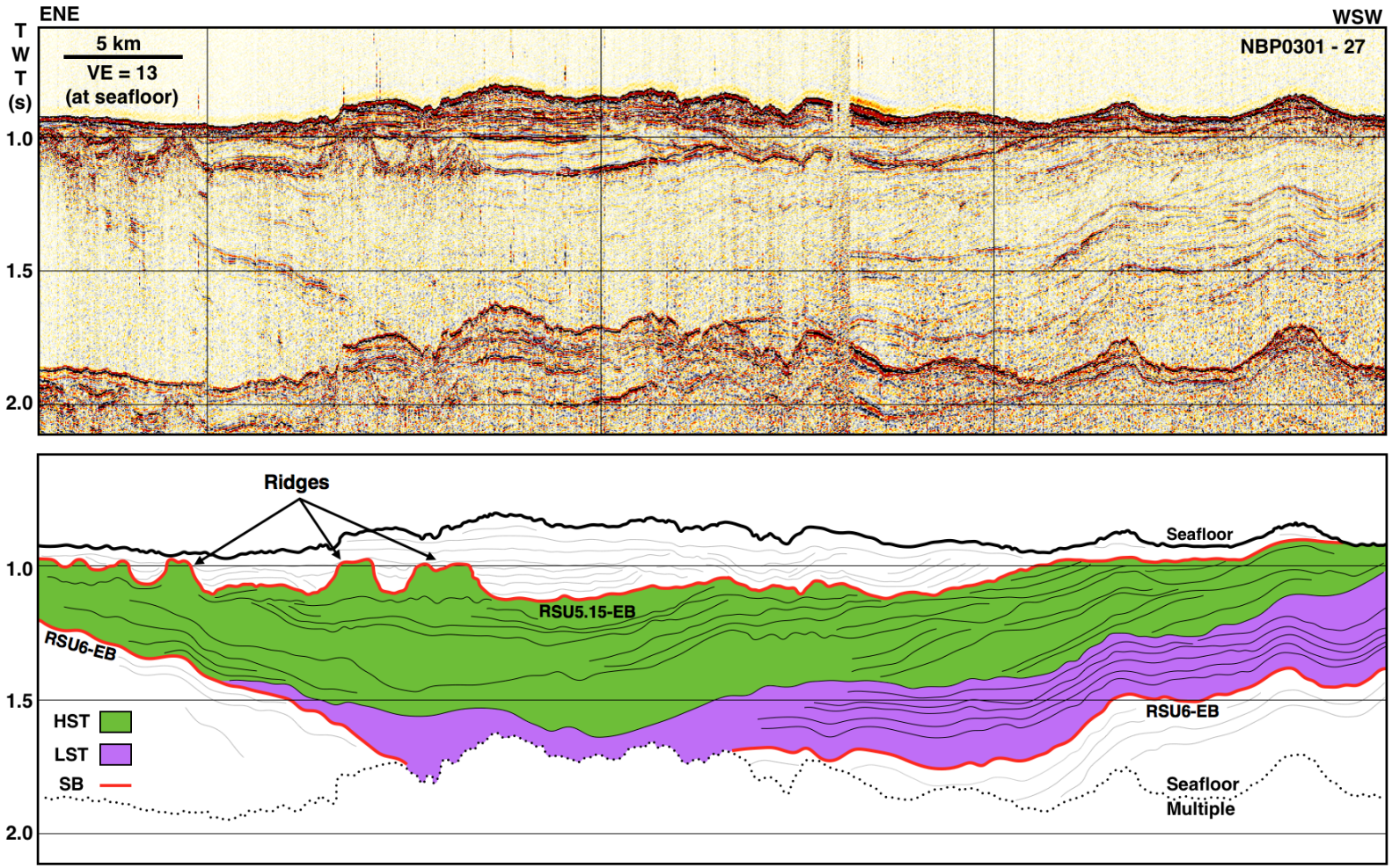

Figure 3.5. Seismic reflection profile NBP0301-27 (see figure 3.1 for location) and interpreted line drawing of sequence 6 identified in the Roosevelt subbasin, eastern Ross Sea. Flat-topped ridges along **SB** - sequence boundary RSU5.15-EB interpreted as glacial moraines on top of a thick **HST** – highstand systems tract. Sequence 6 HST downlaps onto sequence 6 **LST** – lowstand systems tract that onlaps SB RSU6-EB.

3.2. Methods and Data

This study focuses on the stratigraphic record of the Eastern Basin, Ross Sea because it contains a record of West Antarctica sedimentation from at least the late Oligocene (Hayes and Frakes, 1975), has had a relatively simple tectonic history during the late Cenozoic (Decesari et al., 2007a), and has a high density of geophysical data compared to other sectors of the Antarctic margin (Cooper et al., 2008). It uses a third-order sequence stratigraphic model for the Eastern Basin, Ross Sea (Brazell, 2017) and seismic reflection profiles (Table 3.1) to develop a RSL curve that assumes constant subsidence and sedimentation.

The thicknesses of sequences and their systems tracts were measured along seismic profiles PD90-30, BGR-007-1 and NBP0301-27 (Figure 3.1) using a linear velocity function derived from a published velocity model for Eastern Basin (Davey et al., 1982). Stratal stacking patterns were interpreted to infer the relative rates of accommodation and RSL change within a sequence. Variations in accommodation were constrained by chronostratigraphic correlations to DSDP Site 270 and a sea level curve was constructed to reflect relative changes in magnitude and rate of RSL change (Figure 3.4).

3.3 Results and Discussion

3.3.1 Stratal Architecture, Systems Tracts and Relative Sea Level

Six regional sequence boundaries are interpreted on seismic profiles within the Eastern Basin and a seventh, local sequence boundary is interpreted within the Roosevelt subbasin (Figure 3.4). The stratigraphic architecture of the Eastern Basin confirms that at least six cycles

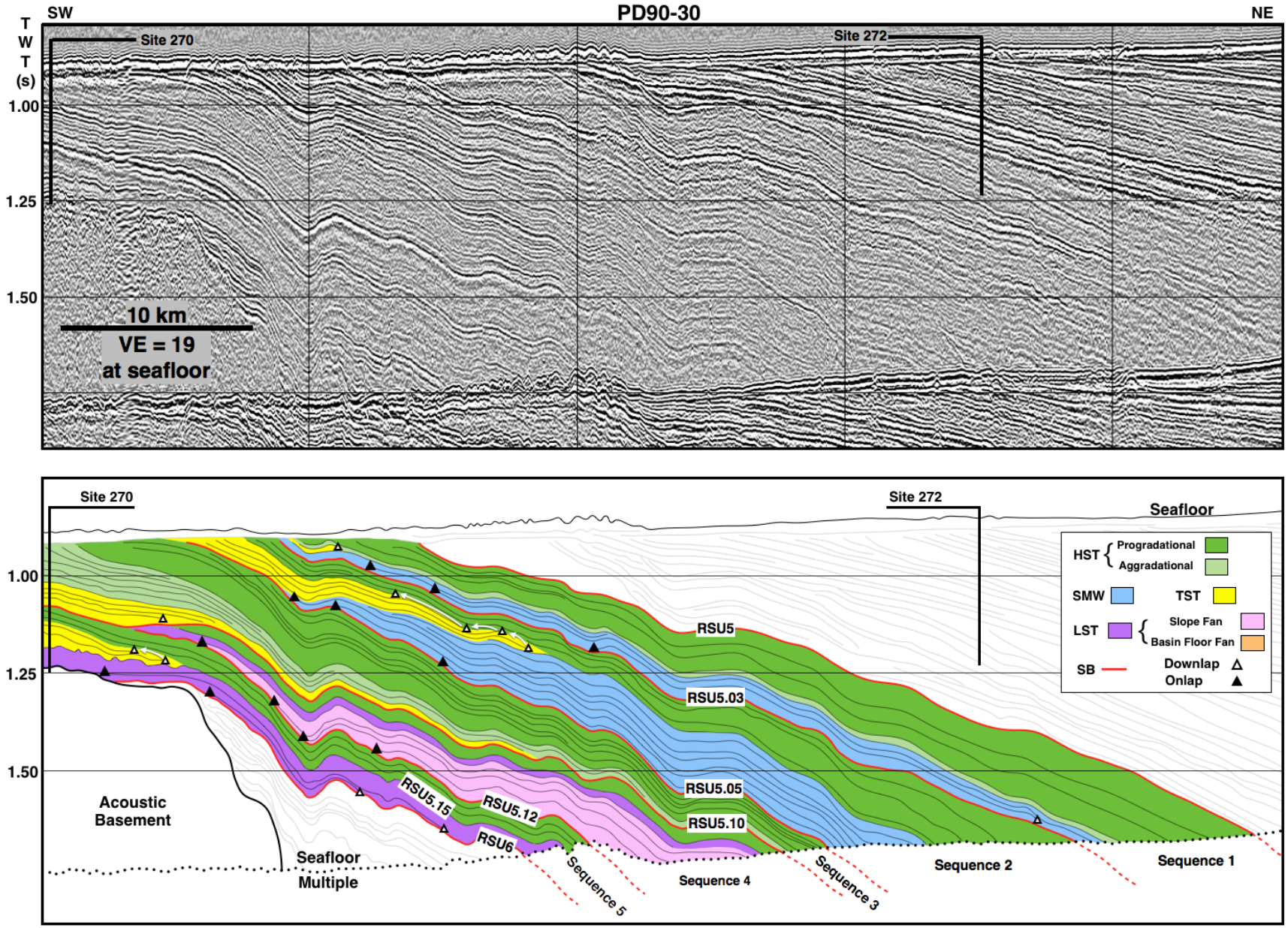
SW
PD90-30
NE
T
W
T
(s)
1.00
1.25
1.50
Site 270
Site 272
10 km
VE = 19
at seafloor
Site 270
Site 272
Seafloor
HST
Progradational
Aggradational
SMW
TST
LST
Slope Fan
Basin Floor Fan
SB
Downlap
Onlap
RSU5
RSU5.03
RSU5.05
RSU5.10
RSU5.12
RSU5.15
RSU6
Acoustic
Basement
Seafloor
Multiple
Sequence 5
Sequence 4
Sequence 3
Sequence 2
Sequence 1

Figure 3.6. Seismic reflection profile PD90-30 in the western sector of the Eastern Basin (see Figure 3.1 for location) and interpreted line drawing of RSS-2-EB. **HST** – highstand systems tracts are in green where light green represents aggradational and dark green represents progradational stacking patters; **SMW** – shelf margin wedge in blue, above type 2 sequence boundaries; **TST** – transgressive systems tracts in yellow; **LST** – lowstand systems tract in purple with pink representing slope fans members of the systems tract; and **SB** – Sequence boundary are labeled using Brazell (2017) nomenclature. Closed triangles locate onlap position. Open triangles locate downlap positions. Erosion at the modern sea floor has removed costal sections of RSS-2-EB.

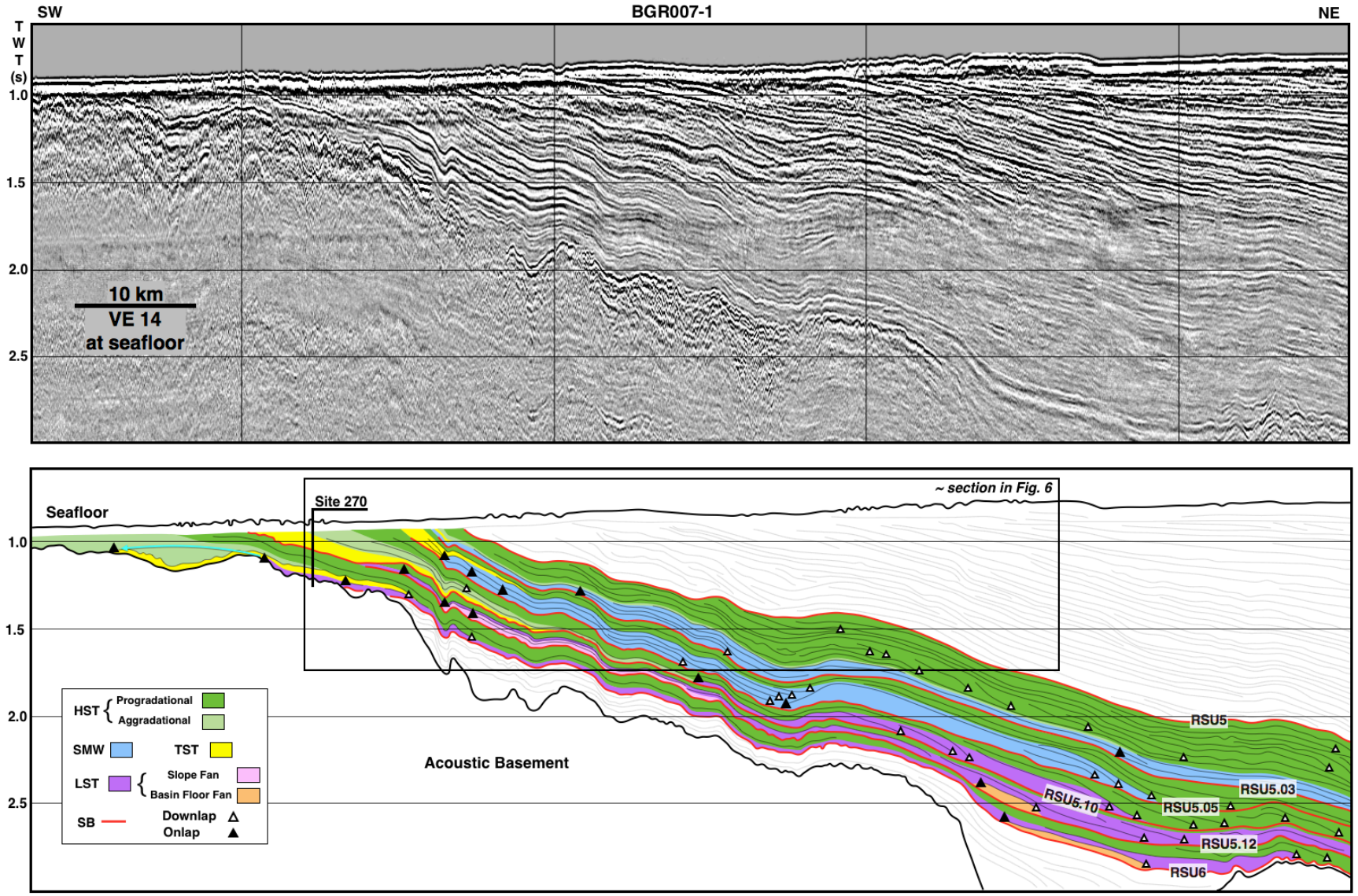
SW
BGR007-1
NE
TWT (s)
1.0
1.5
2.0
2.5
10 km
VE 14
at seafloor
Seafloor
Site 270
~ section in Fig. 6
Acoustic Basement
HST
Progradational
Aggradational
SMW
TST
LST
Slope Fan
Basin Floor Fan
SB
Downlap
Onlap
RSU5
RSU5.03
RSU5.05
RSU5.10
RSU5.12
RSU6

Figure 3.7. Seismic reflection profile BGR007-1 in the western sector of the Eastern Basin (see Figure 3.1 for location) and interpreted line drawing of RSS-2-EB. **HST** – highstand systems tracts are in green where light green represents aggradational and dark green represents progradational stacking patters; **SMW** – shelf margin wedge in blue, above type 2 sequence boundaries; **TST** – transgressive systems tracts in yellow; **LST** – lowstand systems tract in purple with pink representing slope fans members of the systems tract; and **SB** – Sequence boundary are labeled using Brazell (2017) nomenclature. Closed triangles locate onlap position. Open triangles locate downlap positions. Erosion at the modern sea floor has removed costal sections of RSS-2-EB.

of RSL fluctuations are recorded in the eastern Ross Sea during the late Oligocene to early Miocene.

Sequence 6 is bounded at its base by a type 1 (Figure 3.3) sequence boundary RSU6-EB and is comprised of > 830 m of stratified to internally transparent prograding reflectors that are capped by an unconformity correlated to RSU5.15-EB (Figure 3.5). In the Roosevelt subbasin a wedge of reflectors onlap RSU6-EB and have a maximum thickness of ~400 m. This unit is interpreted as a lowstand systems tract deposited during RSL fall. Above the lowstand systems tract is a ~430 m thick section of prograding reflectors interpreted as a highstand systems tract. These two units are capped by a high-amplitude reflector and flat-topped ridges that have been correlated to regional horizon RSU5.15-EB and to lower DSDP Site 270 (Brazell, 2017). The thickness of the section between RSU6-EB and RSU5.15-EB at Site 270, and throughout most of Eastern Basin, is less than 100 m. Additionally, outside of the Roosevelt subbasin, this section is interpreted as the lowstand systems tract of sequence 5 (Figure 3.6). The absence of dip-oriented seismic profiles in the Roosevelt subbasin and significant erosion of up-dip portions of sequence 6 along the eastern margin of the Eastern Basin prevents measurements of onlap positions. Since sequence 6 is only identified within the Roosevelt subbasin, it is interpreted as either the product of a low magnitude RSL cycle (Figure 3.4) or the Roosevelt subbasin may be older than the Eastern Basin and, having experienced a longer period of tectonic subsidence, may have had the necessary accommodation to record a RSL cycle shortly after RSU6-EB time.

Sequence 5 is present along the margins of Central High and Marie Byrd Land and bounded by Type 1 sequence boundaries, RSU6-EB and RSU5.12-EB (Figures 3.6 and 3.7). Sequence 5 represents the lowermost regional third-order sequence within RSS-2-EB that can be correlated throughout the Eastern Basin. Sequence 5 is comprised of an early lowstand systems

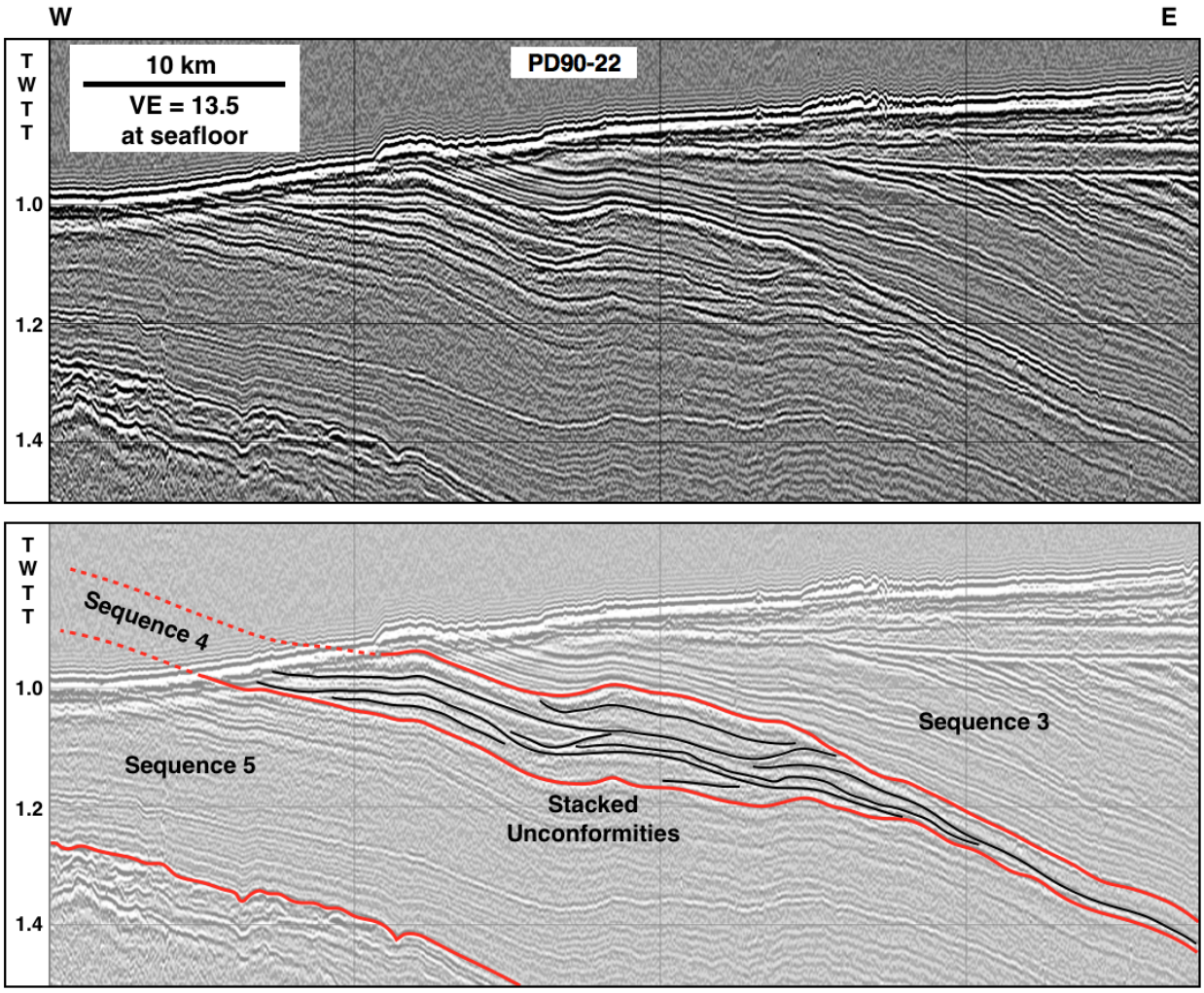

Figure 3.8. Seismic reflection profile PD90-22 (see Figure 3.1 for location). Sequence 4 preserves multiple stacked unconformities along the eastern flank of Central high. These unconformities are interpreted as glacial surfaces of erosions and may be correlated to high frequency glacial/interglacial cycles recorded in the western Ross Sea. The unconformities in Eastern Basin suggest that the WAIS was similarly experiencing ice volume fluctuation ~25 Ma and possibly contributed to glacio-eustatic sea level fluctuations during this time.

tract slope- and basin floor-fan below a prograding late lowstand systems tract, a thin transgressive systems tract and an aggradational to progradational highstand systems tract. Sequence 5 lowstand systems tract is characterized as acoustically transparent to weakly stratified reflectors below RSU5.15-EB that show landward onlap trajectories (Figure 3.6). Above RSU5.15-EB, seismic facies consist of moderate- to high-amplitude stratified reflectors with basinward downlap trajectories. Seismic profile BGR007-1 (Figure 3.7), along Central High, shows type 1 sequence boundary, RSU5.12-EB, truncating the upper portion of sequence 5. Near the Marie Byrd Land coast, modern erosion at the sea floor has removed the shelf break and RSU5.12 appears conformable where it is present.

Sequence 4 is bounded by type 1 sequence boundaries RSU5.12-EB and RSU5.11-EB and is comprised of a thick section of prograding, weakly stratified reflectors with basinward downlap trajectories in the deep basin (Figure 3.7). This unit is interpreted as a lowstand systems tract. Above the early lowstand deposits, weakly stratified reflectors onlap RSU5.12-EB with a landward trajectory and late lowstand reflectors prograde basinward (Figures 3.6 and 3.7). A thin section of weakly stratified reflectors above the lowstand systems tract is interpreted as a section of highstand deposits (Figure 3.6). The overlying sequence boundary, RSU5.11-EB, truncates the up-dip portions of sequence 4 (Figures 3.6 and 3.7) across the basin and suggests the RSL fall of RSU5.11-EB was of greater magnitude than during RSU5.12-EB time (Figure 3.4). This is evidence that RSL fluctuations were not of equal magnitude during the deposition of RSS-2-EB.

Multiple stacked unconformities above RSU5.12-EB are identified in the southwestern sector of Eastern Basin, south of Site 270 (Figure 3.8) These unconformities are interpreted as multiple, higher frequency glacial advance and retreat cycles (Brazell, 2017). The stacked unconformities are ultimately truncated by type 1 sequence boundary RSU5.11-EB.

Unconformity RSU5.11-EB truncates the entirety of sequence 4 along Roosevelt Ridge and offshore Marie Byrd Land.

Sequence 3 is bounded at its base by type 1 sequence boundary RSU5.11-EB and above by type 2 sequence boundary, RSU5.05-EB. It is comprised of a thin lowstand systems tract deposited farther up-dip than previous lowstand systems tracts (Figure 3.7). The thickness and position of Sequence 3 lowstand systems tract suggest a rapid rate of RSL fall (Figure 3.4). Above the lowstand systems tract is a back-stepping transgressive systems tract. Sequence 3 lowstand and transgressive systems tracts are not in contact with one another along the eastern flank of central high (Figures 3.6 and 3.7) and are interpreted as the product of a rapid rate of RSL rise that outpaced sedimentation (Figure 3.4)

The early highstand systems tract is comprised of a thick package of aggradational clinoforms below a thick section of progradational clinoforms during the late highstand. The thick, aggradational early-highstand systems tract suggests a continuation of relatively rapid sea level rise after the inflection point, and the transition to a thick, progradational late-highstand systems tract suggests an abrupt decrease in the rate of accommodation increase. This stacking pattern of the highstand systems tract suggests a rapid reduction in the rate of RSL rise and a prolonged late highstand (Figure 3.4).

Sequence 2, bounded at its base by type 2 sequence boundaries RSU5.05-EB and RSU5.03-EB, is comprised of a thick shelf margin wedge, thin transgressive systems tract, and thick prograding highstand systems tract (Figure 3.6). The lowstand systems tract is comprised of a > 300 m thick shelf margin wedge of high amplitude, stratified reflectors with onlap positions that have a basinward trajectory. A shelf margin wedge is the product of deposition during a RSL fall that does not fall below the position of the self-break. This is interpreted as a

RSL fall during sequence 2 that was smaller in magnitude than the previous RSL fall of sequence 3 (Figure 3.4). Above sequence 2 shelf margin wedge, a set of back-stepping clinoforms is interpreted as a transgressive systems tract (Figure 3.6). The transgressive systems tract of sequence 2 downlaps the shelf margin wedge and may represent a lower rate of RSL rise than during sequence 3 (Figure 3.4). The thick, progradational highstand systems tract may have been deposited when the rate of sea level rise decreased below the rate of sedimentation (Figure 3.4). Sequence 2 is truncated by a regionally extensive erosional unconformity, RSU5.03-EB.

Sequence 1 is bounded by type 2 sequence boundary RSU5.03-EB and Type 1 sequence boundary RSU5-EB. Sequence 1 is comprised of thin, predominately aggradational shelf margin wedge reflectors that onlap RSU5.03 with landward onlap trajectories. The shelf margin wedge is overlain by a thin transgressive systems tract and a thick highstand systems tract composed of strongly progradational clinoforms. The presence of a thin shelf margin wedge lowstand systems tract suggests that the rate of RSL fall was less than or equal to the rate of subsidence and of lower magnitude than the RSL fall during sequence 2 (Figure 3.4). The thick, dominantly progradational highstand systems tract suggests the rate of sea level rise did not outpace the rate of sedimentation and is interpreted as the product of a low-magnitude RSL rise (Figure 3.4).

3.3.2 Sequences and Eustatic Events

Roosevelt subbasin contains a sequence of stacking patterns that cannot be correlated to other sequences preserved in the Eastern Basin. Sequence 6 in Roosevelt subbasin may preserve a complete cycle of glacio-eustatic sea level change and some of the earliest indicators of WAIS growth on the margin. Basal horizon RSU6-EB is regionally recognized as a sequence boundary and associated with a global sea level fall ca. 33 - 30 Ma (Levy et al., 2012). Flat-topped ridges coeval with RSU5.15-EB on seismic profile NBP0301-27 (Figure 3.5) have been interpreted as

moraines (Sorlien et al., 2007a; Brazell, 2017) which support the hypothesis of a regression in Roosevelt subbasin during this time. The presence and timing of sequence 6 may be the product of: 1) differences in subsidence and shelf morphology; 2) differences in sediment supply; or 3) the presence of an unconformity.

Decesari and others (2007b) show a relatively thick section of pre-RSU6-EB strata within Roosevelt subbasin. This suggests that the Roosevelt subbasin was subsiding below sea-level concomitant with deposition. The early sedimentation within the subbasin may have created a more gently sloping shelf capable of trapping sediments resulting in lower paleo-water depths. De Santis and others (1999) show that during RSU6-EB to RSU5.15-EB deposition, the shelf near Central High in the western sector of Eastern Basin was steeply sloping and sediment deposition was likely influenced by down-slope transportation processes until late RSS-2-EB time. If Roosevelt subbasin shelf morphology resulted in increased deposition during this time, the sedimentation may have resulted in a normal regression and appearance of a RSL cycle that is not reflected in the eustatic signature. In the absence of a unique shelf morphology within the Roosevelt subbasin, sedimentation rates during 30 - 25 Ma ± 2 Myrs may have been locally higher within Roosevelt subbasin resulting in crustal loading and increased accommodation. The mechanisms for increased local sedimentation rates are unclear; however, initial glaciation may have resulted in increased sedimentation or the position of Marine Byrd Land and Roosevelt Island highlands may have acted as glacial pinning point or conduit to channel localized sedimentation.

Finally, it is possible that horizon RSU5.15-EB exists as a regional, conformable sequence boundary throughout the Eastern Basin, and it is not recognized because: 1) the resolution of seismic data is too low to identify seismic facies and features that would

corroborate this interpretation; or 2) the location of the unconformable section of the sequence boundary RSU5.15-EB along the modern ice shelf edge, Central High and Marie Byrd Land has been removed. Alternatively, as RSU5.15-EB cannot be directly correlated across Roosevelt Ridge into the Roosevelt subbasin, correlation errors may account for some, but not all the expanded section. The results of this study and Brazell (2017) favors the interpretation that sequence 6 is largely unique to the Roosevelt subbasin, and a RSL fall was minor or absent across much of Eastern Basin.

Sequence 5 RSL fluctuation may correspond to: 1) 30.8 m eustatic sea level rise between 29.7 Ma and 28.3 Ma; or 2) a 47.8 m eustatic sea level rise between 28.0 Ma and 27.3 Ma (supplemental data to Miller et al., 2005). During the eustatic sea level rise between 28.0 Ma and 27.3 Ma, ~80% of the total 47.8 m eustatic fluctuation is calculated to have occurred during 0.2 Ma (supplemental data to Miller et al., 2005). A sea level rise of this magnitude and duration would likely result in a prominent prograding lowstand and back-stepping transgressive systems tract. Comparing sequences 5 and 4, sequence 5 displays a less progradational lowstand systems tract than sequence 4. Given previous chronostratigraphic interpretations of RSU6-EB (Levy et al., 2012) and the stratal stacking patterns of sequence 5, this study favors the interpretation that the post lowstand systems tracts of sequence 5 reflect a more gradual eustatic sea level rise that may correspond to the eustatic sea level rise documented between 29.7 Ma and 28.3 Ma (supplemental data to Miller et al., 2005; Figure 3.4).

The nature of Sequence 4 erosional unconformity RSU5.11-EB (the lower boundary of sequence 3) suggests that the subsequent RSL fall after sequence 4 highstand was of greater magnitude than the RSL fall that created the lower boundary of sequence 4. Limited chronostratigraphic information places Sequence 4 between 30 Ma and 25 Ma. The thick

lowstand systems tract wedge suggests that a rapid and prolonged RSL lowstand is interpreted to correspond to a eustatic sea level fall between 28.3 Ma and 27.7 Ma from the supplemental data to Miller and others (2005) sea level curve (Figure 3.4).

Multiple stacked unconformities, that are interpreted to result from glacial scouring and filling (Brazell, 2017), are located between RSU5.12-EB and RSU5.11-EB. Sequence boundary RSU5.11-EB truncates most of sequence 4 in the western sector of the Eastern Basin; hence, the magnitude of RSL fall during RSU5.11-EB time may have been greater than the magnitude of RSL fall during RSU5.12-EB (Figure 3.4). The stacked unconformities preserved along southeastern Central High may be related to four- or fifth-order (10s – 100s kyrs) glacio-eustatic sea level fluctuations. Fourth-order eustatic sea level fluctuations are recorded in the supplemental data to Miller and others (2005) sea level curve between 27.3 Ma and 24.1 Ma (Figure 3.4). Levy and others (2012) correlate RSU5.11-EB (their Mid-270) to ~25 Ma which corresponds to an ~ 49 m sea level fall and the lowest eustatic sea level position between RSU6-EB and RSU5-EB (supplemental data to Miller et al., 2005). The extent of sequence 4 erosion cannot be quantified, but we suggest that RSU5.11-EB represents one of the most significant regional unconformities during RSS-2-EB time.

Sequence 3 highstand systems tract represents a significant RSL rise, either in magnitude or duration. This study correlates sequence 3 RSL rise to the earliest Miocene (~22 – 24 Ma) (Figure 3.4) which is identified as a period of eustatic sea level fall (Miller et al., 2005). The rate of eustatic sea level fall during this period was an average of 9 m/Myr (supplemental data to Miller et al., 2005) and is comparable to the rate of subsidence along modern passive margins (Xie and Heller, 2009). This may have resulted in an extended period of deposition before the

rate of sea level fall increased to force a regression resulting in a thick late highstand systems tract.

The stratal architecture of RSS-2-EB changes during sequence 2 and we can identify the earliest shelf margin wedge in the Eastern Basin. The shelf margin wedge is the clearest evidence that the magnitude of RSL fall during sequence 2 was lower than during sequence 3 RSL fall. This finding also has implications for the morphology of the Eastern Basin shelf during this time, as it may have been transitioning from a steeply dipping shelf to more gently dipping as sediments filled in the deeper portions of the basin.

Low magnitude RSL fluctuations during sequence 2 continue into sequence 1 time. The presence of a sequence 1 shelf margin wedge is recognized suggesting the magnitude of RSL fall was lower than sequence 2 RSL fall. RSU5.03-EB is recognized as a significant erosional surface along the eastern flank of Central High, but limited ice-proximal facies or features are recognized during sequence 1 (Brazell, 2017). This finding suggests it has an ice-distal or non-glacial origin and may be the product of fluvial or mass wasting processes.

3.3.3 Evidence of Glaciations

3.3.3.1 Seismic Record

Glaciogenic features identified on seismic profiles in the Ross Sea have been correlated to Oligocene (De Santis et al., 1995; Bartek et al., 1996; Sorlien et al., 2007a; Brazell, 2017) and early Miocene time (Pekar et al., 2013). Sorlien and others (2007) identify evidence for ice-proximal features (moraines?) within lower RSS-2-EB sequence in the Roosevelt subbasin. Brazell (2017) has similar interpretations of glaciogenic, ice-proximal features identified in the Roosevelt subbasin and correlated the events to a RSL lowstand during the late Oligocene which correspond to a time of glacial maximum. These interpretations suggest that the eustatic sea level

fall and oxygen isotope event Oi2 (or possibly Oi1, Oi1a or Oi1b; Figure 3.4) contain a signal of WAIS growth and potentially resolves the need to for an EAIS nearly twice as large as the modern.

In the western Ross Sea, Bartek and others (1996) identify three glacio-eustatic events correlated to the late Oligocene via the CIROS-1 drill site. The late Oligocene sequences of purported glaciogenic origin in the western Ross Sea identified by Bartek and others (1996) could not be traced over an extensive portion of the margin leaving the hypothesis of whether these glacial events were of sufficient magnitude to effect eustasy. Late Oligocene glaciogenic facies and features identified in the eastern Ross Sea (De Santis et al., 1995; Sorlien et al., 2007a; Brazell, 2017) correspond to glaciogenic facies and features of the same age identified in the western Ross Sea (Bartek et al., 1996) and suggests that glacial events were regionally extensive and more capable of affecting eustacy than previously recognized.

Seismic records from New Harbour, western Ross Sea suggests increasingly glacial conditions during the late Oligocene to early Miocene and that grounded ice expanded onto the shelf ca. 23 Ma and 19.4 Ma (Pekar et al., 2013). Seismic records from the eastern Ross Sea show increasingly glacial conditions during the late Oligocene and increasingly interglacial conditions during the early Miocene (Brazell, 2017). This apparent conflict suggests that the WAIS was unstable while the EAIS was advancing into the western Ross Sea. Oxygen isotope records indicate a large and rapid decrease in $\delta^{18}O$ enrichment and a warming climate during the latest Oligocene to middle Miocene (Zachos et al., 2001) which may be accounted for if the WAIS was collapsing during this time.

Not all seismic records from the Antarctic margin suggest a glaciated West Antarctica during the Oligocene. Seismic records from the Amundsen Sea, West Antarctica, are correlated

to regional sequences identified in the Ross Sea based on seismic character (Gohl et al., 2013). The earliest evidence of glaciation from the Amundsen Sea margin appears in the middle Miocene ca. 14 Ma (Gohl et al., 2013) and suggests that West Antarctica was not significantly glaciated during the late Oligocene to early Miocene. The lack of evidence of Oligocene glaciation within the Amundsen Sea may be explained by its relatively thin margin compared to the Ross Sea and smaller drainage area that does not reach as far into the interior of West Antarctica as the Ross Sea drainage basin. Ice flowing onto a shelf from a smaller drainage basin area would likely result in thinner ice streams that fringe and collapse more quickly at the ocean-ice interface. A thicker ice stream resulting from a larger basin drainage area would be grounded in deeper water and advance further onto the shelf and would be more likely to leave a record of glaciation.

3.3.3.2 Drill Core Record

Drill core records from the Oligocene-Miocene boundary in the Eastern Basin contain a thick record of glacio-marine sedimentation likely sourced from West Antarctica (Hayes and Frakes, 1975). Foraminiferal records from DSDP Site 270 indicate a deepening of paleo-water depth from subaerial to a depth of 300-500 m by middle RSS-2-EB (Leckie and Webb, 1984). This indicates subsidence outpacing sedimentation during the late Oligocene to early Miocene time. Foraminiferal evidence also indicates the presence of major sea ice buildup during the early Miocene (Leckie and Webb, 1983), reflecting a climate that would have been more favorable for ice accumulation within the continent.

Records from drill core, MSSTS-1, in the western Ross Sea provide evidence for a RSL fall ca 28 Ma. and up to four glacial advances between 28 Ma and 25 Ma and RSL rise ca. 25 Ma (Barrett et al., 1987). The MSSTS-1 records support drill core and seismic reflection evidence

from the Eastern Basin that suggests basement highs may have been subaerialy exposed ca. 30 Ma (Hayes and Frakes, 1975). There are multiple unconformities between 30 Ma and 25 Ma identified on seismic profiles along Central High are interpreted as glacial surfaces of erosion (Sorlien et al., 2007b).

Cape Roberts Project core 2/2A recovered late Oligocene to early Miocene strata off the coast of Victoria Land, western Ross Sea that contains approximately 17, unconformity bounded sequences between 30 Ma and 20 Ma (Cape Roberts Science Team, 1999; Wilson et al., 2000; Fielding et al., 2000) interpreted to represent fluctuations in EAIS ice volume (Naish et al., 2001). Multiple sequences of less than 20 m thickness occur within the CRP 2/2A interval between 25.1 Ma and 25.8 Ma (Fielding et al., 2000; Wilson et al., 2000) and are interpreted as high-frequency glacial advance and retreat cycles (Fielding et al., 2000). The signature identified in CRP 2/2A is correlated to multiple stacked unconformities identified in Eastern Basin below horizon RSU5.11-EB (Figure 3.8) with an approximate age of 25 Ma (Sorlien et al., 2007). Records of eustatic sea level change between 24-26 Ma (Miller et al., 2005) show multiple high-frequency fluctuations and a broad lowering of sea level. This suggests that the EAIS and WAIS were fluctuating in unison by the late Oligocene and both ice sheets likely contributed oxygen isotope events Oi2C and Mi1 and to a eustatic sea level fall of ~ 50 ft during 24-26 Ma (Figure 3.4; Miller et al., 2005).

IRD records from drill core CIROS-1, in the western Ross Sea, contain drop stone free muds deposited from 27 – 26.5 Ma and increasing IRD clasts between 26.5 – 25Ma and is interpreted as a shift from interglacial to an extensive EAIS expansion (Hambrey and Barrett, 1993). Sequence stratigraphic interpretations from seismic data in the eastern Ross Sea suggest significant erosion along the shelf and glaciogenic features prior to 25 Ma (Brazell, 2017) that

likely corresponds to a RSL fall and glacial expansion. Below the 25 Ma sequence boundary in the Eastern Basin is a highstand and transgressive systems tracts deposited between 30 Ma and 25 Ma that may correspond to the same interglacial cycle interpreted during this time in the CIROS-1 core.

3.3.4 Eastern Ross Sea Glacial History

The seismic stratigraphy of the Eastern Basin, Ross Sea has been correlated to eustatic and oxygen isotope events during the late Oligocene and early Miocene. Seismo-stratigraphic stacking patterns, features and facies provide insights about the timing and evolution of the West Antarctic cryosphere and WAIS. Several lines of evidence suggest a cooling climate and that icecaps existed along the flanks of Eastern Basin and Roosevelt Ridge: pre-RSU-6-EB U-shaped channels carved into acoustic basement (De Santis et al., 1995), 18O enrichment (Abreu and Anderson 1998; Zachos et al., 2001; Miller et al., 2005), and a eustatic sea level fall (Haq et al., 1987; Miller et al. 2005) during the early Oligocene.

During the late Oligocene, moraine-like mounds on the flanks of Central High were identified along RSU-6-EB (Brazell, 2017). RSU6-EB has an assumed age between 30 Ma ± 2 Ma and may correspond to oxygen isotope event Oi1, Oi1b or Oi2 (Pekar et al., 2002). Glaciogenic features within sequence 6 observed in our study, including flat-topped ridges (moraines?) and multiple broad scour-and-fill facies within the Roosevelt subbasin (Sorlien et al., 2007a) may be correlated to Oi2 and eustatic sea level fall ~ 30 Ma or the older Oi1b event ~32 Ma. These features provide evidence of ice that existed as either local piedmont glaciers or a thin WAIS that had advanced to the margin of the Ross Sea during the early Oligocene.

Sequence 4 is correlated to a ~ 40 m eustatic sea level fall and oxygen isotope event Oi2a (Figure 3.4). It is mostly removed from the section by a series of stacked unconformities, capped

by erosional unconformity and sequence 3 sequence boundary RSU5.11-EB. The stacked unconformities in Eastern Basin are correlated with a series of higher frequency eustatic sea level fluctuations between 24.3 – 27.3 Ma (Figure 3.4). Multiple, closely spaced glacial surfaces of erosion identified in drill core CIROS-2 in the western Ross Sea (Naish et al., 2001) are correlated by age to the stacked unconformities in the Eastern Basin and suggest that both the EAIS and WAIS were dynamic and likely advanced onto the shelf during this time. This correlation also suggests a synchronization between the two Antarctic Ice Sheets during this time. Moreover, it may reflect the first evidence of the WAIS contributing to the glacio-eustatic signature. The eustatic record reveals that some of the largest sea level falls of the Cretaceous to early Neogene occurred during the Oligocene (Miller et al., 2005) and it is unlikely to be the product of the EAIS alone. If the WAIS did contribute to eustatic sea level fall in a significant way during the late Oligocene, it would either have been as large as it is today (Wilson et al., 2013) or it would have had to be grounded above sea level. No core data exists for this interval within the Eastern Basin and seismic stratigraphic analysis alone is insufficient to unequivocally support the idea.

Sequence 3 is correlated to the Mi1 glaciation event (Figure 3.4). Sequence boundary RSU5.11-EB represents a significant erosional surface that has removed much of sequence 4 in the near Central High and the entire section near Marie Byrd Land. In the easternmost sector of the Ross Sea, glaciogenic scours and mounds may result from increased ice thickness that was grounded below sea level (Sorlien et al., 2007b; Brazell, 2017). These features correspond to the largest magnitude eustatic lowstand during the Paleogene and early Neogene (Miller et al., 2005).

Sequence 2 is correlated to oxygen isotope event Mi1a and a eustatic sea level fall of ~25 m (Figure 3.4). There is a trend of decreasing ^{18}O enrichment during the late Oligocene through early Miocene indicating a collapse of the WAIS during this time (Zachos et al., 2001; Miller et al., 2005). However, sequence boundary RSU5.05-EB shows significant erosion and down-dip features interpreted as glaciogenic (Brazell, 2017). The glaciogenic origin of the features identified within sequence 2 is equivocal and could be related to turbidites and slumping.

Features within Sequence 1 are not interpreted as glaciogenic (Brazell, 2017) and indicate warmer climate and deeper water-depths during the early Miocene. Sequence 1 is correlated with oxygen isotope event Mi1aa and a relatively minor eustatic sea level fall of <10 m (Figure 3.4). Using stratal stacking patterns, RSU5-EB is correlated to have an age of 19.6 Ma (Figure 3.4), which is 1 - 2 Ma younger than previous interpretations for this boundary (Levy et al., 2012); however, RSU5 has never been sampled and ages assigned to RUS5-EB are extrapolated below the bottom of drillcore DSDP Site 272 (Steinhauff et al., 1987).

The magnitude of the latest Oligocene global warming event, as indicated by Zachos and others (2001), suggests that direct records from the Ross Sea should contain evidence of a significant global warming event. While the direct records from the Eastern Basin do indicated reduced ice-volumes during the latest Oligocene and early Miocene there is little evidence of a catastrophic collapse of the West Antarctic Ice Sheet. Pekar and Christie-Blick (2008) show that published oxygen isotope data and other paleoclimate proxies from the late Oligocene to early Miocene should be recalibrated to global sea-level estimates. This recalibration not only indicates cooler global climate during this time-period that would be more conducive for an expanded WAIS, but it resolves conflicts between pCO_2 records that also indicate cooler atmospheric temperatures and an expanded Antarctic Ice Sheet (Pagani et al., 2005). A portion of

increased Antarctic ice-volumes indicated by a recalibrated oxygen isotope record would likely have been supported on West Antarctica. The direct records from the Eastern Basin additionally suggest the WAIS of the Oligocene was fundamentally different that the modern WAIS and perhaps more resilient and stable during past global warming events. Recent modeling by Wilson and others (2013) indicates higher topography in West Antarctica during the Eocene. A terrestrially based WAIS would be less sensitive to fluctuations in ocean temperature. Seismic reflection data does not indicate a foredeepened shelf along the Ross Sea margin during the Oligocene (De Santis et al., 1999). A foredeepened shelf is understood to promote destabilization of and ice sheet's grounding line (Robinson, 2009). Continued Cenozoic erosion and subsidence of the West Antarctic sub-continent, along with the foredeepening of the Ross Sea shelf may have contributed to the modern instability of the WAIS.

3.4 Conclusions

This study utilizes a third-order sequence stratigraphic model and stacking patterns to interpret the relative magnitude of RSL fluctuations and compares them to a eustatic sea level curve and oxygen isotope events. Interpretations of stratal stacking patterns within RSS-2-EB show that RSL events were not of equal magnitude. A dearth age control limits our ability to test the hypotheses about the periodicity of RSL fluctuations. However, a good correlation exists between the relative magnitudes of RSL fluctuations interpreted in the Eastern Basin and the pattern of the eustatic fluctuations during the late Oligocene through early Miocene (Figure 3.4). These patterns were used as qualitative age control for RSS-2-EB and suggest that RSL fluctuations were quasi-periodic during the late Oligocene through early Miocene. By comparing the seismic features identified within the Eastern Basin to a variety of near- and far-field proxy

records of glaciations, a new interpretation of the history of West Antarctica cryosphere evolution has been developed for the late Paleogene through early Neogene:

1. Prior to RSU6-EB (~30 Ma. ± 2 Ma) U-shaped valleys indicate ice, in the form of ice caps and small piedmont glaciers, likely existed along subaerialy exposed portion of the Ross embayment and inland portions of West Antarctica.

2. Approximately 27 - 30 Ma., ice proximal features and facies within the Roosevelt subbasin were the product of significant glaciation that advanced onto the shelf. Little, if any, ice advances to the margin along the eastern Ross Sea.

3. Approximately 28 Ma., U-shaped channels and mounds correlated to Oi2 glaciation records an expansion of EAIS and WAIS onto the Ross Shelf resulting in a eustatic sea level fall of > 40 m.

4. Between 28-25 Ma., multiple stacked unconformities and scour-and-fill deposits suggest EAIS and WAIS are dynamic with multiple advances and retreat cycles. WAIS cannibalizes most of the strata deposited during this interval. After this period, WAIS contributes less to eustatic sea level and may have become marine based.

5. Between 25-22 Ma., significant ice proximal facies within the Eastern Basin represent last seismic evidence of early Miocene glaciers impinging upon the margin. Stacking patterns indicate rising sea level and a collapse of the WAIS.

6. Between 22 – 19 Ma., ice-distal open marine conditions within the Eastern Basin and a significant reduction in the size of the WAIS.

This study further suggests that the WAIS that existed during the Oligocene and early Miocene was more stable than the modern WAIS.

REFERENCES

Abreu, V. S., and Anderson, J. B., 1998. Glacial eustasy during the Cenozoic: Sequence stratigraphic implications. American Association of Petroleum Geologists Bulletin, v. 82, pp. 1385–1400.

Anderson, J.B., and Shipp, S.S., 2001. Evolution of the West Antarctic Ice Sheet, In: Alley, R.B., and Bindschadle, R.A., (Eds). The West Antarctic Ice Sheet: behavior and environment. Antarctic Research Series, v., 77, pp. 45-57.

ANTOSTRAT Project, 1995. Seismic Stratigraphic Atlas of the Ross Sea, Antarctica. In: Geology and Seismic Stratigraphy of the Antarctic Margin, v. 2. Editors, Cooper, A.K., Barker, P.F., and Brancolini, G., 1995. Antarctic Research Series. AGU, Washington D.C., v. 68, plates 1-22.

Bamber, J.L., Riva, R.E.M., Vermeersen, B.L.A., and Le Brocq, A.M., 2009. Reassessment of the potential sea-level rise from a collapse of the West Antarctic Ice Sheet. Science. v. 324(5929): pp. 901-903.

Barker, P.E., Kennett, J.P et al., 1988. Proceedings of the Ocean Drilling Program Scientific Reports. v. 113, Washington, DC. US Government Printing Office. p. 989.

Barrett, P.J., Elston, D.P., Harwood, D.M., McKelvey B.C., and Webb, P.N., 1987. Mid-Cenozoic record of glaciation and sea-level change on the margin of the Victoria Land basin, Antarctica. Geology. v. 15, pp. 634-637.

Barron, J., Larsen, B., and Baldauf, J.G., 1991. Evidence for late Eocene to early Oligocene Antarctic glaciation and observations on late Neogene glacial history of Antarctica: Results from Leg 119. *in* Barron, J. Larsen, B., et al., (Eds). Proceedings of the Ocean Drilling Program, Scientific Results. v. 119. pp. 869-891.

Bartek, L. R., Henrys, S. A., Anderson, J. B., and Barrett, P. J., 1996. Seismic stratigraphy of McMurdo Sound, Antarctica: Implication for glacially influenced early Cenozoic eustatic change. Marine Geology, v. 130, pp. 79–98.

Brazell, 2017. Seismic record of West Antarctic Ice Sheet dynamics during the late Oligocene to early Miocene in the Eastern Basin, Ross Sea. PhD Dissertation. University of North Carolina at Chapel Hill, Chapel Hill, NC, USA.

Cape Roberts Scientific Team 1999. Initial report and scientific results on CRP-2, Cape Roberts Project. Terra Antartica, v. 6(1/2), pp. 1–173.

Catuneanu, O., Galloway, W.E., Kendall, C.G.St.C., Miall, A.D., Posamentier, H.W., Strasser, A., and Tucker, M.E., 2011. Sequence Stratigraphy: Methodology and Nomenclature. Newsletters on Stratigraphy. v. 44/3 pp. 173-245.

Cooper, A.K., G. Brancolini, C. Escutia, Y. Kristoffersen, R. Larter, G. Leitchenkov, P. O'Brien, and W. Jokat, 2008. Cenozoic climate history from seismic-reflection and drilling studies on the Antarctic continental margin, In: F. Florindo and M. Siegert (Eds). Antarctic Climate Evolution, Developments in Earth and Environmental Sciences, v. 8, Elsevier, p. 537.

Coxall, H., Wilson, P.A., Palike, H., Lear, C.H., and Backman, J., 2005. Rapid stepwise onset of Antarctic glaciation and deeper calcite compensation in the Pacific Ocean. Nature, v. 433, pp. 53-57.

Davey, F.J., Bennett, D.J., and Houtz, R.E., 1982. Sedimentary basins of the Ross Sea, Antarctica. New Zealand Journal of Geology and Geophysics. v. 25, i. 2, pp. 245-255.

Decesari, R.C., Wilson, D. S., Luyendyk, B. P., and Faulkner, M., 2007a. Cretaceous and Tertiary extension throughout the Ross Sea, Antarctica. *in* Cooper, A.K., and Raymond, C.R., (Eds.) Antarctica: A Keystone in a Changing World – Online Proceedings of the 10th ISAES, USGS Open File Report 2007-1047, Short Research Paper 052, p. 6.

Decesari, R.C., Sorlien, C.C., Luyendyk, B.P., Wilson, D.S., Bartek, L.R., Diebold, J., and Hopkins, S.E., 2007b. Regional seismic stratigraphic correlations of the Ross Sea: Implications for the tectonic history of the West Antarctic Rift System, *in* Cooper, A.K., and Raymond, C.R., (Eds.) Antarctica: A Keystone in a Changing World – Online Proceedings of the 10th ISAES, USGS Open File Report 2007-1047, Short Research Paper 052, p. 4.

DeConto, R.M., and Pollard, D., 2003. Rapid Cenozoic glaciation of Antarctica induced by declining atmospheric CO2. Nature. v. 421, pp. 245-249.

De Santis, L., Anderson, J. B., Brancolini, G., and Zayatz, I., 1995. Seismic Record of Late Oligocene Through Miocene Glaciation on the Central and Eastern Continental Shelf of the Ross Sea. Antarctic Research Series. American Geophysical Union, Washington, DC, v. 68, pp. 253–260.

De Santis, L., Prato, S., Brancolini, G., Lovo, M., and Torelli, L. 1999. The eastern Ross Sea continental shelf during the Cenozoic: Implications for the West Antarctic Ice Sheet development. *in*: F. M. Van der Wateren, and S. A. P. L. Cloetingh (Eds). Lithosphere dynamics and environmental change of the Cenozoic West Antarctic Rift System. Global Planetary Change, v. 23 (Special Issue), pp. 173–196.

Fielding, C.R., Naish, T.R., Woolfe, K.J., and Lavelle, M.A., 2000. Facies analysis and sequence stratigraphy of CRP-2/2A, Victoria Land Basin, Antarctica. Terra Antarctica, v. 7, pp. 323-338.

Fretwell, P, Pritchard, H.D., Vaughan, D.G., Bamber, J.L., et al., 2013. Bedmap2: improved ice bed, surface and thickness datasets for Antarctica. The Cryosphere, v. 7, pp. 375-393.

Gohl, K., Uenzelmann-Neben, G., Larter, R.D., Hillenbrand, C.D., Hochmuth, K., Kalberg, T., Weigelt, E., Davy B., Kuhn, G., and Nitsche, F.O., 2013. Seismic stratigraphic record of the Amundsen Sea Embayment shelf from pre-glacial to recent times: Evidence for a dynamic West Antarctic ice sheet. Marine Geology, v. 344, pp. 115-131.

Greenlee, S.M., Schroeder, F.W., and Vail, P.R., 1988. Recognition and interpretation of depositional sequences and calculation of sea level changes from stratigraphic data-offshore New Jersey and Alabama Tertiary. *in* Wilgus, C.K., Posamentier, J., Ross, C.A., and Kendall, C.G.St.C. (Eds), Sea Level Changes: an integrated approach. Special Publication. Society of Economic, Paleontology and Mineralogy. v. 42. pp. 329-353.

Hambrey, M.J., Ehrmann, W.U., and Larsen, B., 1991. Cenozoic glacial record of the Prydz Bay continental shelf, East Antarctica. *in* Barron, J. Larsen, B., et al., (Eds). Proceedings of the Ocean Drilling Program, Scientific Results. v. 119. pp. 77-132.

Hambrey, M. J., and Barrett, P. J., 1993. Cenozoic Sedimentary and Climatic Record, Ross Sea Region, Antarctica, Antarctic Research Series, Vol. 60. American Geophysical Union, Washington, DC, pp. 91–124.

Haq, B.U., Hardenbol, J., and Vail, P.R., 1987. Chronology of fluctuating sea levels since the Triassic. Science. v. 235, pp. 1156-1167.

Hayes, D. E., and Frakes, L. A. (Eds)., 1975. Initial Reports of the Deep Sea Drilling Project Leg 28. Washington, DC. US Government Printing Office, v. 28, p. 1017.

Joughin I., and Alley, R.B., 2011. Stability of the West Antarctic ice sheet in a warming world. Nature Geoscience. v. 4, pp. 506-513.

Lear, C.H., Elderfield, H., and Wilson, P.A., 2000. Cenozoic deep-sea temperatures and global ice volumes from Mg/Ca in benthic foraminiferal calcite. Science, v. 287 pp. 269-272.

Lear, C.H., Rosenthal, Y., Coxall, H.K., and Wilson, P.A., 2004. Late Eocene to early Miocene ice-sheet dynamics and the global carbon cycle: Paleoceanography, v. 19, PA4915.

Leckie, R. M., and Webb, P. N., 1986. Late Paleogene and early Neogene foraminifers of deep sea drilling project site 270, Ross Sea, Antarctica. In: J. P. Kennett, C. C. von der Borch, et al. (Eds). Initial Reports of the Deep Sea Drilling Project. Leg 90. US Government Printing Office, Washington, DC, pp. 1093–1118.

Levy, R. H., Harwood, D. M., Sorlien, C. C., Wilson, D. S., Luyendyk, B. P., Decesari, R. C., and Tuzzi, E., 2012. A Revised Chronostratigraphy for Ross Sea Sediments and Predicted Age of the ANDRILL Coulman High Sequences, Abstract PP23C-2070 presented at 2012 Fall Meeting, AGU: San Francisco, Calif., 3-7 Dec.

Miller, K.G., Wright, J.D., and Fairbanks, R.G., 1991. Unlocking the Ice House: Oligocene-Miocene oxygen isotopes, eustasy, and margin erosion. Journal of Geophysical Research. v. 98, no. B4, pp. 6829-6848.

Miller, K.G., Mountain, G.S., Browning, J.V., Kominz, M., Sugarman P.J., Christie-Blick, N., Katz, M.E., and Wright, J.D., 1998. Cenozoic global sea level, sequences, and the New Jersey transect: results from coastal plain and continental slope drilling. Reviews of Geophysics. v. 36, i. 4, pp. 569-601.

Miller, K. G., Kominz, M. A., Browning, J. V., Wright, J. D., Mountain, G. S., Katz, M. E., Sugarman, P. J., Cramer, B. S., Christie-Blick, N., and Pekar, S. F., 2005. The Phanerozoic record of sea-level change. Science, v. 310, pp. 1293–1298.

Naish, T.R., Barrett, P.J., Dunbar, G.B., Woolfe, K.J., Dunn, A.G., Henrys, S.A., Claps, M., Powell, R.D., and Fielding C.R., 2001. Sedimentary cyclicity in CRP drillcore, Victoria Land Basin, Antarctica. Terra Antartica. v. 8, i. 3, pp. 225-244.

Naish, T. R., Powell, R. D., Barrett, P.J., Levy, R. H., Henrys, S.; Wilson, G. S., Krissek, L. A., Niessen, F., Pompilio, M., Ross, J., Scherer, R., Talarico, F., Pyne, A. R., and ANDRILL-MIS Science Team, 2008. Late Cenozoic climate history of the Ross embayment from the AND-1B drill hole: culmination of three decades of Antarctic margin drilling. ANDRILL Research and Publications. Paper 26.

O'Brien, P.E., Cooper, A.K., Richter, C., et al., 2001. Proceedings of the Ocean Drilling Program, Initial Reports. v. 188. Washington DC. US Government Printing Office. p. 65.

Pagani, M., Zachos, J.C., Freeman, K.H., Tipple, B., and Bohaty, S. Marked decline in atmospheric carbon dioxide concentrations during the Paleogene. Science. v., 309, i. 5734, pp. 600-603.

Pekar, S.F., and Lear, C.H., 2007. Estimating Cenozoic ice volume from deep-sea records, *in* Antarctica: A Keystone in a Changing World — Online Proceedings of the 10th ISAES, (Eds) A.K. Cooper, C.R. Raymond, et al., USGS Open-File Report 2007-1047, MWR 02C, p. 14.

Pekar, S.F., Christie-Blick, N., Kominz, M.A., and Miller, K.G., 2002. Calibration between eustatic estimates from backstripping and oxygen isotopic records for the Oligocene. Geology, v. 30, pp. 903-906.

Pekar, S.F., and DeConto, R.M., 2006. High-resolution ice-volume estimates for the early Miocene: Evidence for a dynamic ice sheet in Antarctica. Paleogeography, Palaeoclimatology, Palaeoecology. v. 231, pp. 101-109.

Pekar, S.F., and Christie-Blick, N., 2008. Resolving apparent conflicts between oceanographic and Antarctic climate records and evidence for a decreased in pCO_2 during the Oligocene through early Miocene (34-16 Ma). Paleogeography, Palaeoclimatology, Palaeoecology, v. 260, pp. 41-49.

Pekar, S.F., Speece, M.A., Wilson G.S., Sunwall, D.S., and Tinto, K.J. 2013. The Offshore New Harbour Project: deciphering the Middle Miocene through Late Eocene seismic stratigraphy of Offshore New Harbour, wester Ross Sea, Antarctica. *In* Hambrey, M.J., Barker, P.F., Barrett, P.J., Bowman, V., Davies, B., Smellie, J.L., and Tranter, M. (Eds) Antarctic Palaeoenvironments and Earth-Surface Processes. Geological Society of London Special Publications. v. 381, pp. 199-213.

Posamentier, H. W., and Allen, G. P., 1999. Siliciclastic sequence stratigraphy: concepts and applications. SEPM Concepts in Sedimentology and Paleontology no. 7, p. 210.

Robinson, R., 2009. Role of shelf morphology in grounding-line stability: a numerical approach. LSU Master's Theses. 2510. p. 49.

Sorlien, C. C., B. P. Luyendyk, D. S. Wilson, R. C. Decesari, L. R. Bartek, and J. B. Diebold, 2007a. Oligocene development of the West Antarctic Ice Sheet recorded in eastern Ross Sea strata, Geology, Vol. 35, pp. 467-470.

Sorlien C.C., Wilson, D.S., Luyendyk, D.S., Bartek, L.R., Decesari, R.C., and Diebold, J.B., 2007b. Buried Oligocene glacial topography beneath a smooth middle Miocene unconformity in the southeast Ross Sea: Evolution of West Antarctic glaciation. U.S. Geological Survey and The National Academices, USGS OF-2007-1047. Extended Abstract 099. p. 4.

Spiegel, C., Lindow, J, Kamp, P.J.J., Meisel, O., Mukasa, S., Lisker, F., Kuhn, G., and Gohl, K., 2016. Tectonomorphic evolution of Marie Byrd Land – Implications for Cenozoic rifting activity and onset of West Antarctic glaciation. Global and Planetary Change. v., 145, pp. 98-115.

Steinhauff, D.M., Renz, M.E., Harwood, D.M., and Webb, P.N., 1987. Miocene diatom biostratigraphy of DSDP hole 272: Stratigraphic relationship to the underlying Miocene of DSDP hole 270, Ross Sea. Antarctic Journal, v. 22., pp. 123-125.

Sugden, D.E., Marchant, D.R., and Denton G.H., 1993. The case for a stable East Antarctic Ice Sheet; the background. Geografiska Annaler. v. 75A, pp. 151-155.

Vail, P.R., Mitchum, R.M., Jr., and Thompson, S., III, 1977. Seismic stratigraphy and global changes of sea level, part 3: relative changes of sea level from coastal onlap; in C.E. Payton (ed.) Seismic Stratigraphy - Applications to Hydrocarbon Exploration: American Association of Petroleum Geologists Memoir 26, pp. 63-81.

Wilch, T.I., and McIntosh, W.C., 2000. Eocene and Oligocene volcanism at Mount Petras, Marie Byrd Land: implications for middle Cenozoic ice sheet reconstructions in West Antarctica. Antarctic Science. v. 12, i. 4, pp. 477-491.

Wilson, G S., Bohaty, S. M., Fielding, C.R., Florindo, F., Hannah, M. J., Harwood, D. M., Mcintosh, W. C., Naish, T. R., Roberts, A. P., Sagnotti, L., Scherer, R. P., Strong, C. P., Verosub, K. L., Villa, G., Watkins, D.K., Webb, P. N., and Woolfe, K. J., 2000. Chronostratigraphy of CRP-2/2A, Victoria Land Basin, Antarctica. Terra Antartica, v. 7(4), pp. 647-654.

Wilson, D.S., Pollard, D., DeConto, R.M., Jamieson, S.S.R., and Luyendyk, B.P., 2013. Initiation of the West Antarctic Ice Sheet and estimates of total Antarctic ice volume in the earliest Oligocene. Geophysical Research Letters, v. 40, pp. 4305-4309.

Xie, X., and Heller, P.L., 2009. Plate tectonics and basin subsidence history. Geological Society of America Bulletin. v. 121, pp. 55-64.

Zachos, J. C., Pagani, M., Sloan, L., Thomas, E., and Billups, K., 2001. Trends, rhythms, and aberrations in global climate 65 Ma to present. Science, Vol. 292, pp. 686–693.